Characterisation of human tissue-resident T-regulatory cells in healthy tissues and *in-vitro* generation of tissue-like Treg cells with wound-healing capabilities

DISSERTATION ZUR ERLANGEUNG DES DOKTORGRADES DER NATURWISSENSCHAFTEN (DR.RER.NAT) DER FAKULTÄT FÜR BIOLOGIE UND VORKLINISCHE MEDIZIN DER UNIVERSITÄT REGENSBURG

Vorgelegt von

Lieke Marie Antoinet Sanderink

Aus

Agelo, Niederlande

Im Jahr

2021

Characterisation of human tissue-resident T-regulatory cells in healthy tissues and *in-vitro* generation of tissue-like Treg cells with wound-healing capabilities

DISSERTATION ZUR ERLANGEUNG DES DOKTORGRADES DER NATURWISSENSCHAFTEN (DR.RER.NAT) DER FAKULTÄT FÜR BIOLOGIE UND VORKLINISCHE MEDIZIN DER UNIVERSITÄT REGENSBURG

Vorgelegt von

Lieke Marie Antoinet Sanderink

Aus

Agelo, Niederlande

Im Jahr

2021

Das Promotionsgesuch wurde eingereicht am:

24.09.2021

Die Arbeit wurde angeleitet von:

Prof. Dr. Markus Feuerer

Unterschrift:

Acknowledgments

First and foremost, I would like to thank my Parents, Jan and Annet Sanderink, for always meeting my plans of wanting to move to another country to pursue my next degree with excitement and a statement of: “oh how fun! A new vacation address!”. Your everlasting support has always emboldened me to follow my dreams. Next, I would like to thank my supervisor Prof. Markus Feuerer, for his supervision, help, and insightful questions about the experiments I was doing, always designed to make me think about my research, and improve myself instead of handing answers over. Thanks also to my mentoring team, Dietmar Zaiss and Ralph Witzgall, for keeping up with me over the last few years. Thanks to the RCI core Flow and NGS core facilities. Thanks to Malte Simon, for performing all the bioinformatic analyses in this thesis. Thanks to Florian and Verena in Würzburg, for performing the human skin model experiments for us. Lots of love to my fellow lab Ausländer Asmita, always willing to help, whether it be in the lab or just for a chat about life in Bavaria as a foreigner. I appreciate you, and I’m glad we started at the same time. a big thanks to my other fellow lab members Sebastian, Lisa, Gitte, Vroni, Marina and Kathrin for being going above and beyond in the lab, and for always acting disgusted when I poked around in the newest human sample we got. The biggest thank you goes to Michael Delacher. Thank you for making and keeping science fun. Thank you for the many shared beers in the kitchen, for always being as excited over wobbly human fat as me, listening to heavy metal in the lab late at night, and last but certainly not least, for your excellent coaching and supervision during my PhD. It was always a joy to

work alongside you. Last but not least, thanks to all my wonderful friends who supported me, whether it be the new ones I made in Regensburg, my amazing friends from my Master's, especially Marijne, my immunology buddy, or my friends from back home in Twente, you are wonderful, and I love you all.

Table of Contents

1. Summary

Regulatory T cells (Tregs) are characterized by the expression of FOXP3 and are important for regulating other cellular components of the immune system. Their absence leads to autoimmune diseases like the “Scurfy phenotype” in mice or the Immunodysregulation, Polyendocrinopathy, Enteropathy, X-linked (IPEX) syndrome in humans. Non-lymphoid tissue (NLT) Tregs are distinct from lymphoid tissue (LT) Tregs. Comparing the gene expression profile (transcriptome) and the DNA methylation profile (epigenome) of NLT vs LT Treg cells in mice, our lab identified transcription factors as well as other genes particularly enriched in NLT Tregs. This led to the identification of a tissue specific Treg subset in mice, characterized by the surface expression of Klrg1 and ST2, a T_H2 biased gene program as well as their production of Amphiregulin, which has been shown to aid in tissue repair. In mouse, this program is driven by the Transcription factor Batf.

In this thesis, we worked to identify the human counterpart of this population. We established methods to isolate T-cells from tissues, and when this was optimised, performed the Assay for Transposase Accessible Chromatin following Sequencing (ATAC-seq) on a single cell level (scATAC-seq) to identify changes in chromatin accessibility on murine and human $CD4^+$ T-cells. We found that this was a good and reliable method to identify different populations of T-cells in various tissues, among which Tregs in Non-Lymphoid tissues. From these datasets we identified shared peaks within the human and murine datasets; open chromatin that was conserved between species. We examined BATF binding in this shared peakset and found that

more than half of the shared peaks had a BATF binding site, indicating importance in both human and murine tissue Tregs. Upon closer look we found that *BATF* gene activity score was increased in tissue Tregs compared to blood derived Tregs. Using bulk ATAC sequencing to identify changes in chromatin accessibility, we were able to show that we could induce a tissue Treg-like profile with the combination of cytokines IL-4 and IL-33 in mouse, and that this induction is depended on the Batf, confirming that Batf is both essential in-vitro and in-vivo. Among the shared peakset, we could identify several surface receptors, among which CCR8. Upon closer look we could determine that *CCR8* gene activity was increased in both blood memory Tregs and tissue derived Tregs. This could be confirmed on protein level in blood and in tissues, where we could identify a subpopulation of $CCR8^+$ Tregs in memory Tregs in the blood. In fat and skin, the vast majority of Tregs was $CCR8^+$. We also found that $CCR8^+$ Tregs express a significantly higher amount of FOXP3, BATF and CD25, on both RNA and protein levels. Next we worked to identify more surface markers using LEGENDScreen™. We identified HLA-DR as a reliable positive selection marker for $CCR8^+$ Tregs in blood, fat and skin. CD49d could be identified as a negative selection marker for these same cells. Using single cell RNA sequencing (scRNA-seq) and Single cell TCR sequencing (scTCR-seq) we were able to identify a clonal relationship between $CCR8^+$ from blood, fat and skin, indicating that circulating $CCR8^+$ Tregs are either potential progenitors or recirculating tissue Tregs. Through published datasets and our own RNA-seq data, we were able to show that human tissue Tregs have a Tfh-like phenotype, unlike murine tissue Tregs, which have a Th2-like phenotype. This phenotype could be induced with the cytokines IL-2, TGFβ, IL-12, IL-21, and IL-23. Supernatant

produced by cells cultured with these cytokines were superior at woundhealing compared to IL-2 only Tregs. Finally, we were able to show that Tregs found in tumours share many commonalities with Tregs found in healthy tissue, like BATF, CCR8 and HLA-DR expression.

2. Introduction

2.1. The immune system

The immune system is tightly regulated network of biological processes that functions as our primary defence mechanism. It protects against anything that an organism might experience as harmful. This includes a multiple different pathogens, like bacteria, viruses, or parasites, as well as cancer cells, or anything not deemed “own healthy tissue” (Murphy et al., 2017). In most organisms, the immune system is subdivided into two branches, innate immunity and adaptive immunity. Innate immunity is the first line of defence against pathogens, meaning that recognition of a specific pathogen is not necessary. The innate immune system is composed of natural killer (NK) cells, mast cells, eosinophils, basophils, and phagocytes, including macrophages neutrophils and dendritic cells. The low specificity towards pathogens means that innate immune system has no memory. In contradiction to this stands the adaptive immune system. The adaptive immune system is slower to respond, depending on innate immune cells to process pathogens and present them, so that it may tailor a response to specific pathogens presented to it. The adaptive immune system consists of B- and T-lymphocytes (Bonilla and Oettgen, 2010).

2.1.1. Adaptive immunity

The adaptive system consists of B- and T-Lymphocytes, also called B- and T-cells. Of these 2 groups, B-cells have the majority. B-cells develop in the bone marrow and are antigen specific antibody producing cells. They can be recognised by their B-cell receptor (BCR). By doing this, they mediate humoral immunity, the branch of immunity that deals with molecules secreted into the extracellular fluid (Hoffman et al., 2016). The other major cell type within adaptive immunity is T-cells. T-cells develop in the thymus and can be recognised by their T-cell receptor (TCR).

2.1.2. T-cells

T-cells divided into 2 overarching subsets, namely cytotoxic T-cells (CTLs) expressing Cluster of Differentiation 8 ($CD8^+$ T-cells) and T-helper (Th) cells, expressing CD4 ($CD4^+$ T-cells). T-cells are mediators of both humoral immunity, mostly through Th cells supporting B cell activation, as well as cell-mediated immunity, through CTLs (Goswami and Awasthi, 2020). T-cells can be grouped based on their function. Both $CD4^+$ and $CD8^+$ T cells are developed in the same location, the thymus, and undergo further differentiation in the periphery to perform different tasks.

The CD8 coreceptor on $CD8^+$ T-cells can bind to class I Major Histocompatibility Complex (MHCI) molecules. MHCI molecules are present on nucleated cell and can present antigens to the TCR. The TCR can only recognize antigen (peptides) bound to an MHC molecule. After the TCR recognizes the MHCI-antigen complex, the coreceptor can bind to the MHCI complex and TCR signalling is initiated. TCR signalling will lead to cytotoxic T cell activation, which allows the CD8 T-cell to induce apoptosis in the cell presenting the antigen (Zhang and Bevan, 2011).

The CD4 coreceptor does not recognize MHCI, but rather MHCII. MHCII molecules are not expressed on every cell, but only on a small subset of cells within the immune system, called antigen presenting cells (APCs). APCs include dendritic cells (DCs) and macrophages. APCs can ingest antigens in peripheral tissues and present them to CD4 T-cells in a MHCII-antigen complex upon arriving at secondary lymphoid organs (König et al., 1992).

Once activated, $CD4^+$ T-cell can differentiate into multiple different types of T-helper cells (Figure 1). Which subtype they differentiate into, depends on the environment that the cell is in, and the signals that are provided. These signals are provided by cytokines, proteins that are important in cell signalling. The main functional subsets are Th1, Th2, Th17, Tfh, and T regulatory cell (Treg), with a small subset differentiating into Th9 cells (Murphy *et al.*, 2017).

Th1 cells are characterised by their production of IFNγ and TNFα, and their expression of Transcription factors T-bet and STAT1. They help to eradicate infections by microbes that are able to survive within macrophages, like certain viruses and intracellular bacteria. Upon recognition of these antigens, they release IFNγ, which enhances the macrophage's ability to kIll microbes (Murphy *et al.*, 2017).

Th2 cells are characterised by the expression of GATA3 and STAT6, as well their IL-4, IL-5, and IL-13 secretion. They aid in controlling infections by extracellular parasites, by promoting responses that are mediated by eosinophils and mast cells (Murphy *et al.*, 2017).

Th9 cells express transcription factors PU.1 and IRF4 and are especially known for their secretion on IL-9. Their functions is not yet well understood, but they have

been implicated in various immune related diseases, including tumours, inflammatory diseases and parasite infections (Chen et al., 2019).

Th17 cells can be recognized by their expression of RORγT and STAT3, and their secretion of IL-17. They are an important contributor in the induction of the production of antimicrobial peptides by barrier epithelial cells in the gastrointestinal, respiratory and urogenital tracts, as well as the skin (Murphy *et al.*, 2017).

Tfh cells are characterized by their expressing of the transcription factors BCL6 and STAT3, surface markers Programmed Death 1 (PD-1) and CXCR5, and their secretion of IL-6 and IL-21. They provide help to B-cells in the germinal centre, during B-cell maturation (Liu et al., 2013).

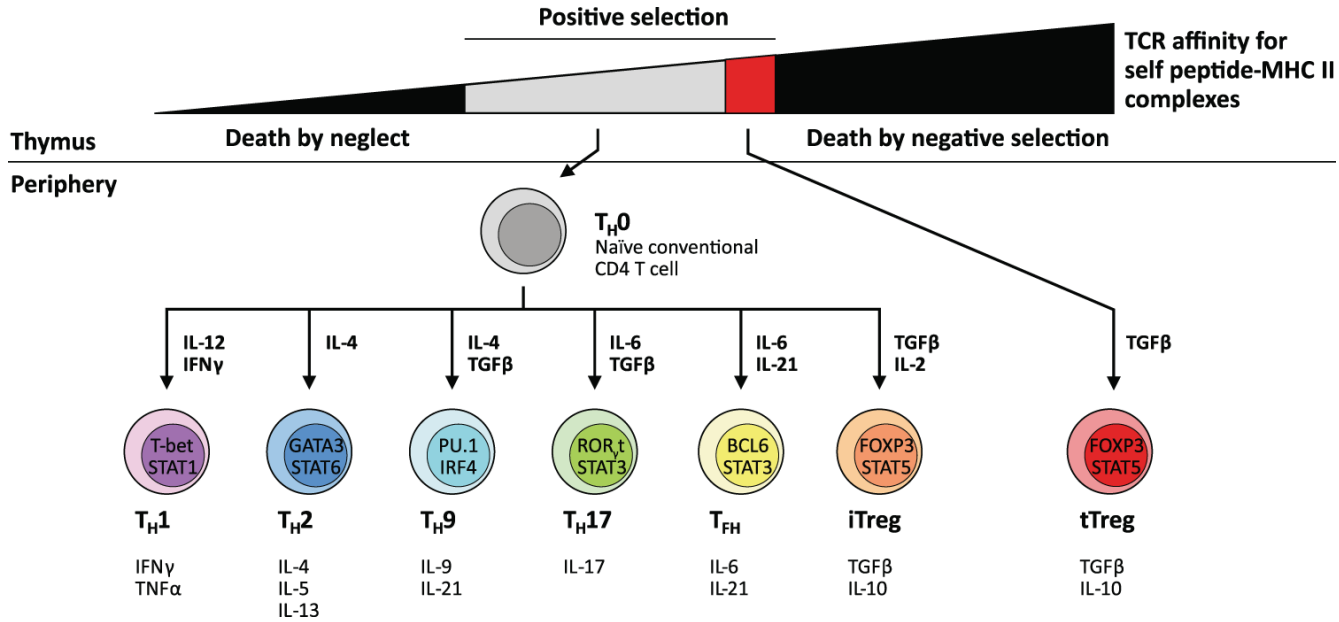

Figure 1. ***CD4 T-cell generation and differentiation into different classes of T-helper cells****. CD4 T-cells, once leaving the thymus, can differentiate into different classes of T helper cells, which are depicted here. Adapted from (Tay et al., 2021) with permission under the creative commons license: http://creativecommons.org/licenses/by/4.0/.*

2.1.3. Regulatory T-cells

Besides conventional T-cells (Tconv), another type of $CD4^+$ T-cell exists, namely, regulatory T-cells (Tregs). Treg cells play a vital role in preventing auto-immune

responses, by restraining self-reactivity of other components of the immune system, as well as excessive inflammatory responses (Sakaguchi et al., 2020). Tregs are characterized by their expression of FOXP3. FOXP3 is essential for Treg function, as a lack of FOXP3 leads to severe autoimmune disease in both mice and humans. In mice, lack of Foxp3 leads to a scurfy phenotype (Brunkow et al., 2001; Wildin et al., 2001). In humans, a lack of FOXP3 is seen in patients suffering from IPEX (immune dysregulation, polyendocrinopathy, enteropathy, and X-linked syndrome) (Vignali et al., 2008). Another trait that sets Tregs apart from Tconv, is their constitutive expression of CD25, even in naïve Tregs. in contrast, only activated Tconv express CD25. In mouse, Naïve Tregs are recognizable by their co-expression of CD62L and CD25. Tregs in human are recognized by their high expression of CD25 and low/no expression of CD127 (Murphy *et al.*, 2017).

Tregs develop from $CD4^+$ cells that are potentially self-reactive (Figure 1). They are selected in the thymus for their higher-than-usual affinity binding to MHC-II/peptide complexes containing self-antigens (Li and Rudensky, 2016).

2.2. Tregs and immune tolerance

Immune tolerance is described as a state of unresponsiveness of the immune system to substances or tissues that have the capacity to elicit an immune response, and is induced by prior exposure of immune cells to a specific antigen (Murphy *et al.*, 2017). Immune tolerance is divided into two categories, central tolerance and peripheral tolerance, differing by where tolerance is induced.

2.2.1. Central tolerance

Central tolerance is the tolerance that is established by deleting autoreactive lymphocyte clones before they mature into fully competent immune cells. Central tolerance takes place during the development stages of lymphocytes in the thymus (for T-cells) or in the bone marrow (for B-cells). During T-cell development, immature T-cells in the thymus are exposed to self-antigens presented by medullary thymic epithelial cells (mTECs). Maturing T-cells that bind too strongly to the self-antigen presented by the mTECs, are removed by the induction of apoptosis (Sprent and Kishimoto, 2001). Cells that have a slight “higher-than usual” binding affinity towards self-antigens, are redirected towards Treg differentiation, as stated before (Li and Rudensky, 2016).

2.2.2. Peripheral tolerance

Peripheral tolerance is the tolerance to antigens that is induced after lymphocytes have left their site of development, the thymus or the bone marrow. Self-reactive T-cells that are not eliminated in the thymus, for example because they are reactive to a tissue restricted antigen not expressed by mTECs in the thymus, can be killed or inactivated in peripheral systems. There are several mechanisms through which peripheral tolerance operates. Anergy is a lack of reaction by T-cells to antigens (Macián et al., 2002). Activation induced cell death is a form of apoptosis that is caused by the interaction the interaction of Fas receptors and Fas ligands, where the cell with the Fas receptor kIL-ls the cell with the Fas ligand (Zhang et al., 2004). Another form of peripheral tolerance is the suppression of other cells by Tregs.

Lastly, In functional deviation cells are directed to become induced Tregs (iTregs) (Hünefeld et al., 2012).

2.2.3. tTregs versus iTregs

Tregs were originally thought to all be thymus derived. Now, however, it is generally accepted that Tregs can also be induced in the periphery (Curotto de Lafaille and Lafaille, 2009). Tregs that are generated in the thymus are called thymic Tregs (tTregs) or natural Tregs (nTregs), and Tregs induced in the periphery are called induced Tregs (iTregs) or peripheral Tregs (pTregs). iTregs are generated when $CD4^+$ T-cells are exposed to Transforming Growth Factor Beta (TGFβ) and antigens in the absence of pro-inflammatory cytokines. Both types of Tregs can quiet T cell signalling in response to self-antigens through several mechanisms. Tregs can supress autoreactive signalling trough contact-dependent mechanisms, as well as contact independent mechanisms.

Tregs express a high level of Cytotoxtic T-lymphocyte associated protein 4 (CTLA-4) on their surface. When CTLA-4 binds to the B7 protein on the surface of T-cells, it can lead to inhibition of T-cell activity. Another Contact dependent mechanism is the induction of anergy in T-cells through the upregulation of cAMP (Vignali *et al.*, 2008).

Tregs can also supress autoreactive signalling through contact independent mechanisms. Tregs constitutively express high amounts CD25, a part of the high-affinity receptor of the IL-2 receptor, they are however, unable to produce IL-2 themselves. This results in Tregs taking away IL-2 from naïve Tconv, who don't express CD25 until they are fully activated. Other contact independent mechanisms relate to the cytokines Tregs secrete. TGFβ can inhibit T-cell proliferation, while IL-10

inhibits the expression of MHC molecules and co-stimulatory molecules by APCs and inhibits the production of pro-inflammatory cytokines. In this way, both T-cell activation, and the effect of the T-cell response are limited (Sakaguchi et al., 2009).

iTregs account for 30% of the Tregs in the intestines. An important function of iTregs in the intestines is to prevent an inflammatory immune response to the commensal microbiota. Here, they seem to be the major producer of IL-10, and a deficiency leads to inflammatory bowel disease (Round et al., 2010).

2.3. Non-Lymphoid tissue resident Tregs

In recent year, studies have shown that Tregs can also act to promote tissue homeostasis and tissue repair when they migrate to non-lymphoid tissues (NLT) and become tissue resident. This has been shown in a variety of tissues, including muscle (Burzyn et al., 2013), lung (Arpaia et al., 2015), the central nervous system (Dombrowski et al., 2017; Ito et al., 2019; Liesz et al., 2009) and visceral adipose tissue (VAT) (Cipolletta et al., 2012; Feuerer et al., 2009; Vasanthakumar et al., 2015). The main agent to mediate wound healing capacity has been described to be amphiregulin (Areg) (Arpaia *et al.*, 2015).

2.3.1. NLT Tregs vs Lymphoid Tregs in mouse

A well described population of tissue Tregs are VAT resident tissue Tregs in the murine system (Feuerer *et al.*, 2009). In the lymphoid compartment Tregs make up about 10-15% of the $CD4^+$ T-cells. In VAT however, Tregs make up about 40-60% of all $CD4^+$

cells. These cells fulfil classical Treg functions and have most of the classical Treg markers, like CD25 and Ctla4, as well as Foxp3 expression.

However, several factors have been shown to be upregulated in VAT Tregs compared to lymphoid tissue (LT) Tregs. This includes factors that are related to extravasation and migration such as CCR2, CCR9 and CXCL10, but also cytokines such as IL-10, which play a role in controlling inflammation (Feuerer *et al.*, 2009).

Recently, one study conducted DNA-methylation and transcription research, and found a Treg population with shared epigenetic and transcriptional features in multiple non-lymphoid tissues, like liver, lung, skin, VAT and colon (Delacher et al., 2017; Delacher et al., 2019; Schmidl et al., 2018). These Tregs can be identified by their expression of Kille rcell lectin-like receptor subfamily G1 (Klrg1) and the IL-33 receptor (ST2). Tissue Tregs that express Klrg1 and ST2 have been found to readily secrete the wound healing factor Areg, as well as IL-10 (Delacher *et al.*, 2017).

2.3.2. An Introduction to BATF and other important transcription factors in NLT Tregs

This tissue Treg population not only expresses classical Treg transcription factors like Foxp3, but also transcription factors that are associated with Th2 differentiation, like GATA binding protein 3 (Gata3), musculoaponeurotic fibrosarcoma (Maf), Interferon regulatory factor 4 (Irf4) and basic leucine zipper ATF-like (Batf). Among these transcription factors, Batf was found to be the most enriched in tissue Tregs

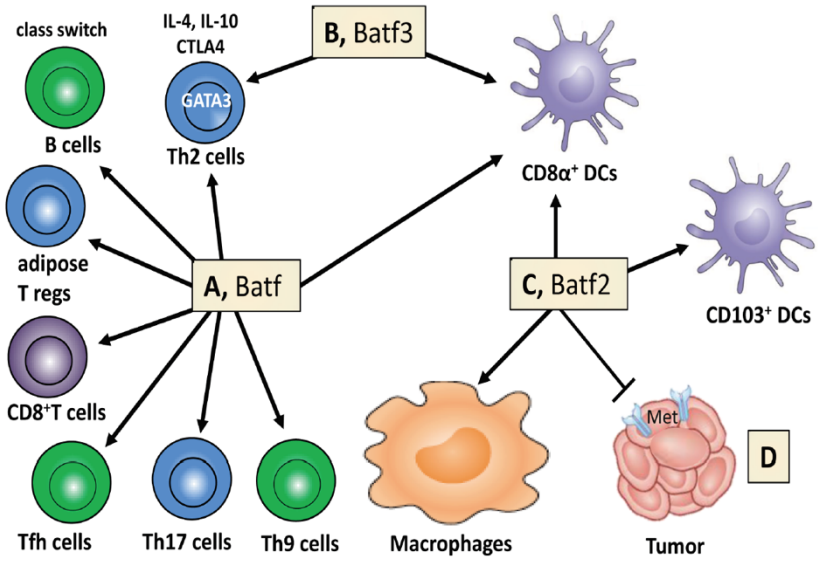

Figure 2. ***Batf is involved in multiple processes in the immune system.*** *Adapted from (Guler et al., 2015) with permission under the creative commons license: http://creativecommons.org/licenses/by/4.0/.*

versus lymphoid Tregs (Delacher *et al.*, 2017). Batf (Figure 2) has been shown to be an important transcription factor in many cell populations in the immune system (Morman et al., 2016). Most prominently, it is essential for the development of Tfh cell development (Liu *et al.*, 2013), Th17 cell development (Pham et al., 2019), and $CD8^+$ T-cell effector differentiation (Kurachi et al., 2014).

2.4. Tregs in Tumours

Tregs have long had a negative connotation in relation to tumours. Tregs, in their immunosuppressive capacity, often suppress anti-tumour immunity, as the tumour tissue cannot be identified as foreign. However, the effect of Treg presence in the tumour on disease prognosis seems to differ per tumour. In head and neck cancer, in breast cancer and in lung cancer, the presence of Tregs in high frequencies leads to a bad prognosis (Ménétrier-Caux et al., 2012; Tanaka and Sakaguchi, 2017). In contrast, high numbers of Tregs in the colon lead to an improved prognosis (Saito et al., 2016). Studies have been conducted to examine Tregs and other T-cells in tumours on a single cell level (Azizi et al., 2018; Plitas et al., 2016; Sakaguchi *et al.*, 2020; Szabo et al., 2019), and markers have been identified like surface markers Programmed cell death protein 1 (PD-1) (Ishida et al., 1992), Chemokine (C-C motif) receptor 8 (CCR8) (Plitas *et al.*, 2016), Lymphocyte activation gene 3 (LAG3), T-cell immunoglobulin and mucin-domain containing-3 (TIM-3) and T cell immunoreceptor with Ig and ITIM domains (TIGIT) (Yano et al., 2019) and transcription factors like Thymocyte selection-associated high mobility group box protein (TOX) (Easton et al., 2007).

2.5. Next generation sequencing

2.5.1. Introduction to next generation sequencing

Next generation sequencing is a term that is applied to a generation of sequencing that came after sanger sequencing, which is sequencing method based on selective incorporation of dideoxynucleotides that are chain terminating during DNA replication

(Sanger et al., 1977). NGS is mostly accomplished by fragmenting nucleic acids into tiny fragments, adding adapters, and sequencing all tiny fragments.

The most popular method of NGS is sequencing by synthesis, which use modified dNTPs containing a terminator which blocks further polymerization, so only one base can be added to a copy strand of the fragment to be sequenced (Fuller et al., 2009).

In sequencing by synthesis, strands of 100-150 base pairs are used. These strands are provided with adapters, along with a sequencing binding site, indeces, and sequence regions that allow for binding on the flow cell, a glass slide with lanes on which clustering happens. The flow cell is covered in oligos that the prepared strands can bind to. Complement sequences of the original strands are generated, after which the original fragment is denatured and washed away. The complement strands form a “bridge” by folding over and binding to another adapter on the flow cell that is complementary to the sequence on the end of the complement strand. A complementary strand is once again generated, resulting in 2 strands, which can each bridge and attach to adapters on the flow cell. in this way, each original strand is amplified. Sequencing is done like mentioned above, by flooding the flow cell with competing dNTPs containing a terminator. When a dNTP binds to a complementary base, it emits a light. This process of flooding is repeated until the strand is complete. The colour of each light is assigned to a base, A, T, C or G. the sequencer records the lights, and the order they appear in. In this way, the sequences of the strands are read. Sequences are then mapped to a reference genome for further bioinformatic analysis. (Meyer and Kircher, 2010).

2.5.2. RNA-sequencing

In RNA sequencing (RNA-seq), NGS is used to determine the quantity of RNA present in a pre-determined biological sample, at a given moment in time, and thereby analysing the transcriptome (Chu and Corey, 2012). RNA-seq can be used for a variety of purposes, including the analysis of alternative slice variant transcripts, gene mutations or single nucleotide polymorphisms (SNPs), gene fusion, post translational modifications, or changes that can be found in gene expression between samples or over time. In RNA-seq, RNA is isolated from a sample, after which double stranded complementary DNA (ds-cDNA) is synthesized. RNA is transcribed into cDNA because DNA is more stable, and allows for amplification, which uses DNA polymerases. This cDNA is then sequenced as described above (Mortazavi et al., 2008).

In single cell RNA-seq (scRNA-seq) the nuclei from a sample are isolated and pair with a bead with a unique barcode. This nuclei-bead pair is encapsulated in a Gel-bead-in-Emulsion (GEM) in an oIL-y environment, which guarantees that nucleic acids stay separated during amplification. This allows for bulk amplification of a cells, while cells are still uniquely traceable due to their assigned beads. Once amplification is completed, the oIL- is removed and samples can be sequenced like described above (Islam et al., 2014)

2.5.3. ATAC-sequencing

The Assay for Transposase Accessible Chromatin using sequencing (ATAC-seq) is a technique that uses NGS to visualize accessible chromatin, i.e., chromatin that is ready to be transcribed. In sample preparation for ATAC-seq, tn5 is added to the extracted DNA of a sample. Tn5 is a transposase, which means it can bind to DNA, cut it and insert a new fragment into it. ATAC sequencing exploits this mechanism with a hyperactive non-specific form of Tn5, which binds to any open chromatin it can find, and inserts sequencing adapters. The strands with adapters can then be amplified through polymerase chain reaction (PCR), and sequenced and processed like described above (Buenrostro et al., 2013).

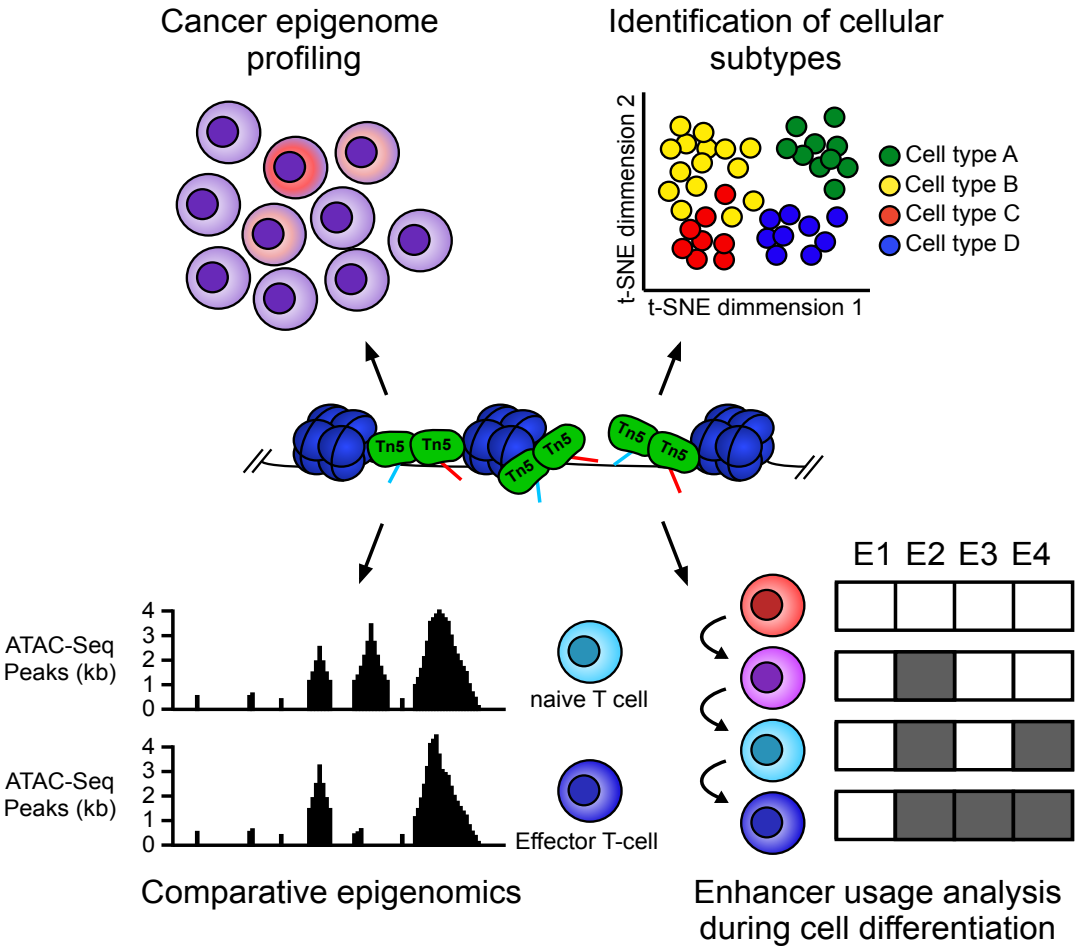

Figure 3. ***ATAC-seq allows for the visualization of open chromatin.*** *Adapted from Wikimedia commons, with permission under the creative commons license: http://creativecommons.org/licenses/by/4.0/.*

In Single Cell ATAC-seq (scATAC-seq), addition of tn5 happens in bulk. After this, nuclei are assigned their own unique beads and DNA is processed like in scRNA-seq. in analysis, strands are mapped to a reference genome (Satpathy *et al.*, 2019).

2.5.4. Single cell TCR-sequencing

T-cells have a natural barcode, the TCR receptor, which is unique to each cell and its clone, and consist of V, D and J fragment, made up into and alpha and beta chain. Through single TCR sequencing (scTCR-seq), T-cells that are related to each other can be tracked throughout an organism. In scTCR-seq, nuclei containing TCR alpha and beta chain mRNA are separated in GEMs like mentioned above, followed by reverse transcription and amplification using multiplex PCR that uses overlapping primers. These overlapping primers allow for the creation of one strand containing both the alpha and beta chain. These newly created strands are further amplified and sequenced as described above. In analysis, strands are mapped against a VDJ reference (De Simone et al., 2018).

2.6. Aim of this thesis

Tissue resident Tregs have been well studied in mice and contribution to tissue regeneration has been well established. Both in our lab and others, markers have been identified and Batf has been identified as the main driver of the tissue program in mice. However, the human counterpart of this population remains poorly understood. In this thesis, we attempted to identify this population, and gain a better understanding of its biology, its markers, and its drivers. We characterized murine and human $CD4^+$ cells

on a single cell level by examining chromatin accessibility. To do this, we used cutting edge methods to identify factors shared between human and mouse tissue Tregs.

Out of those factors, we could establish a profile that characterized human tissue Tregs.

From this profile we attempted to identify surface markers of this population, to be able to identify it in different tissues. Using these markers, we attempted to find this population in multiple tissues, and assess the relationship between them.

We attempted to induce a tissue-like program in naïve blood derived Tregs and evaluated both their likeness to tissue Tregs and their wound healing capacity.

Finally, we attempted to compare healthy tissue Tregs to tumour Tregs, as to potentially help to elucidate the mechanisms by which Tregs operate in the tumour microenvironment.

3. Materials and methods

3.1. Experimental model

3.1.1. Ethics Statement

Human skin and adipose tissue used for scATAC-seq and scRNA/scTCR-seq were obtained from five healthy female donors with an average age of 44.6 years (± 14; range from 26 to 56) undergoing abdominoplasty procedures after weight loss (4 donors) and epigastric hernia repair (1 donor). The average BMI of all patients was 31.0 (±8.9).

Human skin and adipose tissue used for bulk RNA-seq of skin and fat tissue Treg cells ($CD4^+CD127^-CD25^+$) were obtained from 7 donors undergoing abdominoplasty

procedures after weight loss (5 donors) and epigastric hernia repair (2). The average BMI of all patients was 33.2 (±6.3).

Human skin and adipose tissue used for bulk RNA-seq of skin and fat tissue CCR8$^+$ Treg cells (CD4$^+$CD127$^-$CD25$^+$CD45RA$^-$CCR8$^+$) were obtained from 5 patients undergoing abdominoplasty procedures after weight loss (4 donors) and epigastric hernia repair (1 donor). The average BMI of all patients was 26.1 (±2.8).

Human primary liver tumours (4 hepatocellular carcinomas and 2 cholangiocellular carcinomas) and surrounding healthy liver tissue as well as PBMCs used for bulk RNA-seq of CD45RA$^-$CCR8$^+$ Treg cells, CD45RA$^-$CCR8$^-$ Treg cells and CD45RA$^+$ Treg cells were obtained from six patients (3 male and 3 female) with an average age of 74.5 years (± 7; range from 62 to 82) undergoing major liver surgery.

Collection of skin, fat and blood samples from donors was performed after ethical approval by the local ethical committee (Regensburg University, reference number 19-1453-101) and signed informed consent. Collection of primary liver tumours, surrounding liver tissue and blood samples from tumour patients was performed after ethical approval of the local ethical committee (Regensburg University, reference number 18-1075-101) and signed informed consent.

Human primary keratinocytes for the generation of epidermal models were isolated from foreskin biopsies obtained from juvenile donors under informed consent, according to ethical approval granted by the local ethic committee (Würzburg University, reference numbers 182/10 and 280/18sc) and the written consent of guardians.

Peripheral blood mononuclear cells for CD4 T cell enrichment were isolated from leukocyte reduction chambers from healthy female donors donating thrombocytes.

Collection of immune cells from those donors was performed in compliance with the Helsinki Declaration after ethical approval by the local ethical committee (Regensburg University, reference number 13-0240-101 and 19-1414-101) and signed informed consent.

3.1.2. Mice

To generate scATAC-seq data of SPF animals, we used adult male C57BL/6 mice of 10 or more weeks of age. To generate scATAC-seq data of germ-free animals, we used adult male wIL-d type C57BL/6 mice of 9 or more weeks of age housed under germ-free conditions at the Helmholtz Centre for Infection Research (Braunschweig). Proof of germ-free hygiene status was performed bi-weekly through Sytox cell staining and 16S rRNA gene analysis of stool samples. *Nfil3*(GFP) mice were housed under SPF conditions and described previously (Delacher et al., 2020). *Foxp3*(huCD2) mice ($Foxp3^{tm1(CD2/CD52)Shori}$) were a gift from S. Hori (Komatsu et al., 2009). For generation of *Areg*(GFP) BAC-transgenic mice, a fusion construct composed of the DNAs for iCre and eGFP, separated by a 2A sequence, was generated and inserted at the start codon of the *Areg* gene in the BAC RP23-190I9 (BioScience) using Escherichia coli DH10B (Copeland et al., 2001). The final construct was linearized and injected into the pronuclei of fertilized C57BL/6N mouse eggs at the animal facility of the German cancer Research Center (DKFZ). Genotyping was carried out by PCR from genomic DNA of tailbiopsies. Animals were housed under specific pathogen-free conditions at the DKFZ animal care facility or the Regensburg University Clinics animal care facility, and the governmental committee for animal experimentation (Regierungspräsidium Karlsruhe, Germany for DKFZ Heidelberg or Regierungspräsidium Unterfranken, Würzburg for Regensburg) approved these animal experiments.

Tumour bearing BALB-NeuT transgenic mice (Hosseini et al., 2016) were a gift from Christoph Klein. Mice were screened at 3–4 weeks of age for hemizygosity ($neuT^+/neuT^-$). Mammary glands of BALB-NeuT female mice were inspected twice a week and $CD4^+$ T cells from growing tumours were analyzed by scATAC-seq. Experimental animal procedures regarding BALB-NeuT were approved and conducted according to German federal and state regulations (Regierungspräsidium Unterfranken, Würzburg).

3.2. Tissue digestion for flow cytometry and FACS sorting

3.2.1. T cell isolation from murine tissue

3.2.1.1. Visceral Adipose Tissue (VAT)

To isolate T cells from VAT tissue, gonadal fat pads of male mice were excised, cut into small pieces and digested for 45 minutes at 37°C (base medium DMEM (Gibco #41965), 1 mg/ml collagenase type II (Sigma-Aldrich #C6885), 20 µg/ml DNAse I (Roche #11284932001), 20 mg/ml bovine serum albumin (Sigma-Aldrich #A4503)) on a MACSmix tube rotator (Miltenyi Biotec 130-090-753), followed by incubation with 2 mM EDTA-PBS for 2 minutes and centrifugation and filtration steps.

3.2.1.2. Skin

To isolate T cells from skin tissue, hair and hair follicles from the back of the animal were removed with an electric shaver and depilatory cream. Skin was separated from the dorsal surface, cut into small pieces and digested (base medium DMEM (Gibco #41965), 4 mg/ml collagenase type IV (Sigma-Aldrich #C5138), 10 µg/ml DNAse I (Roche #11284932001), 2% fetal bovine serum). Digestion was performed directly in

a GentleMACS C tube (Miltenyi Biotec #130-096-334) and the program "37_C_Multi_H" for 90 minutes, followed by centrifugation and filtration steps

3.2.1.3. Lung

To isolate T cells from lung tissue, animals were perfused by opening the inferior vena cava and flushing the left ventricle with 10ml PBS to clear the body circulation. Lungs were excised, cut in small pieces and digested (base medium DMEM (Gibco #41965), 1 mg/ml collagenase type IV (Sigma-Aldrich #C5138), 20 μg/ml DNAse I (Roche #11284932001), 5 mg/ml bovine serum albumin (Sigma-Aldrich #A4503)) for 30-45 minutes at 37°C on a MACSmix tube rotator, followed by centrifugation and filtration steps. Lung samples were pre-enriched using biotinylated antibodies (Clone PC61, Biolegend) and anti-biotin ultrapure, anti-PE ultrapure or anti-APC microbeads (Miltenyi Biotec #130-105-637, #130-105-639, #130-090-855).

3.2.1.4. Colon

To isolate T cells from colon tissue, colons were isolated, cleared of feces and prepared according to manufacturer's instructions with a lamina propria dissociation kit (Miltenyi #130-097-410). Samples were either pre-enriched with CD4 (Clone RM4-5, Biolegend) or CD25 (Clone REA568, Miltenyi Biotec) antibody followed by bead-based magnetic purification or measured directly. More detailed protocols about T-cell isolation from murine tissues are published (Cossarizza et al., 2019).

3.2.1.5. Tumour

To isolate T cells from tumour tissue of HER2-transgenic tumour-bearing animals, mammary carcinoma depots were surgically excised, cut into small pieces and digested for 45 minutes at 37°C (base medium DMEM (Gibco #41965), 1 mg/ml

collagenase type II (Sigma-Aldrich #C6885), 20 µg/ml DNAse I (Roche #11284932001), 20 mg/ml bovine serum albumin (Sigma-Aldrich #A4503) on a MACSmix tube rotator, followed by incubation with 2 mM EDTA-PBS for 2 minutes and centrifugation and filtration steps. Cells were pre-enriched with anti-mouse CD45 microbeads (Miltenyi #130-052-301), followed by column-based magnetic enrichment and staining for FACS-based sorting.

3.2.1.6. Spleen and lymph nodes

To isolate T cells from murine spleen and lymph nodes, tissues were mechanically dissociated on a 70 µm filter unit and red blood cells lysed using ACK lysis buffer (Thermo Fisher # A1049201). Samples were either pre-enriched with CD4 (Clone RM4-5, Biolegend) or CD25 (Clone PC61, Biolegend) antibody followed by column-based magnetic purification or measured directly.

3.2.2. Establishment of human tissue isolation protocol

For the establishment of human tissue digestion, multiple different protocols were tested for the skin and for the fat.

For the skin, we tested the Miltenyi human skin digestion kit (Miltenyi 130-101-540), a protocol was adapted from a methods paper by He. Et al (Au - He et al., 2016), and we tested our already established mouse protocol.

For all protocols, skin was separate from fat and cut into small pieces

For skin dissociation with the Miltenyi kit, manufacturer's protocol was used.

Another method we tried was adapted from He. Et al. (Au - He *et al.*, 2016). Briefly, skin was cut into small pieces in GentleMACS in DMEM supplemented with penicillin/streptomycin, pyruvate, glutamax, and collagenase I-A. Digestion was

performed directly in a GentleMACS C tube and the program “37_C_Multi_H” for 90 minutes, followed by centrifugation and filtration steps. For the mouse protocol, see above.

For the fat, we tested the Miltenyi human fat digestion kit (reference), as well as our already established mouse protocol. For fat dissociation with the Miltenyi kit, manufacturer’s protocol was used. For the mouse protocol, see above.

3.2.3. T cell isolation from human tissue

3.2.3.1. Fat

To isolate T cells from human skin and subcutaneous fat tissue, skin and underlying fat were first mechanically separated, followed by tissue-individual preparation steps. fat was cut in into small pieces and digested for 90 minutes at 37°C (base medium DMEM (Gibco #41965), 1 mg/ml collagenase type II (Sigma-Aldrich #C6885), 20 μg/ml DNAse I (Roche #11284932001), 20 mg/ml bovine serum albumin (Sigma-Aldrich #A4503), 10 mM HEPES) on a MACSmix tube rotator, followed by filtration and centrifugation steps as well as red blood cell lysis using ACK lysis buffer (Gibco # A1049201).

3.2.3.2. Skin

To isolate T cells from human skin tissue, skin was cut into small pieces and digested (base medium DMEM (Gibco #41965), 4 mg/ml collagenase type IV (Sigma-Aldrich #C5138), 10 μg/ml DNAse I (Roche #11284932001), 2% fetal bovine serum, 10 mM HEPES). Digestion was performed directly in a GentleMACS C tube and the program “37_C_Multi_H” for 90 minutes, followed by centrifugation and filtration steps. Dead cell removal was performed with a dead cell removal kit.

3.2.3.3. Liver

To isolate T cells from human liver and liver tumour tissue, samples were cut into small pieces and digested (base medium DMEM (Gibco #41965), 1 mg/ml collagenase type IV (Sigma-Aldrich #C5138), 25 µg/ml DNAse I (Roche #11284932001), 10% fetal bovine serum, 10 mM HEPES). Digestion was performed directly in a GentleMACS C tube. Tissues were minced using the program "h.tumour" on the GentleMACS, and were subsequently attached to a MACSmix tube rotator and placed at 37°C for 60 minutes. Digestion was stopped and cells were washed with PBS $^{+}$ 2mM EDTA. Single cell solution was obtained by centrifugation and filtration steps as well as red blood cell lysis using ACK lysis buffer (Gibco # A1049201).

3.3. Peripheral blood mononuclear cell isolation and pre-enrichment of blood lymphocytes

To isolate T cells from human blood, leukocyte reduction chambers (provided by Transfusion Medicine, University Clinics Regensburg) were used. Leukocytes were first diluted 3 times with DPBS (Gibco #14190-094), and the resulting blood and PBS mixture was split in two fractions and underlayed with an equal amount of Pancoll (PAN biotech #P04-601000). Samples were centrifuged at 1,000xg for 20 minutes at RT, with acceleration set to 4 and brake to 0. The PBMC layer was isolated and washed twice by centrifugation steps. Cells were pre-enriched with either biotinylated anti-human CD4 (clone OKT4, Biolegend), biotinylated anti-human CD8 (clone HIT8a, Biolegend) or PE-labeled or biotinylated anti-human CD25 (Clone BC96, Biolegend; Clone 2A3, BD), followed by column-based magnetic separation with anti-biotin or

anti-PE ultrapure microbeads (Miltenyi Biotec #130-105-637 or #130-105-639) following manufacturer's protocol.

3.4. Flow cytometric sorting and acquisition

3.4.1. Staining

3.4.1.1. Surface staining

T cells were isolated and pre-enriched as described in the previous sections. Cells were stained in 1.5 mL Eppendorf tubes or 96-well plates in FACS buffer (2%FCS in PBS). Surface staining was performed at 4 °C for 20 minutes in 50-100μl staining volume. Antibodies were used, if not indicated otherwise, as recommended by the manufacturer. The following anti-human antibodies were used for surface staining: CD4 (OKT4/L200 SK3), CD3 (OKT3), TCR-β chain (IP26), CD8 (RPA-T8/HIT8a), CD19 (HIB19), CD25 (BC96/2A3), CD45RA (HI100), CD45RO (UCHL1), CD127 (A019D5), CD45 (HI30/2D1/REA747), CD14 (MϕP9), CCR8 (433H), CD39 (TU66), HLA-DR (L243), CD71 (CY1G4), CD195 (3A9), CD49d (9F10) CD279 (REA1165), CD206 (19.2). The following anti-mouse antibodies were used for surface staining: CD4 (RM4-5), CD3 (17A2), TCR-β chain (H57-597), CD8 (53-6.7), CD19 (6D6), CD45 (30-F11), Ccr8 (SA214G2), CD25 (PC61), Klrg1 (2F1/KLRG1), Pd1 (29F.1A12), St2 (DIH9).

3.4.1.2. Intracellular staining

Intracellular staining was performed with the Foxp3/Transcription Factor Buffer Set (eBioscience 00-5521-00) according to manufacturer's protocol with the following adaptations: intracellular staining steps were performed for 60 minutes at room

temperature. The following antibodies were used for intracellular staining of mouse and human proteins: FOXP3 (206D) at a dilution of 1:20, BCL-6 (7D1) at a dilution of 1:20, Helios (22F6) at a dilution of 1:20, IL-10 (JES5-16E3) at a dilution of 1:25, Amphiregulin (IPO0314111) at a dilution of 1:50 and BATF (D7C4) at a dilution of 1:400. For BATF staining, secondary intracellular staining was performed with AF647 (Cell Signaling Cat#4414) or AF488 (Cell Signaling Cat#4412) coupled anti-rabbit antibody at 1:1000. Dead cells were excluded with a fixable live/dead dye (Fixable ViabIL-ity Dye eFlour780, eBioscience Cat# 65-0865-14).

3.4.2. Acquisition and sorting

T cells were isolated, pre-enriched and stained as described previously. Afterwards, samples were filtered with a 40μM filter unit and acquired on a BD LSRII™, BD FACSymphony™ or BD FACSFusion™ flow cytometer. BD CS&T beads were used to validate machine functionality. Fluorescence spIL-lover compensation was performed with lymphocytes stained with CD4 (OKT4) in the respective colours. Flow cytometry data were analyzed using BD FlowJo™ (Version 10.6.2). Sorting was performed with a BD FACSAriaII™ or BD FACSFusion™ cell sorter with 85μm nozzle and 45 psi of pressure. Post-sort quality controls were performed as applicable. For scATAC-seq, target cells were sorted into 500 μl 10%FCS-PBS, followed by nuclei preparation. For scRNA-seq, target cells were sorted into 500 μl 10%FCS-PBS. For bulk RNA-seq, cells were sorted directly into 500 μL RLT$^+$ lysis buffer (Qiagen RNEasy Plus Micro Kit #74034). For bulk ATAC-seq, target cells were sorted into 500 μl 10%FCS-PBS. For cultivation experiments, cells were sorted directly into cell culture medium. All procedures were performed in DNA low-bind tubes (Eppendorf

#0030108051). For cytokine re-stimulation experiments, cells were incubated with either 1X cell stimulation cocktail with transport inhibitor or transport inhibitor only (both eBiosciences) in cell culture medium for 4 hours at 37°C. Afterwards, cells were surface-stained, followed by intracellular staining with the Foxp3 Fix/perm kit.

3.5. Single-cell ATAC sequencing of blood and tissue T cells

3.5.1. From mice

Murine T cells were isolated, pre-enriched, stained and sorted as described previously. From spleens of SPF animals, we sorted 100,000 $CD45^+Dead^-CD19^-CD3^+TCR\beta^+CD8^-CD4^+$ and two independent runs of 100,000 $CD45^+Dead^-CD19^-CD3^+TCR\beta^+CD8^-CD4^+CD25^+$ T cells. From colons of SPF animals, we sorted 79,000 $CD45^+Dead^-CD19^-CD3^+TCR\beta^+CD8^-CD4^+$ T cells. From skin of SPF animals, we sorted 73,000 $CD45^+Dead^-CD19^-CD3^+TCR\beta^+CD8^-CD4^+$ T cells. From lung of SPF animals, we sorted 100,000 $CD45^+Dead^-CD19^-CD3^+TCR\beta^+CD8^-CD4^+$ T cells. From VAT of SPF animals, we sorted 70,000 and 100,000 $CD45^+Dead^-CD19^-CD3^+TCR\beta^+CD8^-CD4^+$ T cells in two independent runs.

Sorted cells were pelleted by centrifugation (300xg, 5min 4°C). Supernatant was removed and cells were resuspended in 50 µl - 100 µl 0.04%BSA-PBS buffer. Cells were centrifuged (300xg, 5min 4°C), supernatant was completely removed and chilled nuclei lysis buffer (10mM TRIS-HCL pH7.4, 10mM NaCl, 3mM $MgCl_2$, 0.1% Tween-20, 0.1% NP-40, 0.01% Digitonin, 1% BSA in nuclease-free water) was added. Lysis was performed for 2 minutes at 4°C, followed by addition of 50 µl washing buffer (10mM TRIS-HCl ph7.4, 10mM NaCl, 3mM MgCL2, 1%BSA, 0.1% Tween-20 in nuclease-free water). After centrifugation (300xg, 5min 4°C), supernatant was

removed and 45 µl chilled diluted nuclei buffer (10X Genomics) was added. After centrifugation (300xg, 5min 4°C), supernatant was removed and 7µl chilled diluted nuclei buffer (10X Genomics) was added. Nuclei were counted (where applicable) and transposition mix was prepared with 5 µl of nuclei suspension based on the manufacturer's protocol. Transposition was performed for one hour at 37°C, followed by supplementation of master mix and beads (Single Cell ATAC Gel Beads V1.0 or V1.1 and reagents, 10X Genomics #1000175), loading on 10X Chromium Next GEM Chip H (10X Genomics #1000161) and processing on 10X Chromium Controller (10X Genomics #120212). GEM incubation was performed with 12 cycles of PCR. Library was prepared according to the protocol with cycle numbers dependent on input nuclei concentration. scATAC libraries were sequenced on an Illumina NextSeq™ 550 with NextSeq™ 500/550 High Output Kit v2.5 (75 cycles, Illumina #20024906).

3.5.2. From humans

Human T cells were isolated, pre-enriched, stained and sorted as described previously.

From peripheral blood of healthy donor 1, we sorted 100,000 $CD3^+Dead^-CD19^-TCR\beta^+CD8^-CD4^+$ and two independent runs of 100,000 $CD3^+Dead^-CD19^-TCR\beta^+CD8^-CD4^+CD25^+CD127^-$ T cells. From peripheral blood of healthy donor 2, we sorted 100,000 $CD3^+Dead^-CD19^-TCR\beta^+CD8^-CD4^+$ and two independent runs of 100,000 $CD3^+Dead^-CD19^-TCR\beta^+CD8^-CD4^+CD25^+CD127^-$ T cells. From peripheral blood of healthy donor 3, we sorted two independent runs of 100,000 $CD3^+Dead^-CD19^-TCR\beta^+CD8^-CD4^+CD25^+CD127^-CD45RA^-CD45RO^+CCR8^+$ T cells.

From fat tissue of donor 3, we sorted 100,000 $CD45^+Dead^-CD14^-CD19^-CD3^+TCR\beta^+CD8^-CD4^+$ and 15,000 $CD45^+Dead^-CD14^-CD19^-CD3^+TCR\beta^+CD8^-CD4^+CD25^+CD127^-$ T cells. From fat tissue of donor 4, we sorted 100,000 $CD45^+Dead^-CD14^-CD19^-CD3^+TCR\beta^+CD8^-CD4^+$ T cells. From skin tissue of donor 4, we sorted 70,000 $CD45^+Dead^-CD14^-CD19^-CD3^+TCR\beta^+CD8^-CD4^+$ T cells. From fat tissue of donor 5, we sorted 100,000 $CD45^+Dead^-CD14^-CD19^-CD3^+TCR\beta^+CD8^-CD4^+$ and 25,000 $CD45^+Dead^-CD14^-CD19^-CD3^+TCR\beta^+CD8^-CD4^+CD25^+CD127^-$ T cells. From skin tissue of donor 5, we sorted 90,000 $CD45^+Dead^-CD14^-CD19^-CD3^+TCR\beta^+CD8^-CD4^+$ T cells.

Sorted cells were pelleted by centrifugation (300xg, 5min 4°C) and processed as described above (Single Cell ATAC Gel Beads V1.1). scATAC libraries were sequenced on an Illumina NextSeq™ 550 with NextSeq™ 500/550 High Output Kit v2.5 (75 cycles).

3.6. Bioinformatic processing and analysis of single cell ATAC-seq data

All Bioinformatic analyses have been performed by Malte Simon, Charles Imbusch, and Agnes Holz-Wagenblatt, at the German cancer research center (DKFZ) in Heidelberg as follows:

3.6.1. Preprocessing of scATAC-seq data

All preprocessing steps were performed using “Cell Ranger ATAC version 1.1.0” (10X Genomics). Read fIL-tering, alignment, peak calling and count matrix generation from fastq files were done per sample using ‘cellranger-atac count’. Reference genome assemblies mm10 (refdata-cellranger-atac-mm10-1.1.0) and hg19 (refdata-cellranger-atac-hg19-1.1.0) provided by 10xGenomics were used for murine and

human samples, respectively. Gel bead and barcode multiplets were detected with a custom script provided by 10xGenomics (clean_barcode_multiplets_1.1.py), which leverages the frequency of adjacent fragment ends within and between barcodes. Subsequently, barcodes were annotated as cells if they met the following criteria: at least 1,000 (scATAC-data derived from HER2-transgenic tumour samples) or at least 5,000 read-pairs (scATAC-data derived from murine and human tissues) passed read filters defined by Cell Ranger ATAC version 1.1.0; less than 20% read-pairs with low mapping quality (< 0.2 fraction of unmapped + low mapping quality (mapq < 30) + chimeric read-pairs); less than 90% read pair duplicates; less than 10% read pairs from mitochondrial DNA; no annotation as gel bead or barcode multiplets. Then, $CD4^+$ T cell samples were aggregated using the command 'cellranger-atac aggr' on barcodes annotated as cells without normalization for library size (--normalize=none). To reduce the influence of cell count depth on the downstream analysis, fragments from barcodes with more than 50,000 unique fragments which passed filters were randomly subsampled to 50,000 fragments.

All further analysis steps were performed in R (Version 3.6.0). Fragments were loaded into R using the package Seurat (version 3.1.2 (Stuart et al., 2019). Transcription start site (TSS) scores were calculated for each barcode as previously described (Satpathy *et al.*, 2019). Briefly, the per-base coverage was obtained in a 1,000 bp flanking region around all transcription start sites from the R packages 'TxDb.Mmusculus.UCSC.mm10.knownGene' (version 3.4.7, murine samples) or 'TxDb.Hsapiens.UCSC.hg19.knownGene' (version 3.2.2, human samples). These values were divided by the mean coverage at the 100 bp end regions of the flanking regions for normalization. Finally, the normalized coverage values were smoothed

within a window of 50 bp and the highest value was maintained as TSS score. Barcodes with a TSS score smaller than 8 were excluded from further analysis. Peaks were filtered out if they met any of the following criteria: less than 10 fragments across all cells; overlap with chromosomes chrY, chrM or unplaced sequences; overlap with blacklisted regions provided by the ENCODE consortium using the blacklist assembly provided in R package Signac (version 0.1.3, blacklist_mm10 for murine cells and blacklist_hg19 for human cells).

For normalization and dimensionality reduction, the R package Signac (version 0.1.3, https://github.com/timoast/signac) was used. The peak-barcode matrix was then binarized and normalized using the implementation of the TF-IDF transformation described in ((Stuart *et al.*, 2019), RunTFIDF(method=1)). Subsequently, singular value decomposition was run (RunSVD) on the upper quartile of accessible peaks (FindTopFeatures(min.cutoff = 'q75')). Batch correction for donors in the human and pooled samples in the murine $CD4^+$ T cell data was done with Harmony (Korsunsky et al., 2019). Harmony was run on the previously calculated SVD embeddings with the command 'HarmonyMatrix' with default parameters for lambda and theta. Sigma was set to 1 for human data and to 0.3 for murine data, respectively. The first 20 components from the SVD or Harmony reduction were used for secondary dimensionality reduction with UMAP (RunUMAP(metric = 'euclidean')).

3.6.2. Gene activity scores of scATAC-seq data

To calculate gene activity scores we first obtained gene body coordinates by using the command genes (TxDb.Mmusculus.UCSC.mm10.knownGene) for murine samples and genes (TxDb.Hsapiens.UCSC.hg19.knownGene) for human samples

from the package GenomicFeatures in R. The coordinates were filtered for standard chromosomes (keepStandardChromosomes(pruning.mode='coarse')) and extended by 2,000 bp upstream of the transcription start sites to include promoter regions (Extend(upstream=2000)). Then, the command 'FeatureMatrix' from the Signac package was used with the 'features' parameter set to the extended gene coordinates to sum up the number of unique reads within gene regions for each cell. Eventually, these gene activity scores were log-normalized and multiplied by the median read counts per cell (nCount_Reads) with the command NormalizeData(normalization.method='LogNormalize',scale.factor=median(nCount_Reads). Normalized gene activities were capped at the 95th quantIL-e for plotting.
For the tumour T cell dataset from (Satpathy *et al.*, 2019), the provided Cicero gene activity scores (Pliner et al., 2018) were used to visualize gene activities

3.6.3. Signature scores of scATAC-seq data

To calculate an accessibility score for a set of regions for each cell, we first filtered the dataset for peaks overlapping with any of the signature regions (subsequently referred to as signature peaks). For each cell in the dataset of n cells, the number of peaks (n_peaks) was counted. The relative frequency for each peak in the dataset was calculated by dividing the number of cells with a signal for this peak through the total peak count of the binarized peak-cell matrix. For a peak x in the dataset:

$$freq(peak_x) = \sum_{i=1}^{n} peak_x \; / \; \sum_{i=1}^{n} n\_peaks$$

We then simulated cells with (1000, 2000, 3000, .., max(n_peaks)) peaks for our datasets. Due to the higher number of peaks, we used (1000, 6000, 11000, ..,

max(n_peaks)) for the human tumour T cells from (Satpathy *et al.*, 2019). For each of these cells, we sampled the respective number of peaks from the dataset with probabilities given by the previously calculated frequencies for each peak. We then counted the number of signature peaks among these samples. For each simulated cell, sampling was repeated 48 times and the average sum of signature peaks + 1 was assigned as final value. These values represent the number of signature peaks overlapping by chance with random peaks for cells with increasing count depth. Finally, we calculated the enrichment of signature peaks for each cell by dividing the sum of observed signature peaks + 1 for the cell by the simulated cell with the closest number of observed peaks.

3.6.4. Cell clustering of scATAC-seq data

We identified cell clusters using graph-based clustering implemented in the Seurat package. The shared nearest neighbor graph was constructed based on the Harmony or SVD embeddings as indicated in the table below (FindNeighbours(dims=1:20)). Subsequently, clusters were determined using the function 'FindClusters' with the indicated resolutions: Mouse SPF tissue and spleen $CD4^+$ with 1.7 (Harmony); Mouse gnotobiotic tissue and spleen $CD4^+$ with 1.7 (SVD); Mouse tumour $CD4^+$ with 0.5 (SVD); Human tissue and blood $CD4^+$ with 1.0 (Harmony).

3.6.5. Identification of differential chromatin accessibility between scATAC clusters

To identify differentially accessible regions between cell clusters, we buIL-t a logistic regression model for each region and used a likelihood ratio test to compare it to a null

model with the number of peaks per cell as latent variable. Regions were filtered for Bonferroni-corrected p-value below 0.05 and average log-fold change above 0.25 (FindMarkers(test.use = 'LR', latent.vars='n_peaks', min.pct=0.1, logfc.threshold=0.25) from Seurat).

3.6.6. Usage of bigWig tracks

For the generation of per-cluster BigWig tracks, we first identified all barcodes within the clusters. We then used Sinto (https://github.com/timoast/sinto) to extract reads associated with these barcodes from the sample bam files and combined them into one bam file per cluster (samtools merge). Eventually 'bamCoverage' was called to generate BigWig coverage tracks from the bam file. BigWig and broadPeak files from BATF-ChIP-seq data of human B cells (replicate 2) were downloaded from GSM803538 for comparisons with the chromatin accessibility BigWig data.

3.6.7. Homer transcription factor analysis of scATAC-seq data

We used Homer (Heinz et al., 2010) for the identification of known transcription factor motifs and de novo motif discovery in sets of cluster-specific peaks (findMotifsGenome.pl peaks.bed hg19 -mask -size given -len 8,10,12,14). We used the motif position weight matrices provided on the Homer website as reference for known transcription factors (http://homer.ucsd.edu/homer/custom.motifs). To generate BATF transcription factor footprints for human $CD4^+$ T cells from different clusters, we first converted the per-cluster bam files into tag directories (makeTagDirectory). We then centered the peaks from the human $CD4^+$ T cell dataset around the BATF (Th17-BATF-ChIP-Seq(GSE39756)/Homer) transcription factor

binding motif (annotatePeaks.pl -center -mask -size -1000,1000). Finally, we quantified the tags within 2,000 bp around the BATF motif using the centered peaks (annotatePeaks.pl -fragLength 1 -size -1000,1000 -hist 1).

3.6.8. Cross-species regions liftover of murine and human scATAC-seq data

We used the liftOver tool from UCSC (Kuhn et al., 2013) to transfer mouse signature regions (original peaks) to the human genome (liftover regions). First, liftOver was called with the mm10 to hg19 chain file on the original peaks (http://hgdownload.cse.ucsc.edu/goldenpath/mm10/liftOver/mm10ToHg19.over.chain.gz). Subsequently the liftover regions were lifted back to the mouse genome with the hg19 to mm10 chain file (http://hgdownload.cse.ucsc.edu/goldenpath/hg19/liftOver/hg19ToMm10.over.chain.gz). We used `minMatch=0.2` to require a substantial sequence conservation between the corresponding murine and human DNA sequences. We filtered out all liftover regions with an overlap smaller than 90% or a width difference greater than 40% with the original peaks after transfer back to the mm10 genome. To include information on the localization with respect to genes, we obtained gene regions and extended these by 2,000 bp upstream to include promoter regions (Signac::Extend(upstream=2000)). We then annotated both the original peaks and liftover regions with the gene symbols of overlapping genes as well as the closest gene. We used biomart (Durinck et al., 2009) to translate MGI symbols to HGNC symbols and filtered out all liftover regions without any matching gene symbol to the original peak.

To derive a repair Treg signature that is conserved between mouse and human, we searched peaks from the human tisTreg signature which overlap by more than 40%

with the liftover regions or vice versa. This set of peaks was further filtered for peaks within gene bodies or promoter regions and same direction of chromatin accessibility difference in mouse and human.

3.7. Bulk RNA sequencing of human tissue Tregs

All Bioinformatic analyses have been performed by Malte Simon, Charles Imbusch, and Agnes Holz-Wagenblatt, at the German cancer research center (DKFZ) in Heidelberg as follows:

Human T cells were isolated, pre-enriched, stained and sorted as described previously. Sort gates are shown in. From human fat samples of five individual donors, we sorted 2,500 to 10,000 Treg cells ($CD45^+CD3^+TCRb^+CD4^+CD8^-CD25^+CD127^-$). From human skin samples of five individual donors, we sorted 3,500 to 10,000 Treg cells ($CD45^+CD3^+TCRb^+CD4^+CD8^-CD25^+CD127^-$). From human peripheral blood samples of five individual donors, we sorted 10,000 naive Treg cells ($CD45^+CD3^+TCRb^+CD4^+CD8^-CD25^+CD127^-CD45RA^+CD45RO^-$), 10,000 memory Treg cells ($CD45^+CD3^+TCRb^+CD4^+CD8^-CD25^+CD127^-CD45RA^-CD45RO^+$), and 10,000 CCR8 Treg cells ($CD45^+CD3^+TCRb^+CD4^+CD8^-CD25^+CD127^-CD45RA^-CD45RO^+$ $CCR8^+$). Total RNA was isolated using a DNA/RNA micro kit (Qiagen Cat#80284) and RNA was eluted in 14 μL RNAse-free water. RNA quality was assessed using a Tapestation 4200 and High-Sensitivity RNA Screentape (Agilent Cat# 5067-5579). 8 μl of the RNA was used for generating RNA-seq libraries using the SMART-seq Stranded Kit (Takara Cat# 634444). Indexed libraries were pooled in

an equimolar ratio and sequenced on an Illumina NextSeq 550 machine with NextSeq 500/550 High Output Kit v2.5 (75 cycles).

To isolate and compare CCR8$^+$ Treg cells from healthy and tumour patients, we sorted 800 to 5,500 CCR8$^+$ Treg cells (CD45$^+$Dead$^-$CD206$^-$CD3$^+$CD4$^+$CD8$^-$CD25$^+$CD127$^-$CD45RA$^-$CCR8$^+$) from human fat, 850 to 2,500 CCR8$^+$ Treg from human skin, 1,000 to 10,000 CCR8$^+$ Treg or Treg from human NAT liver tissue, and 2,000 to 10,000 CCR8$^+$ Treg or Treg from human liver tumour tissue. From blood of skin and fat donors, we sorted 750 to 2,500 CCR8$^+$ Treg cells, 2,000 to 2,500 CCR8$^-$ Treg cells and 2,000 to 2,500 CD45RA$^+$ Treg cells. From blood of tumour patients, we sorted 2,000 CCR8$^+$ Treg cells, 2,000 CCR8$^-$ Treg cells and 2,000 CD45RA$^+$ Treg cells. RNA was isolated, reversely transcribed, indexed and sequenced as described above.

3.8. Bioinformatic processing and analysis of bulk RNA-seq data

All Bioinformatic analyses have been performed by Malte Simon, Charles Imbusch, and Agnes Holz-Wagenblatt, at the German cancer research center (DKFZ) in Heidelberg as follows:

For all samples, low quality bases were removed with Fastq_quality_filter from the FASTX Toolkit 0.0.13 (http://hannonlab.cshl.edu/fastx_toolkit/index.html) with 90% of the reads needing a quality phred score > 20. Homertools 4.7 (Heinz *et al.*, 2010) were used for PolyA-tailtrimming and reads with a length < 17 were removed. PicardTools 1.78 (https://broadinstitute.github.io/picard/) were used to compute the quality metrics with CollectRNASeqMetrics. With STAR 2.3 (Dobin et al., 2013), the filtered reads were mapped against human genome 38 using default parameters. Count data and

RPKM tables were generated by mapping filtered reads against union transcripts using a custom pipeline. Mapping was carried out with bowtie2 version 2.2.4 (Langmead and Salzberg, 2012) against union human genes: every gene is represented by a union of all its transcripts (exons). The count values (RPKM and raw counts) were calculated by running CoverageBed from Bedtools v2.26.0 (Quinlan and Hall, 2010) of the mapped reads together with the human annotation file (Ensembl 90) in gtf format and parsing the output with custom perl scripts. The input tables containing the replicates for groups to compare were created by a custom perl script. For the pairwise comparisons DESeq2 (Love et al., 2014), DESeqDataSetFromMatrix was applied, followed by estimateSizeFactors, estimateDispersions, and nbinomWald testing. The MA plots were generated using the plotMA function of DESeq2 using all data. The PCA plots were generated by DESeq2's plotPCA after transforming the counts using varianceStabilizingTransformation and selecting the genes from the DESeq2 result according to the adjusted p-value (<0.05, <0.01, <0.001). Dendrogram was generated using R. First, tables were integrated (read.csv) followed by conversion (as.matrix.data.frame). Heatmap was generated using library (pheatmap) and pheatmap function (cutree_rows=2, cellwidth =50, cellheight =1, scale="row", colour=greenred(500)). As source data, all genes identified in bulk RNA-seq were first sorted in a comparison of skin – or fat Treg cells vs naive Treg cells. All values unequal to zero in either comparison were allowed. Next, correlated genes were identified by dividing skin Treg/fat Treg (0.5<x>2.0) and top 1000 genes with increased expression in fat Treg vs naive Treg and bottom 1000 genes in the comparison fat Treg vs naive Treg were selected and displayed as dendrogram.

3.9. Single-cell RNA/TCR sequencing of human tissue and blood T cells

All Bioinformatic analyses have been performed by Malte Simon, Charles Imbusch, and Agnes Holz-Wagenblatt, at the German cancer research center (DKFZ) in Heidelberg as follows:

Human T cells were isolated, pre-enriched, stained and sorted as described previously. Sort gates are shown in.

From fat tissue of donor 6, we sorted 40,000 $CD45^+Dead^-CD14^-CD19^-CD3^+TCR\beta^+CD8^-CD4^+$ T cells. From skin tissue of donor 6, we sorted 40,000 $CD45^+Dead^-CD14^-CD19^-CD3^+TCR\beta^+CD8^-CD4^+$ T cells. From peripheral blood of donor 6, we sorted 50,000 $CD45^+Dead^-CD14^-CD19^-CD3^+TCR\beta^+CD8^-CD4^+$ T cells, 50,000 $CD45^+Dead^-CD14^-CD19^-CD3^+TCR\beta^+CD8^-CD4^+CD25^+CD127^-$ Treg cells, 50,000 $CD45^+Dead^-CD14^-CD19^-CD3^+TCR\beta^+CD8^-CD4^+CD25^+CD127^-CD45RA^-CD45RO^+$ memory Treg cells and 27,000 $CD45^+Dead^-CD14^-CD19^-CD3^+TCR\beta^+CD8^-CD4^+CD25^+CD127^-CD45RA^-CD45RO^+CCR8^+$ Treg cells.

From fat tissue of donor 7, we sorted 40,000 $CD45^+Dead^-CD14^-CD19^-CD3^+TCR\beta^+CD8^-CD4^+$ T cells. From skin tissue of donor 7, we sorted 40,000 $CD45^+Dead^-CD14^-CD19^-CD3^+TCR\beta^+CD8^-CD4^+$ T cells. From peripheral blood of tissue donor 7, we sorted 50,000 $CD45^+Dead^-CD14^-CD19^-CD3^+TCR\beta^+CD8^-CD4^+$ T cells, 50,000 $CD45^+Dead^-CD14^-CD19^-CD3^+TCR\beta^+CD8^-CD4^+CD25^+CD127^-$ Treg cells and 50,000 $CD45^+Dead^-CD14^-CD19^-CD3^+TCR\beta^+CD8^-CD4^+CD25^+CD127^-CD45RA^-CD45RO^+$ memory Treg cells.

After sorting, cells were centrifuged (1000xg, 5min, 4°C) and reconstituted in 38 μl 10%FCS-PBS buffer. Master Mix (Chromium Next GEM Single Cell 5' Gel bead V1.1,

10X Genomics #1000165) was added to the cells and samples were loaded on 10X Chromium Next GEM Chip G (10X Genomics #1000120). GEM incubation was performed for 45 minutes at 53°C according to manufacturer's protocol. Single-cell libraries were prepared as by manufacturer's protocol (Chromium Next GEM Single Cell 5′ Library and Gel Bead Kit v1.1). scRNA libraries were sequenced on an Illumina NextSeq™ 550 with NextSeq™ 500/550 High Output Kit v2.5 (75 cycles). scTCR libraries were sequenced on an Illumina NextSeq™ 550 with NextSeq™ 500/550 Mid Output Kit v2.5 (300 cycles, Illumina Cat# 20024905).

3.10. Bioinformatic analysis of single cell RNA/TCR sequencing

All Bioinformatic analyses have been performed by Malte Simon, Charles Imbusch, and Agnes Holz-Wagenblatt, at the German cancer research center (DKFZ) in Heidelberg as follows:

3.10.1. Single Cell RNA sequencing

Fastq files were processed using Cell Ranger (version 3.1.0) based on 10xGenomics provided hg19 reference genome (version 3.0.0). Cell Ranger was run per sample (using cellranger count). For downstream analysis, the R package Seurat (Butler et al., 2018) (version 3.4.1) together with R (version 3.6.0) was used. Cells with fewer than 500 were discarded as well as cells exceeding a 5% threshold of mitochondrial transcripts. The data was log normalized (using NormalizeData) and scaled (using ScaleData). Highly variable genes were identified (using FindVariableFeatures) with default parameter settings and principle components

calculated (using RunPCA(npcs = 40)). UMAP dimensionality reduction was performed (using RunUMAP).

3.10.2. Single cell TCR sequencing

Fastq files were processed using Cell Ranger (version 3.1.0) based on 10xGenomics provided VDJ reference (version 3.1.0). Clones from different samples were matched by TRA and TRB amino acid sequences. Clonal abundance pie charts were generated using ggplot2 (version 2.3.3) and R (version 3.6.0). Different TCR numbers between samples and respective pie charts based on removal of duplets or certain clusters.

3.11. LEGENDScreen™ with human Peripheral Blood Mononuclear Cells

Human peripheral blood T cells from three donors isolated and pre-enriched using CD25-biotinylated antibody and anti-biotin ultrapure microbeads. Samples were surface stained with antibodies against CCR8, CD45, CD3, CD4, CD8, CD19, Dead cells, CD45RO, and CD127 for 20 minutes at 4°C. CD25 was detected by Streptavidin staining. Pre-enriched and pre-stained cells were distributed among LEGENDScreen™ plates and stained, washed and fixed according to manufacturer's protocol. Samples were acquired on a BD FACSSymphony™ using a high-throughput sampling unit (BD HTS™) with following settings: Sample flow rate 3.0 µL/sec, sample volume 100 µL, mixing volume 50 µL/sec, mixing speed 200 µL/sec, 5 number of mixes per well, wash volume 400 µL and BLR period of 5 seconds, throughput mode standard. Analysis was performed using BD FlowJo™. Clustermap was generated using R. First, tables were integrated (read.csv) followed by conversion

(as.matrix.data.frame). Clustermap was generated using library (pheatmap) and pheatmap function (cutree_rows=9, cellwidth =10, cellheight =8, scale="row").

3.12. Induction of tissue-like Treg *in-vitro* from naïve Tregs

3.12.1. In mice

Spleens and lymphnodes were isolated and processed like described above, in a sterile environment. CD25 pre-enrichment was performed with anti-mouse CD25 PE-conjugated, or biotin conjugated antibody and PE-labeled or biotinylated ultrapure magnetic beads and magnetic columns. Staining and sorting was performed like described above. Dead-TCRb^{+}CD4^{+}CD8-CD19-MHCII-CD25^{+}CD62L^{+} cells were sorted into T cell culture medium (base medium DMEM, 10% FCS, 0,5% MEM vitamin solution, 1% Sodium pyruvate, 1% non-essential amino acids, 1% pen/strep, 1% HEPES, 1% glutamine and 0,1% β-Mercapto ethanol) and stimulated for 3 days with anti-mouse CD3/CD28 microbeads at a 4:1 ratio and 2000 units IL-2 for 3 days. On day 3 each well was supplemented with an equal amount of T cell culture medium with 2000 units of IL-2. On day 4, one well of each condition was harvested and checked for BATF and FOXP3 expression through intracellular staining like described above.

3.13. Induction of tissue-like Tregs *in-vitro* followed by bulk ATAC sequencing and RNA sequencing in mice and humans

3.13.1. Tissue-like induction in murine naïve Tregs *in-vitro*

Spleens and lymphnodes were isolated and processed like described above. CD25 pre-enrichment was performed with anti-mouse CD25 biotin-conjugated antibody and biotinylated ultrapure magnetic beads and magnetic columns. Staining and sorting

was performed like described above. Dead-TCRb^{+}CD4^{+}CD8-CD19-MHCII-CD25^{+}CD62L^{+} cells were sorted into T cell culture medium (base medium DMEM, 10% FCS, 0,5% MEM vitamin solution, 1% Sodium pyruvate, 1% non-essential amino acids, 1% pen/strep, 1% HEPES, 1% glutamine and 0,1% β-Mercapto ethanol) and stimulated for 3 days with anti-mouse CD3/CD28 microbeads at a 4:1 ratio and 2000 units IL-2 for 3 days. On day 3 each well was supplemented with an equal amount of culture medium with 2000units of IL-2. On day 4, one well of each condition was harvested and checked for BATF induction and FOXP3 expression through flow cytometric analysis like described above. On day 5, cells were harvested, and live cells were sorted into PBS supplemented with 10% FCS using FACS sorting like described above.

3.13.2. Tfh induction in human naïve Tregs *in-vitro*

Human peripheral blood was separated by Ficoll gradient centrifugation and pre-enriched with anti-human CD25 biotinylated antibody and anti-biotin beads or anti-human CD25 PE-conjugated antibody and anti-PE ultrapure beads. Cells were purified using magnetic columns followed by fluorescence-activated cell sorting of CD45^{+}Dead^{-}CD19^{-}CD3^{+}TCRβ^{+}CD8^{-}CD4^{+}CD25^{+}CD127^{-}CD45RA^{+} antigen-naive Treg cells. 100,000 cells per well were activated with anti-human TransAct and either treated with IL-2 only (500 units/mL, “IL-2 Treg”) or with IL-2 (500 units/mL), IL-12, IL-21, IL-23 and TGF-b (50 ng/ml, “Tfh-like Treg”) in TexMACS medium (Miltenyi130-097-196) for 3 days, followed by re-supplementation of cytokines and additional cultivation for 3 days. After five days, a QC staining was performed: samples meeting quality requirements (>85% FOXP3, induction of BCL-6 and BATF) were FACS-sorted

on day 6 ($CD45^+Dead^-CD19^-CD3^+TCR\beta^+CD8^-CD4^+$) and 100,000 cells were subjected to bulk ATAC-seq and 50,000 cells were subjected to bulk RNA-seq.

3.13.3. ATAC sequencing

Chromatin accessibility mapping was performed using the ATAC-seq method as previously described (Buenrostro *et al.*, 2013; Corces et al., 2017), with minor adaptations. Briefly, in each experiment 30,000 – 100,000 sorted cells were pelleted by centrifuging for 10 min at 4 °C at 500 x g. After centrifugation, the pellet was carefully lysed in 50 µl resuspension buffer supplemented with NP-40 (Sigma), Tween-20 and Digitonin (10 mM Tris-HCl pH 7.4, 10 mM NaCl, 3 mM MgCl2, 0.1 % NP-40, 0.1 % Tween-20, 0.01 % Digitonin) and incubated for 3 minutes on ice. Then, 1 ml of ice-cold resuspension buffer supplemented with Tween-20 was added, and the sample was centrifuged at 4 °C at 500 x g for 10 minutes. The supernatant was discarded, and the cell pellet was carefully resuspended in the transposition reaction (25 µl 2 x TD buffer (20 mM Tris-HCL pH 7.6, 10 mM $MgCl_2$ 20% Dimethyl Formamide in Ambion water), 2.5 µl TDE1 (Illumina), 16.5 µl PBS, 5 µl nuclease-free water, 0.5 µl 1% Digitonin (Promega), 0.5 µl 10% Tween-20 (Sigma)) for 30 min at 37 °C on a shaker at 1000 rpm. Following DNA purification with the Clean and Concentrator-5 kit (Zymo) eluting in 23 µl, 2 µl of the eluted DNA was used in a quantitative 10 µL PCR reaction (1.25 µM forward and reverse custom Nextera primers (Corces *et al.*, 2017), 1x SYBR green final concentration) to estimate the optimum number of amplification cycles with the following program; 72°C 5 min, 98°C 30 s; 25 cycles: 98°C 10 s, 63°C 30 s, 72°C 1 min. the final amplification of the library was carried out using the same PCR program and the number of cycles according to the Cq value of the qPCR. Library

amplification using custom Nextera primers was followed by SPRI size selection with AmpureXP beads to exclude fragments larger than 1,200 bp and smaller than 150 bp (e.g., primer dimers). DNA concentration was measured with a Qubit fluorometer (Life Technologies). The libraries were sequenced using the Illumina NextSeq 550 system.

3.13.4. RNA sequencing

RNA was isolated using the RNEasy Plus Micro Kit (Qiagen #74034), and samples meeting quality criteria (RIN>9.5) were used to generate libraries with the Truseq total RNA kit (100 ng total RNA as input, IL-umina Cat# 20020596). Indexed samples were pooled in an equimolar ratio and sequenced on an Illumina NextSeq™ 550 with NextSeq™ 500/550 High Output Kit v2.5 (75 cycles).

3.14. Bioinformatic processing and analysis Bulk-ATAC sequencing data

All Bioinformatic analyses have been performed by Malte Simon, Charles Imbusch, and Agnes Holz-Wagenblatt, at the German cancer research center (DKFZ) in Heidelberg as follows

3.14.1. Preprocessing and analysis of ATAC-seq data

ATAC-seq reads were trimmed using Skewer (Jiang et al., 2014) and aligned to the hg19 assembly of the human genome using Bowtie2 (Langmead and Salzberg, 2012) with the '-very-sensitive' parameter and a maximum fragment length of 2,000 bp. Duplicate and unpaired reads were removed using the sambamba (Tarasov et al., 2015) 'markdup' command, and reads with mapping quality >30 and alignment to the nuclear genome were kept. All downstream analyses were performed on these filtered

reads. For visualization purposes bigwig files were created using the bamCoverage function from deeptools with the “RPGC” normalization option.

3.14.2. Analysis of chromatin accessibility data

Peak calling for each sample was performed using MACS2 with the parameters ‘--nomodel --extsize 147 -g 2700000000’ and a qvalue cutoff of 5.00e-02. Peaks overlapping blacklisted features as defined by the ENCODE project were discarded. For the analysis of sample sets we always created a consensus region set by merging the called peaks from all involved samples, and we quantified the accessibility of each region in each sample by counting the number of reads from the filtered BAM file that overlapped each region.

To normalize the chromatin accessibility signal across samples, we performed quantIL-e normalization followed by GC content normalization by regression using DESeq2’s “varianceStabilizingTransformation” approach (Love *et al.*, 2014). DESeq2 was used to identify differential chromatin accessibility between samples. Significant regions were defined as having an FDR-corrected p-value below 0.05, an absolute log2 fold change above xxx, and a mean accessibility equal or greater than 10.

Motif enrichment analysis was done using HOMER (Heinz *et al.*, 2010) with the function findMotifsGenome using “-size 500 -len 8,10,12 -h” parameters. Statistical significances of motif enrichment using HOMER were calculated using hypergeometric testing indicated by the “-h” parameter. Histograms of reads around transcription factor binding motifs were generated using HOMER by centering the peaks of interest on the investigated motifs using the annotatePeaks function, followed by counting reads from individual experiments at single base pair resolution in a radius

of 1,000 bp (or 150 bp) around the peak centers using the annotatePeaks function with the parameters “-hist -fragLength 1”. Tn5 background was calculated by processing publicly avaIL-able sequencing data of tagmented “naked” DNA fragments (ERR2213810_1, ERR2213810_2, ERR2213806_1, and ERR2213806_2) (Henriksson et al., 2019) similar to all other ATAC-seq data.

3.15. *In-vitro* wound healing assay

3.15.1. Generation of supernatant

Human peripheral blood was separated by Ficoll gradient centrifugation and pre-enriched with anti-human CD25 biotinylated antibody and anti-biotin ultrapure beads or anti-human CD25 PE-conjugated antibody and anti-PE ultrapure beads. Cells were purified using magnetic columns followed by fluorescence-activated cell sorting of $CD45^{+}Dead^{-}CD19^{-}CD3^{+}TCR\beta^{+}CD8^{-}CD4^{+}CD25^{+}CD127^{-}CD45RA^{+}$ antigen-naive Treg cells. 100,000 cells per well were activated with anti-human TransAct and either treated with IL-2 only (500 units/mL, “IL-2 Treg”) or with IL-2 (500 units/mL), IL-12, IL-21, IL-23 and TGF-b (50 ng/ml, “Tfh-like Treg”) in TexMACS medium (Miltenyi 130-097-196) for 3 days, followed by re-supplementation of cytokines and additional cultivation for 2-3 days. After five to six days, cells were washed vigorously to remove all remaining cytokines. Cells were resuspended in fresh medium with IL-2 and TransAct and allowed to produce metabolites for 20 hours. After 20 hours, supernatant was collected and cells were used for flow cytometry-based quality control, where FOXP3, HELIOS, BATF and BCL-6 expression were evaluated.

3.15.2. *In-vitro* wound healing assay with HaCaT cells

The human keratinocyte cell line HaCaT (RRID: CVCL_0038) was grown in TexMACS medium supplemented with 1% Penicillin/streptomycin. 25.000 Cells/ well were seeded in an ImageLock plate (Essen Bioscience Cat# 4379) and were allowed to settle and expand for 18h at 37°C. Wounds were made with a WoundMaker™ (Essen Bioscience). Supernatant was diluted at various ratios ($1^{+}1$, $1^{+}3$, $1^{+}7$, $1^{+}15$) and added to HACAT cells, which were then placed at 37 degrees. Culture plate was placed in the IncuCyte Zoom (Essen Bioscience) and scans of the wells were scheduled for every 60 minutes for 48h. Relative wound density was calculated win IncuCyte® Scratch Wound Cell Migration and Invasion System software (Essen Bioscience). Relative wound density values were analysed, and statistical significance was established with GraphPad Prism (GraphPad software).

3.15.3. *In-vitro* wound healing assay with Open-sourced Reconstructed Epidermis

These experiments were performed by Florian Groeber-Becker and Verena Schneider at the Frauenhofer ISC Würzburg, as follows;

The reconstructed human epidermis wound healing assay was performed using models generated with primary human epidermal keratinocytes (hEK) isolated from juvenile foreskin samples, according to the open source method described in literature (Groeber et al., 2016). In short, hEKs were seeded on a polycarbonate membrane and cultivated using supplemented EpIL-ife medium. At day 12 of airlift culture, models were wounded using a 2 mm biopsy punch. After wounding, models were supplemented with fresh cell culture supernatant of either IL-2 Treg cells or Tfh-like

Treg cells at a 1+5 dilution on day 0. On day 2 after wounding, IL-2 or Tfh-like Treg supernatant was supplemented again. On day 4 after wounding, cell culture supernatant was washed off and growth medium was used. Impedance spectroscopy measurement was performed before wounding, 3 h after wounding, and 2 days, 4 days and 7 days after wounding. Seven days after wounding, models were fixed in Roti Histofix (Carl Roth GmbH, Germany) and embedded in paraffin. Cross sections of 5 *µ*m were cut and hematoxylin & eosin staining (H&E; Morphisto, Germany) was performed, followed by computer-assisted histological studies. In this context, slides were scanned at 40-fold magnification with the high-resolution microscope system TissueFAXSiPLUS (TissueGnostics, Vienna, Austria) operated by TissueFAXS software (TissueGnostics). This technique allows both image processing and automated stitching of single images to one data set automatically (Schmid et al., 2015). The StrataQuest digital image analysis software was used to quantify the progress of *Stratum corneum* reconstruction, known to be associated with wound healing in the applied assay (Kiesewetter et al., 2019). Based on the tissue detection algorithm, the area of the *Stratum corneum* including the adjoining transition zone to the *Stratum granulosum* was determined.

3.16. Calculation of signatures and correlations

All Bioinformatic analyses have been performed by Malte Simon, Charles Imbusch, and Agnes Holz-Wagenblatt, at the German cancer research center (DKFZ) in Heidelberg as follows.

3.16.1. Tissue Treg and tumour Treg signatures

DEG between skin and fat $CD4^+CD25^+CD127^-CD45RA^-CCR8^+$ Treg cells and blood $CD4^+CD25^+CD127^-CD45RA^+$ naive Treg cells were selected (padj<0.05, log2 fc >2 or <-2, 1,393 genes). For those genes, expression data for all groups were extracted and shown in a heatmap. DEG between HCC $CD4^+CD25^+CD127^-CD45RA^-CCR8^+$ Treg cells and blood $CD4^+CD25^+CD127^-CD45RA^+$ naive Treg cells were selected (padj<0.05, log2 fc >2 or <-2, 1,408 genes). For those genes, expression data for all groups were extracted and shown in a heatmap. All signatures are listed in.

3.16.2. Correlation between RNA-seq data of Tfh-like Treg and skin $CCR8^+$ Treg

DEG between skin $CD4^+CD25^+CD127^-CD45RA^-CCR8^+$ Treg cells and blood $CD4^+CD25^+CD127^-CD45RA^+$ naive Treg cells were selected (padj<0.05, 4,136 genes). DEG between *in-vitro* IL-2 Treg cells and Tfh-like Treg cells were selected (padj<0.05, log2 fc >1 or <-1, 2,222 genes). In the comparison of DEG between IL-2 Treg and Tfh-like Treg cells with skin CCR8 specific DEG, 499 genes were identified. Of those 499 genes, 228 showed increased expression in Tfh-like Treg cells and skin $CCR8^+$ Treg cells.

3.17. Statistical analysis

Data were analysed using Graphpad Prism or by algorithm, which were performed in R. Algorithms were used or created by Malte Simon and Charles Imbusch of the German cancer Research Center (DKFZ) to analyse statistical significance in the context of bioinformatic analyses. DetaIL-s about statistical tests, significance, and population size can be found in the Figure legends.

4. Results

4.1. Establishing protocols for the digestion of human fat and skin tissue

To isolate T-cells out of human non-lymphoid tissue, isolation and digestion protocols had to be established. Two different protocols were compared for fat digestion and skin digestion, respectively (Figure 4). For fat digestion, one commercially avaIL-able digestion protocol (Miltenyi # 130-101-540) was tested as well as the in-house protocol for murine fat digestion. For skin digestion, an already published protocol for human skin digestion (Au - He *et al.*, 2016) was tested as well as the already established in house murine skin digestion protocol. To compare which protocol would yield us the most Tregs per tissue, single cells were stained with fluorescent antibodies and acquired on a flow cytometer. Dead cells, as well as cells positive for CD8, CD14, CD19 and CD206 were excluded. Tregs were gated as being $CD25^{+}CD127^{-}$. For the fat digestion, the in-house mouse protocol yielded 692 Tregs (4,53% of total live CD4) whereas the Miltenyi protocol yielded us 35 Tregs (2,6% of total live CD4) from 5 grams of fat tissue. For the skin, the in-house mouse protocol yielded 267 Tregs (5,07% of total CD4), whereas the published protocol yielded 202 Tregs (6,38% of total CD4) from 1 gram of skin tissue.

Based on these results, we decided to use the in-house protocols for both fat and skin digestion moving forward.

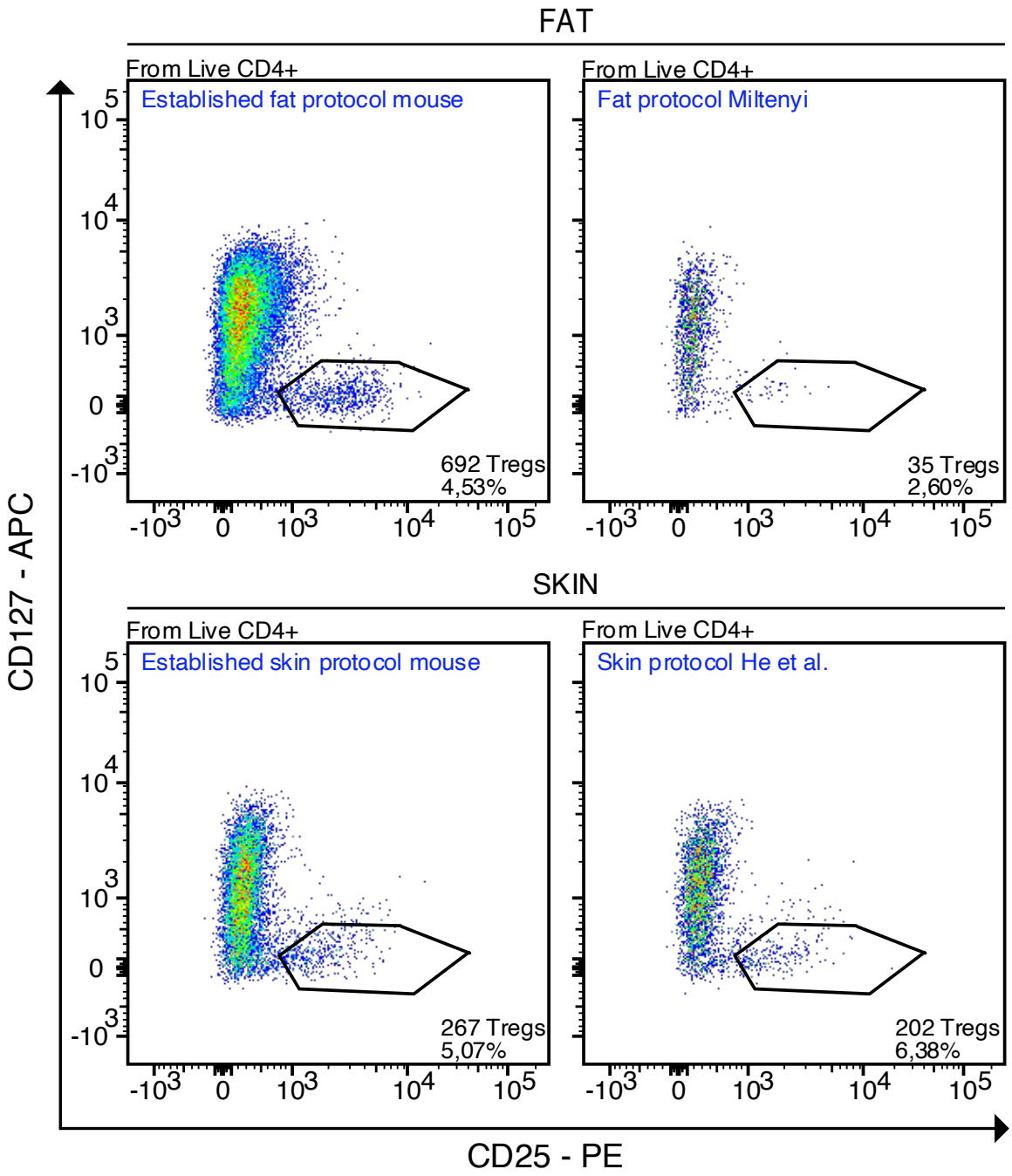

Figure 4. ***In-house established mouse protocol best for both skin and fat digestion.*** *flow cytometry plots of CD4⁺ populations from human skin and fat. Treg populations in each plot are gated as CD127⁻CD25⁺. different protocols highlighted in blue within the plot. Numbers and percentages of Tregs are listed in the plots Full protocols for each digestion can be found in the materials and methods. Dot plots are representative for 2 donors.*

Next, we compared the Treg yield between 2 different timepoints of digestion (Figure 5). Following the now established digestion protocols, we researched whether the Treg yield would still be comparable to digestion directly after tissue receival, if the tissue was stored at 4°C for 24h. Upon receiving the tissue, a part was processed directly, and a part was stored at 4°C for 24h. Both timepoints were processed in the same way and stained with identical antibodies. Whereas the Treg yield from the directly digested tissue was 692 Tregs (4,53% of total live CD4) for the fat (5g) and 267 Tregs (5,07% of total CD4) for the skin (1g), this decreased after 24h at 4°C. Only 29 Tregs (2,61% of total CD4) were isolated from 5 grams of fat after 24h at 4°C, and only 62 Tregs (5,49% of total $CD4^+$) were isolated out of 1 gram of skin after 24h at 4°C. Based on these data it was the decided that tissue should be digested immediately upon arrival.

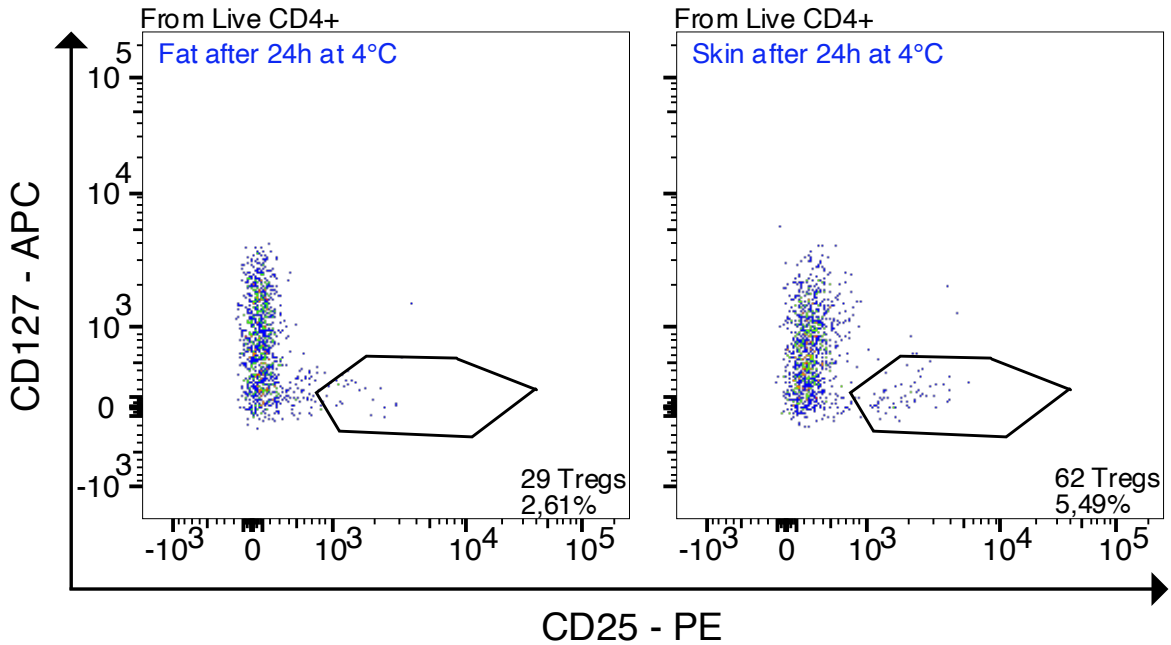

*Figure 5. Ti**ssues need to be processed immediately upon arrival. .** flow cytometry plots of $CD4^+$ populations from human skin and fat. Treg populations in each plot are gated as $CD127^-CD25^+$. Timepoints are highlighted inside the plot in blue. Numbers and percentages of Tregs are listed in the plots. Dot plots are representative for 2 donors.*

4.2. Mouse Treg populations can be successfully identified using single cell ATAC-sequencing

Once protocols for tissue digestion had been established, the characterisation of human NLT Tregs could start. Murine NLT Tregs had been very well characterized already (Cipolletta *et al.*, 2012; Delacher *et al.*, 2020; Delacher *et al.*, 2017; Feuerer *et al.*, 2009), by our lab and others, so this served as a good baseline for comparison against human NLT Tregs. To research this comparison, $CD4^+$ and $CD4^+CD25^+$ were isolated from murine spleen, colon, lung, visceral adipose tissue (VAT) and skin (Figure 6). From each of the tissues, CD45-negative cells were excluded, as well as dead cells, $CD19^+$ cells, $CD3^-TCR\beta^-$ cells, and $CD8^+$ cells. 100.000 $CD4^+$ cells were sorted of each tissue. In the spleen the number and percentage of $CD4^+$ cells were high enough to also allow for the sorting of 100.000 $CD4^+$ $CD25^+$ cells.

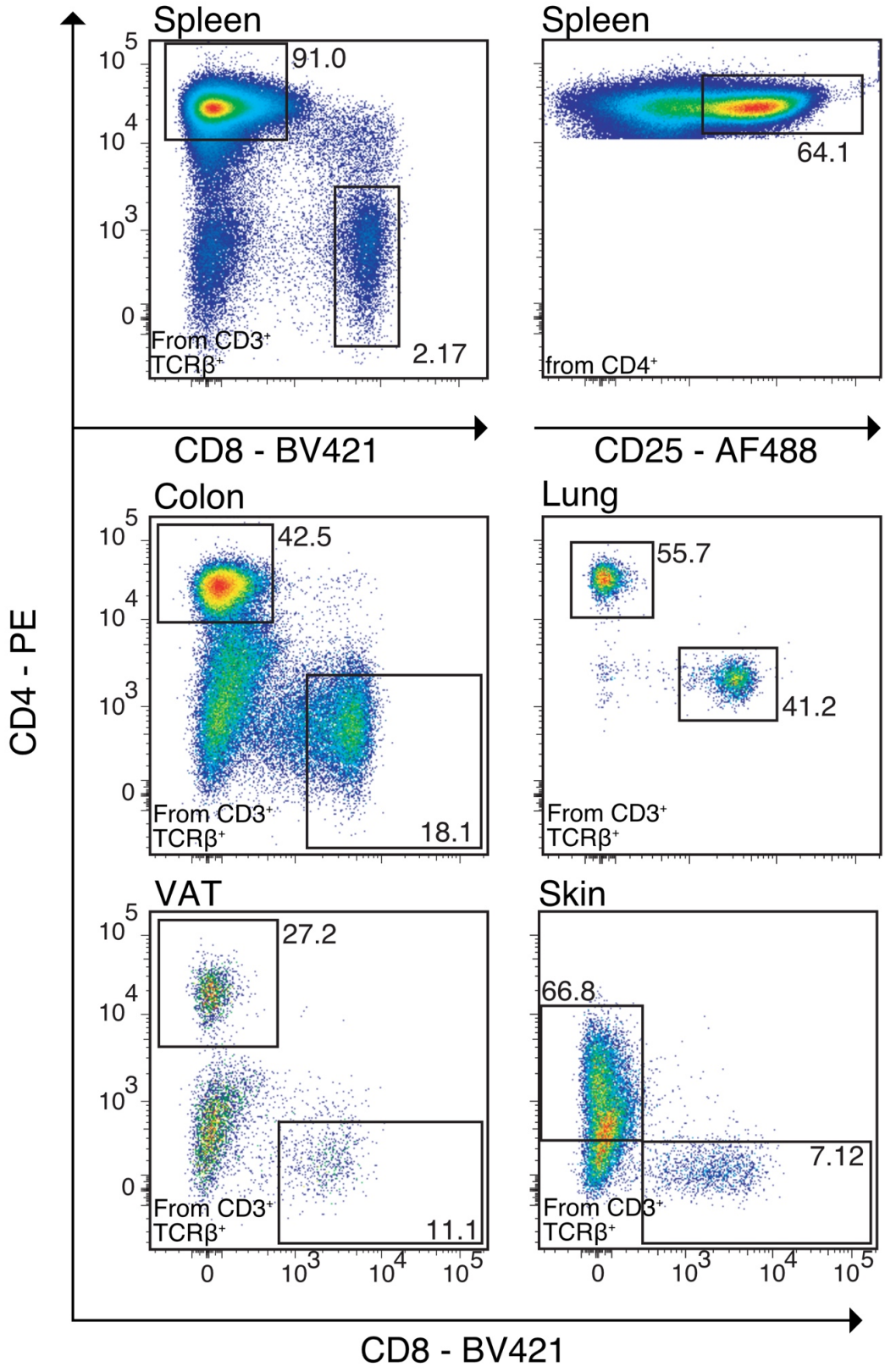

Figure 6. ***Murine CD4+ populations were sorted for scATAC-seq.*** *Flow cytometry plots of CD4+ populations from several mouse tissues. Tissues are listed on top of the plots. From spleen, CD4+CD25+ cells were also sorted, on top of whole CD4+ cells. VAT = Visceral adipose tissue. Data derived from four experiments with 18 C57BL/6J mice. Representative plots from each organ were chosen.*

After sorting the above populations, all single cells were subjected to Assay for Transposase Accessible Chromatin (scATAC). This could be performed on a single cell level with the help of the 10x Chromium controller (10x genomics), in which every single cell is labelled with a specific barcoded bead. scATAC profiles were generated for a total of >26.000 $CD4^+$ T cells. On a cell-to-cell basis, around 18.000 to 35.000 unique nuclear fragments were identifiable. Harmony (Korsunsky *et al.*, 2019) was used for group normalisation and the data were visualised using UMAP (Uniform Manifold Approximation and Projection for Dimension Reduction) (Figure 7). UMAP plots allow for the displaying of multiple dimensions of the same data in a 2D way. Cells are assigned a spot on the plot based on how similar or different they are to each other. Cells that were derived from the same organ were assigned the same colour code (Figure 7A). To identify certain populations of different $CD4^+$ cell types, the gene activity score of $CD4^+$ subtype defining were assessed (Figure 7B-F). To identify Tregs in different tissues, *Foxp3*, the master transcription factor for Tregs was used (Figure 7B). Opposed to Tregs, Tconv were found to be the only ones with open chromatin at the *IL2* locus (Figure 7C), while they did not have open chromatin at the *Foxp3* locus. To find naïve $CD4^+$ cells, both Tregs and Tconv, the gene activity of *Sell* (encoding CD62L) was examined (Figure 7D). These cells are antigen-inexperienced, and a good population to compare tissue-resident Tregs against. To identify Th1 polarized clusters, the *Tbx21* (encoding for T-bet) gene activity score was evaluated. The *Tbx21* locus was only open in tissue resident effector T-cells, but not in Tregs (Figure 7E). This result was confirmed by the *Ifng* activity score (Figure 7F). The *Ifng* locus was, like the *Tbx21* locus, only accessible in tissue resident effector T-cell fraction, but not in the Treg fraction, which has been described as Th2-biased (Delacher *et al.*, 2017).

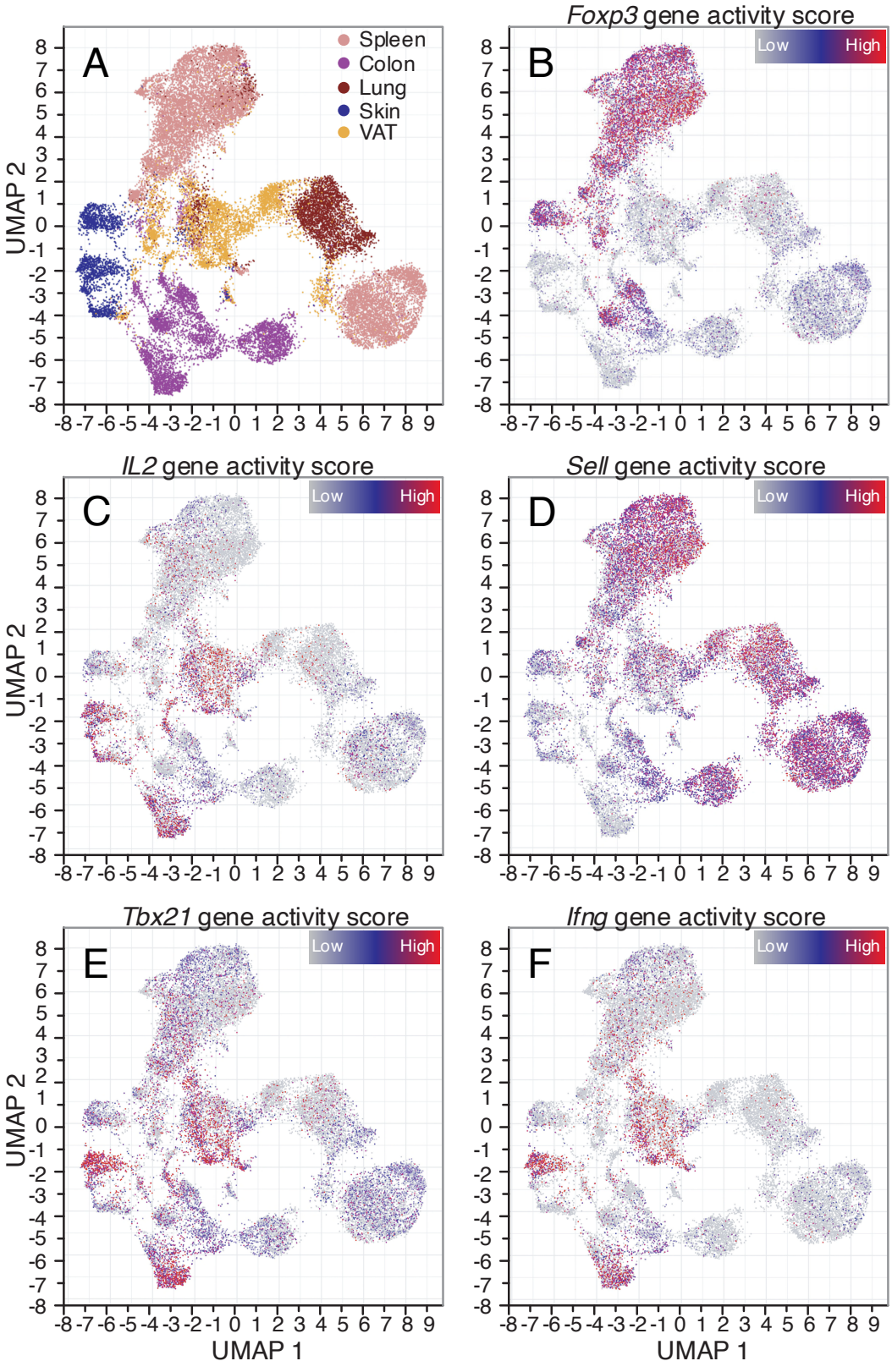

Figure 7. ***Murine tissue resident Tregs can be identified through scATAC-seq.*** *UMAP plots of of scATAC-seq data derived from FACS-sorted CD4⁺ and CD25⁺ T cell populations from the spleen, colon, lung, skin and VAT. All plots batch corrected using Harmony. A: cells were assigned colour based on tissue of origin. B-F: gene acivity scores based on chromatin accessibility with blue=low and red=high. B: gene activity score of FoxP3. C: gene activity score of IL-2. D: gene activity score of Sell. E: gene activity score of Tbx21. F: gene activity score of IFN□. Bioformatic analysis and UMAP generation was done by Malte Simon (DKFZ). Data derived from four experiments with 18 C57BL/6J mice.*

Based on these results, scATAC could reliably be used to identify T-cell populations within several murine tissues, including Tregs.

4.3. Human Treg populations can be successfully identified using Single cell ATAC-sequencing

Once scATAC on murine tissues was successfully carried out, we researched if we could apply the same technique to identify human tissue resident T-cells, and whether it would be possible to compare these populations to murine tissue resident T-cells. To this end, Total $CD4^+$ cells were sorted from blood, fat, and skin, and Tregs were sorted from blood and fat from healthy donors undergoing cosmetic surgery (Figure 8). Two independent runs of 2 donors yielded 100.000 peripheral blood derived $CD4^+$ cells each, as well as 100.000 $CD25^+CD127^-$ Tregs each. 100.000 $CD4^+$ cells each were sorted from 3 adipose-tissue donors, as well as a total of 40.000 Tregs divided between 2 donors. The skin yielded a total of 160.000 $CD4^+$ cells, divided between 2 donors, with 70.000 and 90.000 $CD4^+$ cells respectively.

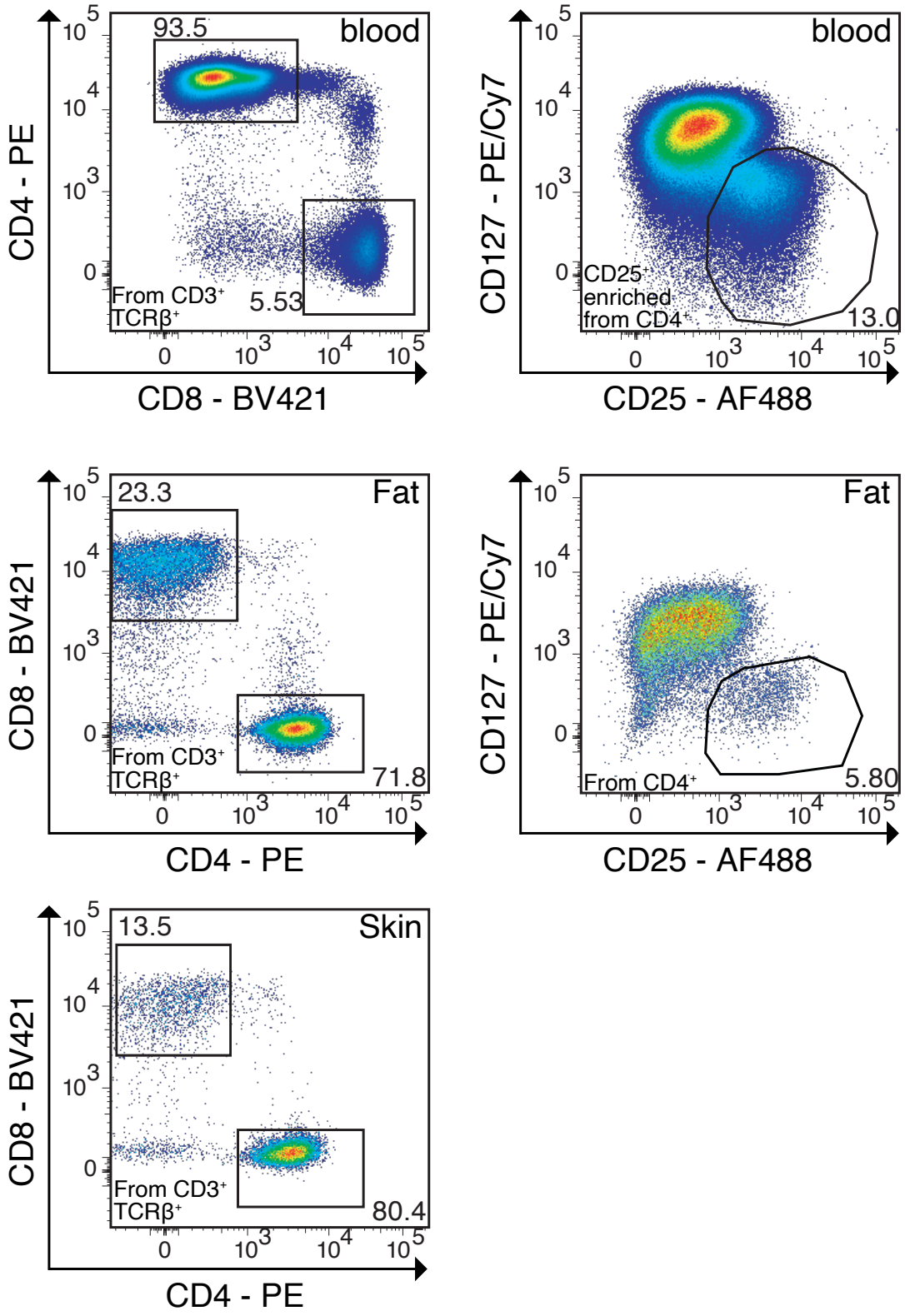

Figure 8. ***Human CD4+ populations were sorted for scATAC-seq.*** *Flow cytometry plots of CD4+ populations from human skin, fat and blood. Tissues are listed inside the plots. From fat and blood, CD4+CD127-CD25+ cells were also sorted, on top of whole CD4+ cells. N=2 for blood, N=3 for fat, N=2 for skin. Representative plots were chosen for each organ.*

scATAC-seq was carried out with the populations mentioned above. In total, the skin yielded >20.000 identifiable single $CD4^+$ cell profiles and $CD4^+$ and $CD4^+CD127^-CD25^+$ cells from the fat combined yielded >20.000 identifiable single cell profiles. Lastly, more than 35.000 identifiable single cell profiles were obtained from blood derived $CD4^+$ and $CD4^+CD127^-CD25^+$ cells per donor. Like with the mouse data, Harmony (Korsunsky *et al.*, 2019) was used to normalise the data between donors, and UMAPs were generated. Once again, cells derived from each tissue were assigned their own colour (Figure 9A). Parallel to the mouse system, FOXP3 is the master transcription factor of Tregs in humans and the gene activity score of *FOXP3* was used to identify the Treg populations in different tissues as well as blood (Figure 9B). Most notably, Tregs from fat and skin grouped together away from other $CD4^+$ cells, confirming their separate identity from both blood derived Tregs as well as tissue resident CD4 Tconv cells. In both tissue and blood derived Tregs, the *IKZF2* (encoding Helios) locus is opened (Figure 9C), showing thymic origin. The *SELL* locus was found to be accessible in antigen inexperienced CD4 Tconv and Tregs in the blood, analogous to naïve $CD4^+$ cells from the murine spleen (Figure 9D). The *IL2* gene activity score was high in activated $CD4^+$ Tconv cells, mostly present in the tissue (Figure 9E). Cells that had an accessible *IL2* locus did not overlap with cells with a high FOXP3 gene activity score, confirming their separate identity. Likewise, *IFNG* gene activity was observed in activated $CD4^+$ Tconv cells, but not in Tregs from derived from either the blood or the tissue (Figure 9F). These results showed that scATAC can also reliably be used to identify human tissue resident T cell populations on a single cell level.

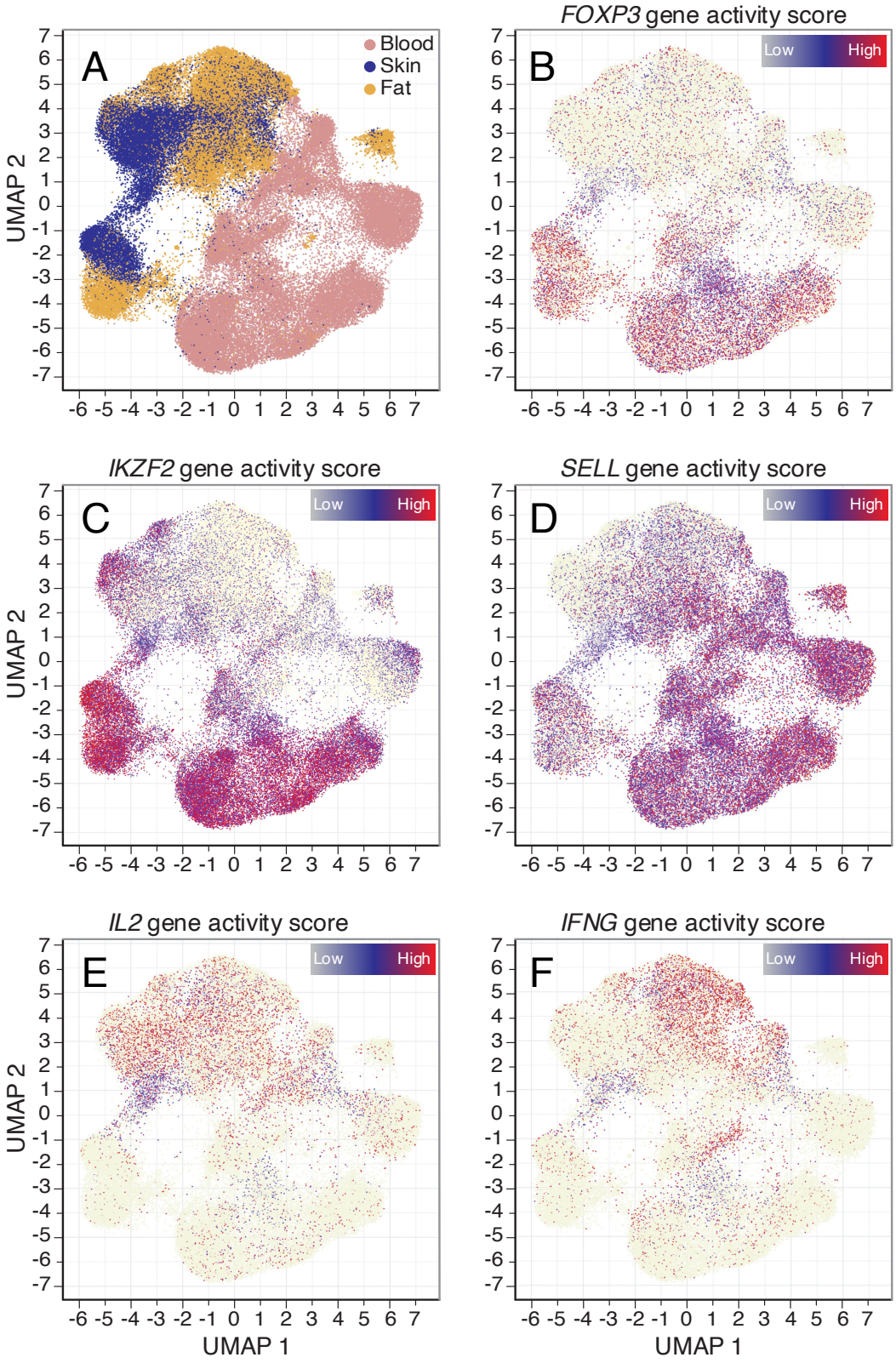

Figure 9. ***Human tissue resident Tregs can be identified through scATAC-seq.*** *UMAP plots of of scATAC-seq data derived from FACS-sorted CD4⁺ and CD127⁻CD25⁺ T cell populations from the blood, fat, and skin. All plots batch corrected using Harmony. A: cells were assigned colour based on tissue of origin. B-F: gene acivity scores based on chromatin accessibility with blue=low and red=high. B: gene activity score of FOXP3. C: gene activity score of IKZF2. D: gene activity score of SELL. E: gene activity score of IL-2. F: gene activity score of IFN. Representative plots were chosen for each organ. . N=2 for blood, N=3 for fat, N=2 for skin. Bioinformatic analysis and UMAP generation was performed by Malte Simon (DKFZ).*

4.4. Peak liftover of open chromatin from mouse to human identifies shared features

4.4.1. BATF binding sites are detected in majority of shared peaks between mouse and human tissue resident Tregs

With the knowledge that scATAC could reliably identify Treg populations in different tissues, came to opportunity to compare murine tissue resident Tregs with human tissue resident Tregs. To compare these populations, murine naïve Tregs were compared to murine fat and skin resident Tregs, and a murine tissue specific signature was established, encompassing 14.595 peaks. Next, the same was done for the equivalent human populations. Human tissue resident Tregs were compared to human blood derived naïve Tregs were compared, and a human tissue specific signature was established, encompassing 12.236 peaks. Shared peaks between the mouse and human signature were identified by performing a peak liftover. The liftover was performed with the peaks present in the murine mm10 genome that could be mapped to the human hg19 genome. Peaks that qualified for liftover had to be located inside the gene body or 2000 base pairs up or down stream, and the same gene activity score change direction (i.e both upregulated chromatin accessibility, or both downregulated chromatin accessibility). The list of candidates that met these criteria counted 643 peaks (Figure 10). This list contained, among others, surface receptors, like CCR2, CCR5, CCR6, CCR8, and Transcription Factors, like TOX, GATA3, BACH2 and BATF.

The importance of BATF in murine tissue resident Tregs had already been described (Delacher *et al.*, 2020), so the next step was to research if BATF had any binding sites within this shared peakset. Consequently, Chromatin Immunoprecipitation following

sequencing (CHIP-seq) data were extracted (Pope et al., 2014). This dataset showed that 145 out of 278 peaks shared between murine and human tissue resident Tregs had BATF binding sites. In contrast, only 70 out of 365 peaks shared between naive murine and human Tregs had BATF binding sites. These data show that BATF is of import in both mouse and human tissue resident Tregs.

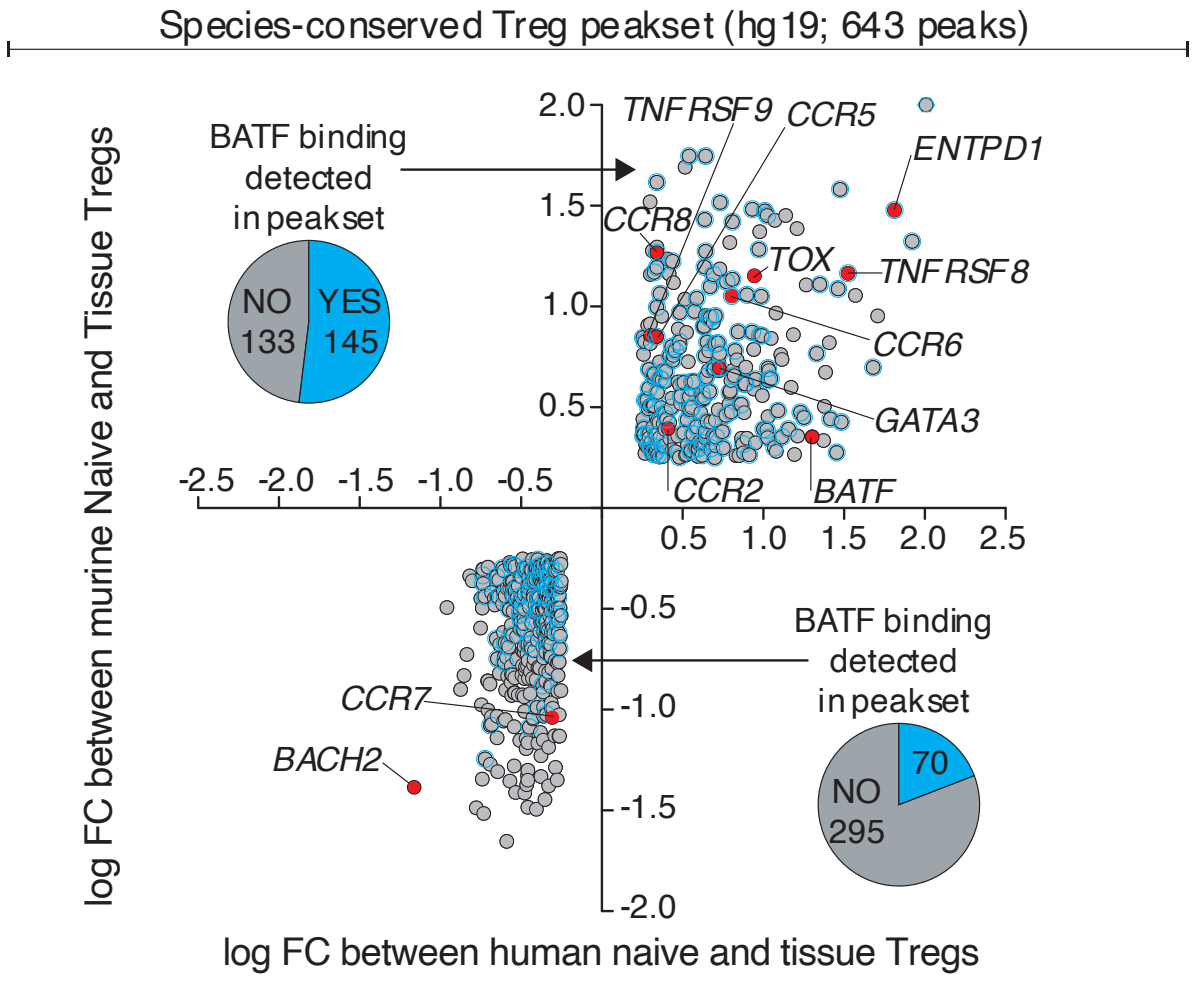

Figure 10. ***Peak lift-over identifies shared peaks between human and mouse tissue Tregs.*** *Shared peaks in murine and human tissue Treg data sets. logFC of peaks compared to naïve Tregs of corresponding species (No cut off, all shared peaks included in plot). Peaks overlapping with ChIP-seq confirmed BATF binding sites (B-cells, GSM803538), were coloured blue in the plots and counted in pie charts next to shared sections. Bioinformatic analyses performed by Malte Simon.*

To research this connection between BATF and human tissue resident Tregs further, the scATAC dataset was re-evaluated. This time, only the Treg populations from blood, fat and skin were taken and a new UMAP with these populations was generated (Figure 11). In this UMAP, a clear distinction between naïve and memory blood derived Tregs can be made. It also shows that memory blood derived Tregs cluster closer to skin and fat Tregs than naïve Tregs, showing a similarity to tissue resident Tregs that is lacking in naïve Tregs. *BATF* gene activity score in these populations was assessed. Chromatin accessibility was clearly increased in tissue resident Tregs compared to blood derived Tregs, once again showing an increased role of *BATF* in tissue resident Tregs compared to both naïve and memory blood derived Tregs.

Combined, these data show that besides being important in the murine tissue resident Tregs, BATF also has an important presence in human tissue resident Tregs.

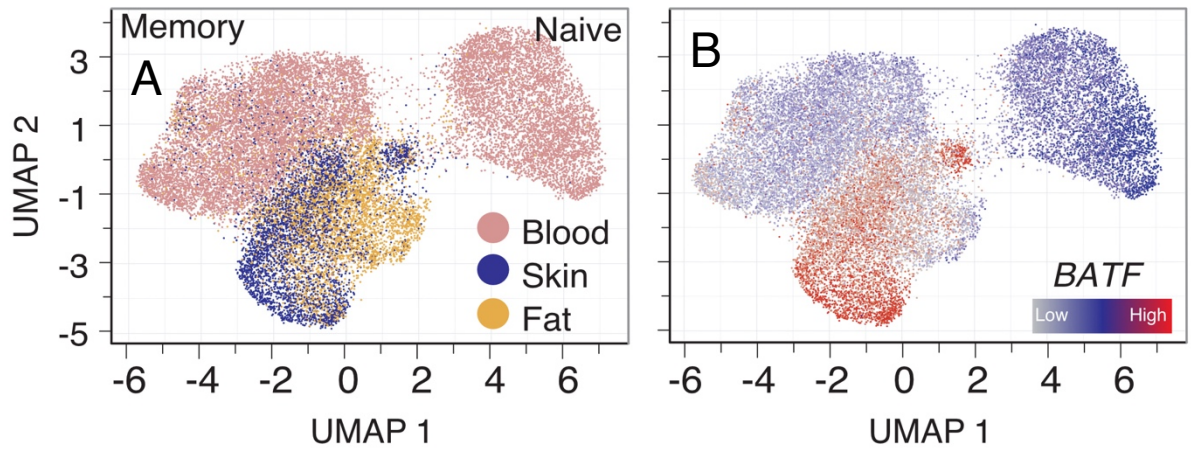

Figure 11. ***BATF gene activity score higher in tissue derived Treg compared to blood.*** *UMAPs of Treg populations derived from blood, fat and skin. Batch corrected by harmony. A: colours were assigned based on tissue of origin. B: gene activity score of BATF based on chromatin accessibility with blue = low and red = high. Bioinformatic analysis and UMAP generation was done by Malte Simon (DKFZ).*

4.4.2. A tissue Treg-like phenotype cannot be induced through cytokines in Batf$^{-/-}$ mice

Given the importance of Batf in both the murine and human system, the next question was whether a tissue repair phenotype could be present in the absence of Batf. To address this question, an induction model of a tissue repair phenotype in mice was used. Murine tissue Tregs have been described to be Th2 biased, and to express the IL-33 receptor (ST2) (Arpaia *et al.*, 2015; Delacher *et al.*, 2017). They have also been described to express Nfil3 as a marker transcription factor (Delacher *et al.*, 2020). So, in order to induce a tissue phenotype in naïve murine Tregs, a Th2 profile needed to be induced, as well as ST2 and Nfil3 expression. To achieve this, naïve ($CD4^+CD25^+CD62L^+$) spleen derived Tregs were sorted and cultured with either IL-2, IL-2 and IL-4, IL-2 and IL-33, or IL-2, IL-4 and IL-33 for 6 days (Figure 12). IL-4 has been described to induce a Th2 phenotype (Murphy *et al.*, 2017), and IL-33 is the ligand for ST2.

Upon culture with IL-2 only, neither Nfil3 nor ST2 were induced. Upon addition of IL-4 to this cocktail, only Nfil3 was induced, but not ST2. Upon culture with IL-2 and IL-33, a small subpopulation of $ST2^+$ Tregs appeared. It was only upon culture with a mixture of all 3 cytokines, that a subpopulation that was both Nfil3 positive as well as ST2 positive appeared. This data indicates that both IL-4 and IL-33 are necessary for a tissue phenotype induction in naïve murine Tregs.

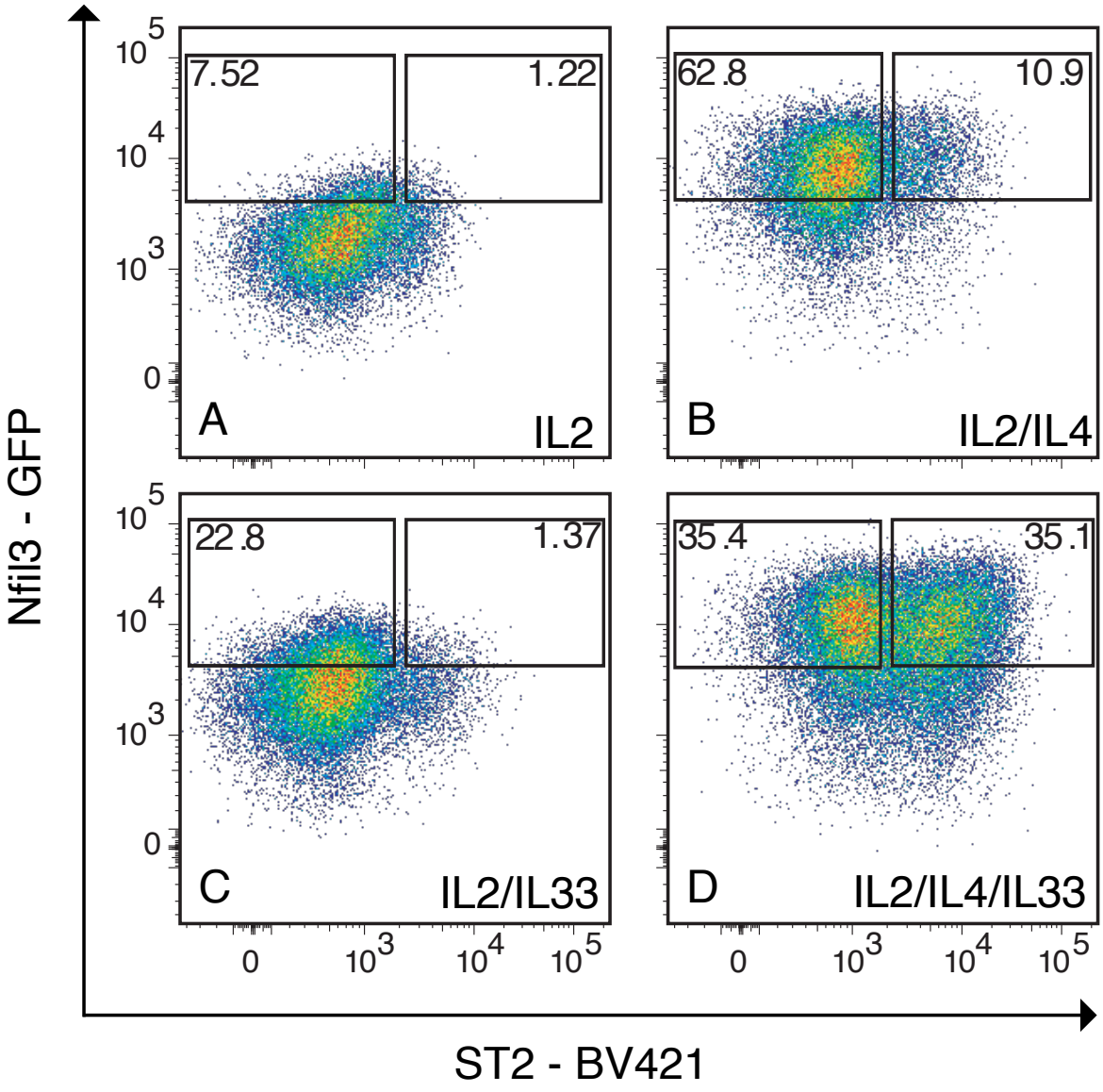

Figure 12. ***A tissue phenotype can be induced in murine Tregs with IL-4 and IL-33.*** *Flow cytometry plots of naïve murine Tregs cultured with different cytokine combinations for 5 days. Cytokine combinations are listed in the plots. Naïve Tregs were sorted as CD4⁺CD25⁺CD62L⁺. N=5 mice. Representative dot plots were chosen for each condition.*

To confirm that this tissue phenotype induction is also visible on transcription factor level, Gata3, a Th2 driving transcription factor, and Batf expression was examined (Figure 13). In all mice, both Gata3 and Batf expression increased significantly upon culture with IL-4 and IL-33.

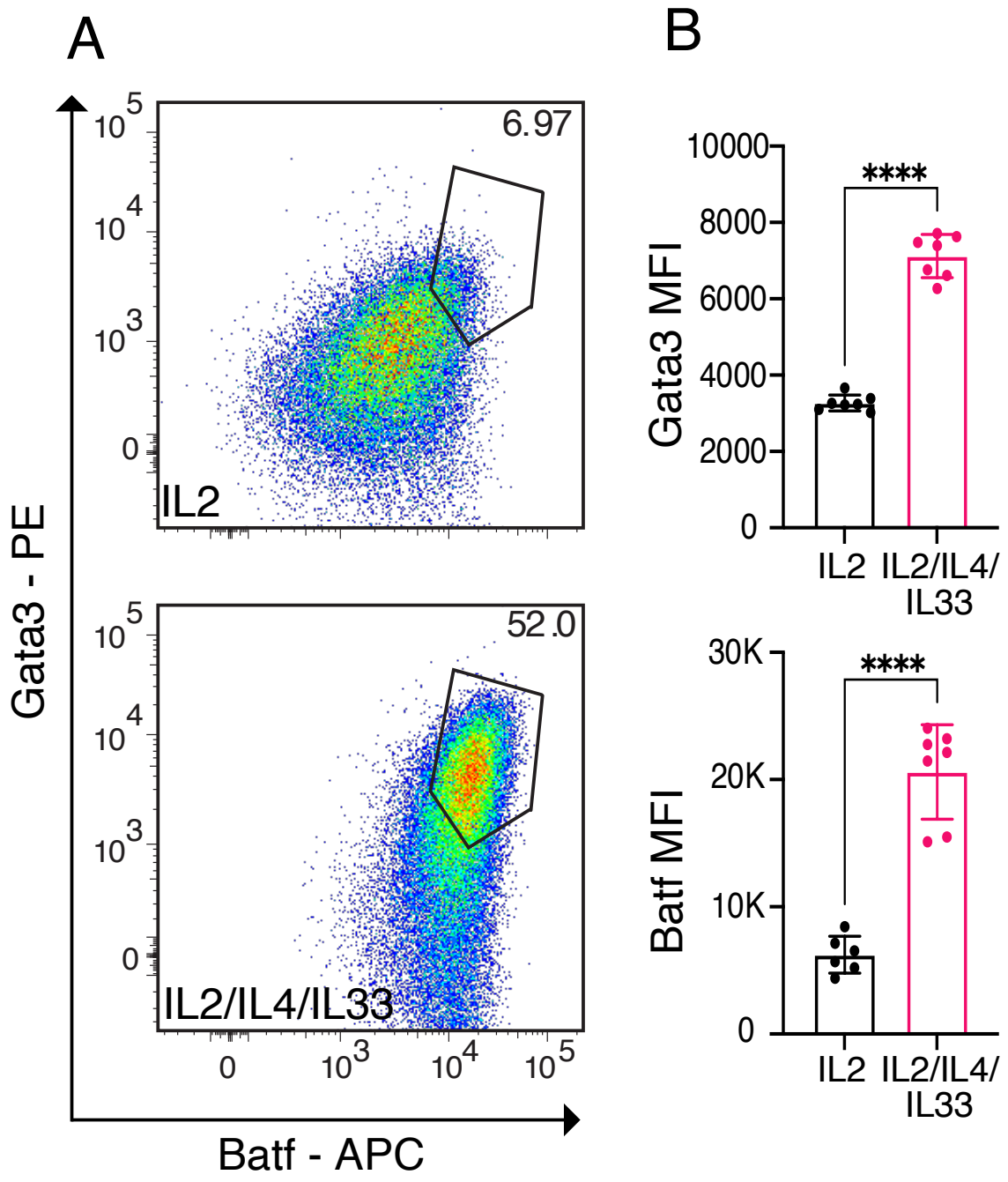

Figure 13. ***Gata3 and Batf are significantly upregulated in tissue-like Tregs.*** *A: Flow cytometry plots of naïve murine Tregs cultured with different cytokine combinations for 5 days. Cytokine combinations are listed in the plots. Naïve Tregs were sorted as CD4⁺CD25⁺CD62L⁺. B: MFI of Gata3 and Batf in IL-2-Tregs vs IL-2/IL-4/IL-33 Tregs. N=6 mice for IL-2 Tregs, N=7 for IL-2/IL-4/IL-33 Tregs. 2-way ANOVA to test for significance.*

With this model well established, we cultured WT and *Batf*$^{-/-}$ Naïve Tregs with either IL-2, IL-4 and IL-33 or IL-2 only for 6 days. After 6 days, life cells of all 4 conditions were sorted and subjected to bulk ATAC sequencing (Figure 14). In a principal component analysis plot, where samples group based on their likeness, *Batf*$^{-/-}$ Tregs treated IL-4 and IL-33 clearly grouped together with *Batf*$^{-/-}$ and WT IL-2 treated Tregs, while IL-4/IL-33 treated WT Tregs grouped separately in the opposite corner of the plot, indicating that without Batf, IL-4/IL-33 treated Tregs have more in common with IL-2 treated Tregs than tissue-like Tregs (Figure 14A). In a heatmap showing normalised accessibility comparison between samples (Figure 14B) across 28033 different peaks, chromatin that becomes accessible when WT Tregs are cultured with IL-4 and IL-33, stay closed in *Batf*$^{-/-}$ Tregs cultured with the same cytokines, confirming that Batf is necessary to induce a tissue phenotype in vitro. This was confirmed by examining individual gene loci associated with tissue Tregs, like *Pparg*, *Il1rl1* (encoding ST2), *Maf* or *Il10* (Figure 14C). Peaks were barely or not all present at Batf binding sites (indicated by the pink bars) in *Batf*$^{-/-}$ Tregs cultured with IL-4/IL-33. In contrast to this, WT cells cultured with IL-4 and IL-33 had peaks at Batf binding sites comparable to those found in VAT derived tissue Tregs. Combined, these data show that Batf is necessary to induce a tissue-like phenotype in Naïve Tregs *in-vitro*.

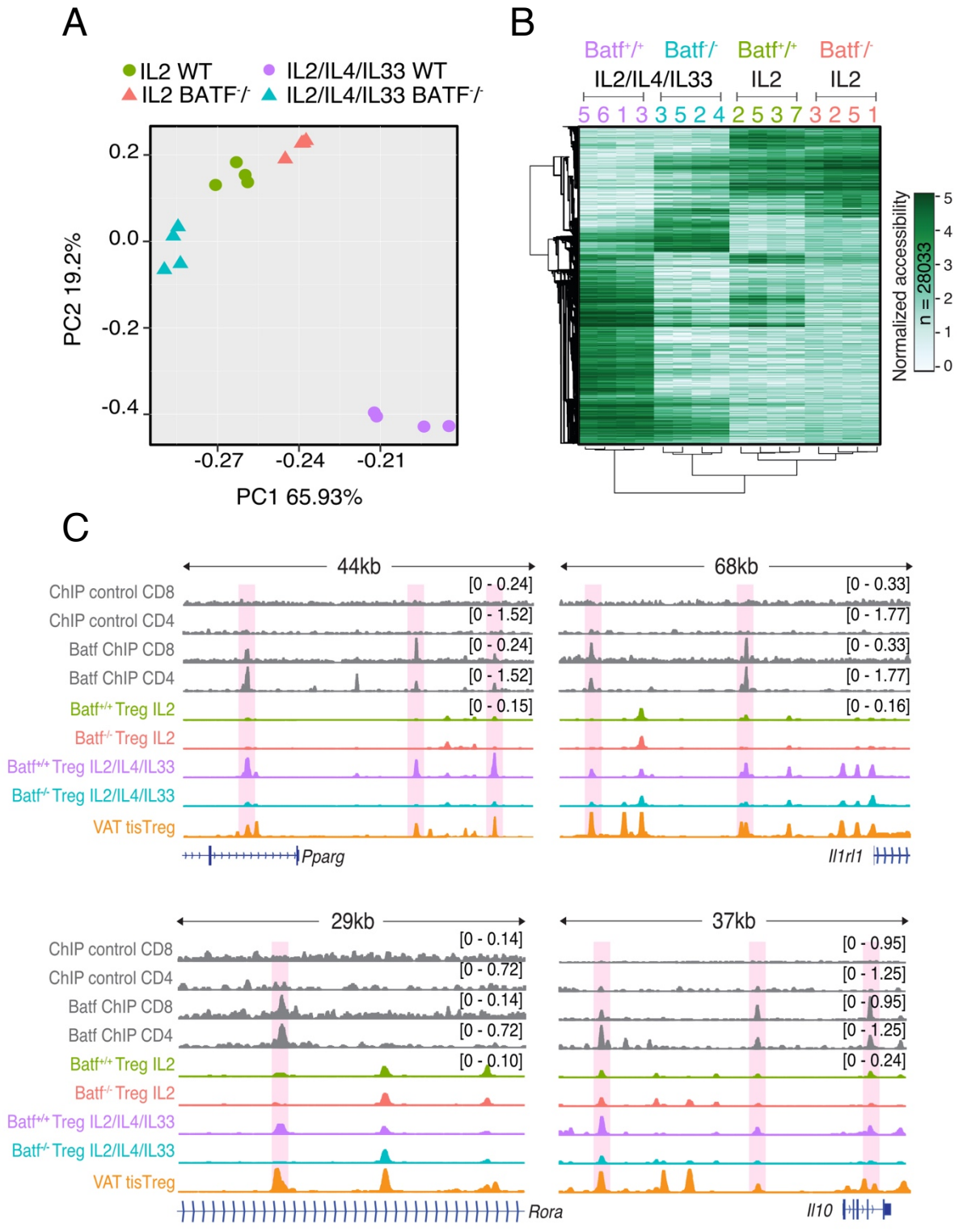

Figure 14. ***A tissue phenotype cannot be induced in BATF$^{-/-}$ Tregs.*** *BATF$^{-/-}$ and WT Tregs were cultured with IL-2/IL-4/IL-33 or IL-2 only for six days, followed by bulk ATAC sequencing. A: PCA plot based on ATAC-sequence reads of each group (N=4). B: heatmap showing unsupervised hierarchal clustering of ATAC dataset containing 28.033 peaks, using the same groups as in A (N=4). C: ATAC-seq data for all four conditions mentioned above, as well as tissue derived VAT Tregs. Gene loci and associated promotor area for Pparg, Il1rl1, Rora and IL-10 are shown (N=4). Top 4 tracks are derived from public BATF ChIP-seq data for CD4^{+} and CD8^{+} T-cells, including controls. peak hieight normalized to max peak height in brackets. For ChIP -seq, peak height was group normalized (value In brackets). Bioinformatic analysis, PCA plot, heatmap and bigwig track generation was performed by Christian Schmidl (RCI).*

4.4.3. CCR8 can be used to identify tissue Tregs in human non-lymphoid tissue as well as potential progenitors in peripheral blood.

Among the shared peakset between human and mouse tissue resident Tregs with BATF binding sites were several genes encoding for surface receptors. One of these surface receptors was CCR8, which was chosen for closer research in the human system. Upon examination of the UMAP of only the Treg populations from blood, skin and fat, *CCR8* chromatin accessibility was seen to be increased in memory blood derived Tregs compared to Naïve blood derived Tregs (Figure 15). In skin and fat derived Tregs this difference was seen to be more pronounced, with a higher gene activity score compared to memory blood derived Tregs. This could also be seen at the *CCR8* gene locus (Figure 15C). Whereas no peaks were present in naïve blood derived Tregs, small peaks could be seen in memory blood derived Tregs, and larger peaks could be seen in tissue Tregs. This was true for gene body as well as the BATF binding site.

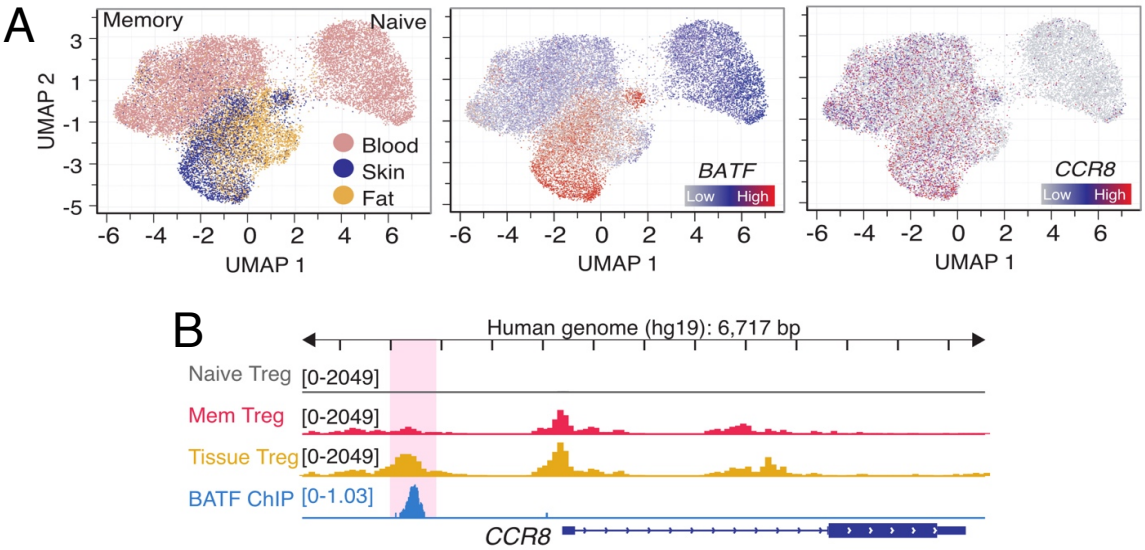

Figure 15. ***CCR8 gene activity score is higher in blood memory Tregs and tissue Tregs.*** *UMAPs of Treg populations derived from blood, fat and skin. Batch corrected by harmony. A: left; colours were assigned based on tissue of origin. Middle; gene activity score of BATF based on chromatin accessibility with blue = low and red = high. Right; gene activity score of CCR8 based on chromatin accessibility with blue = low and red = high. B: ATAC-seq data for the CCR8 locus in all 3 populations shown in UMAP, combined with public BATF ChIP data. Peak height normalized to numbers in the brackets. Bioinformatic analysis, UMAP and BigWig track generation performed by Malte Simon.*

Having established that *CCR8* chromatin is open in both memory blood derived Tregs and tissue Tregs, a next question was to see if this could also be seen on protein level. To this end, PBMCS were isolated from a leukocyte reduction system chamber (LRSC) and fluorescently labelled for flow cytometry. $CD45RO^+$ (memory) Tregs showed a subpopulation of 35,6% $CCR8^+$ Tregs, whereas this subpopulation was not present in $CD45RA^+$ (Naïve) Tregs (Figure 16A). In Tconv, the same dynamic between memory and naïve cells could be seen, but the subpopulation of $CCR8^+$ memory Tconv was significantly smaller than $CCR8^+$ memory Tregs. In both Tregs and Tconv, the subpopulation of memory $CCR8^+$ cells were significantly bigger than in naive cells (Figure 16B).

Having shown that CCR8 protein expression in blood mirrors the chromatin accessibility of the *CCR8* locus, the next question was if this could be confirmed in tissues as well. To research this, tissues were digested and processed as mentioned above. Blood and tissues were fluorescently labelled and examined through flow cytometry (Figure 16C). As before, naive blood derived Tregs showed no presence of CCR8. In memory blood derived Tregs, CCR8 MFI increased with the presence of the $CCR8^+$ subpopulation. In skin and in fat, CCR8 MFI increased even more, indication the presence of a bigger $CCR8^+$ population than in the blood. These results mirror the gene activity score for the *CCR8* locus (Figure 15C).

These results show that CCR8 can confidently be used to identify human tissue resident Tregs, as well as $CCR8^+$ subpopulation in the blood.

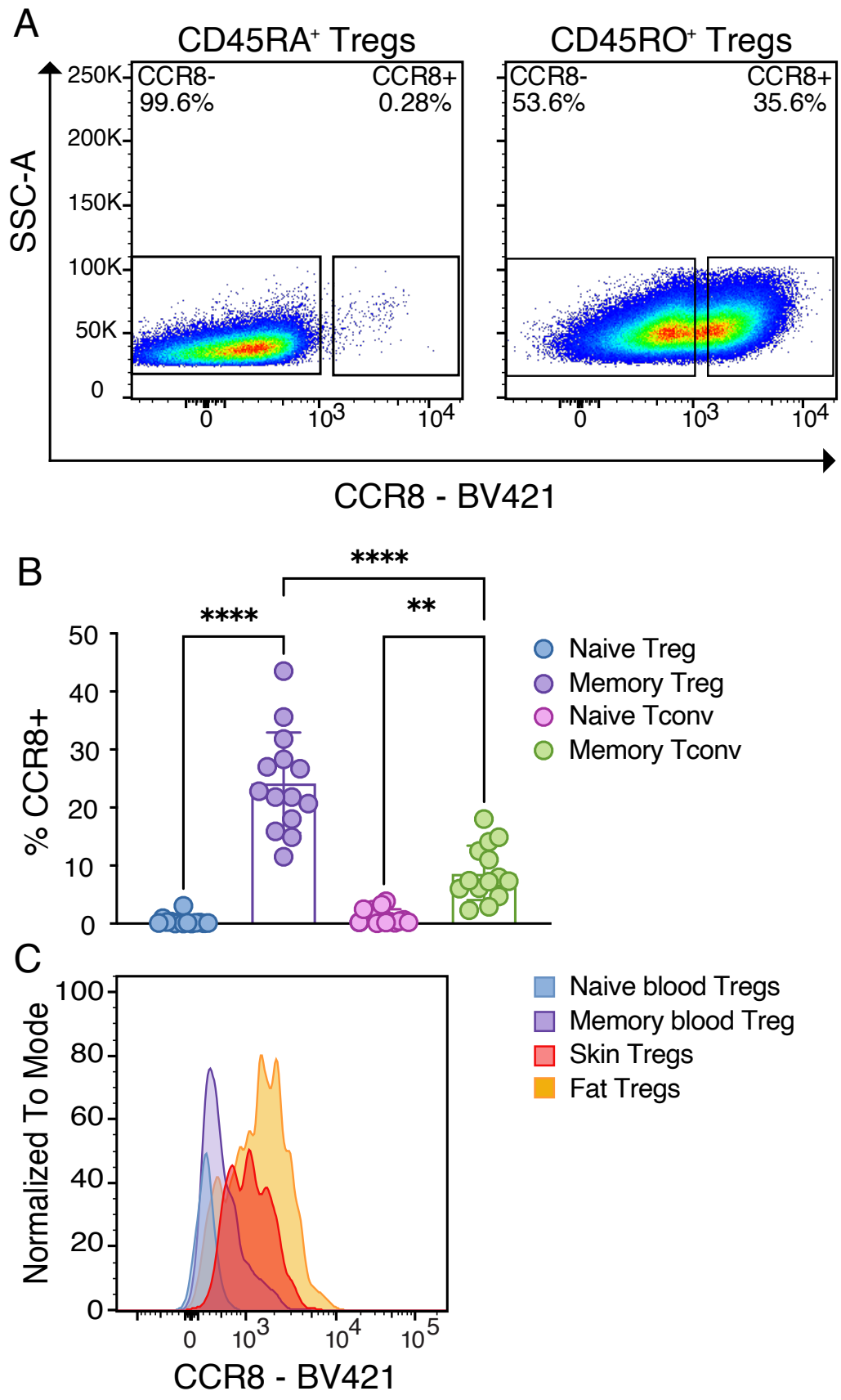

Figure 16. ***CCR8 chromatin accessibility can be confirmed on protein level.*** *A: flow cytometry plots of CCR8 protein expression in CD45RA+ and CD45RO+ Tregs. B: percentage of CCR8+ in Naïve/Memory Tregs and Tconv (N=14, one-way ANOVA). C: flow cytometry plots of CCR8 protein expression in blood, fat and skin.*

To research human (tissue) Treg associated transcription factors on protein and RNA level in blood derived Tregs, naïve Tconv, naïve Tregs, CCR8$^-$ memory Treg and CCR8$^+$ memory Tregs were sorted and subjected to intracellular staining. Naïve Tconv, naïve Treg and CCR8$^+$ Tregs were also subjected to RNA sequencing. As expected Tconv had the lowest amount of FOXP3 on both a protein level as well as an RNA level (Figure 17A). Naïve Tregs predictably had a higher amount of FOXP3 expression on both a protein and an RNA level. CCR8$^-$ memory Tregs had a slightly increased, but similar FOXP3 protein level compared to naïve Tregs. CCR8$^+$ Tregs had an increased level of FOXP3 expression on both protein and RNA level. This increase was significant on RNA level compared to both naive Tconv and Naïve Tregs. CD25 expression on protein level, and *IL-2RA* (encoding CD25) expression on RNA level, followed a similar trend (Figure 17B). Little to no CD25/*IL-2RA* was expressed in naive Tconv. Naïve Tregs and CCR8$^-$ memory Tregs had an increased amount of CD25/*IL-2RA* compared to naïve Tconv on both protein and RNA level, but CD25 protein expression level was almost identical in the 2 populations. Once again, CD25/*IL-2RA* expression in CCR8$^+$ Tregs was increased compared to all other populations. This increase was significant on RNA level compared to both naïve Treg and Naïve Tconv. Lastly, BATF protein and RNA expression was examined. Like with the previous factors, BATF expression was lowest on both protein and RNA level in naïve Tconv and increased in naïve Tregs (Figure 17C). In CCR8$^-$ memory Tregs, BATF protein expression levels were increased compared to the previous 2 populations. Both protein and RNA expression levels of BATF were highest in CCR8$^+$ Tregs. RNA expression of BATF was significantly increased in CCR8$^+$ Tregs compared to both Naïve Tconv and Tregs, confirming the increased chromatin

accessibility seen in these populations.

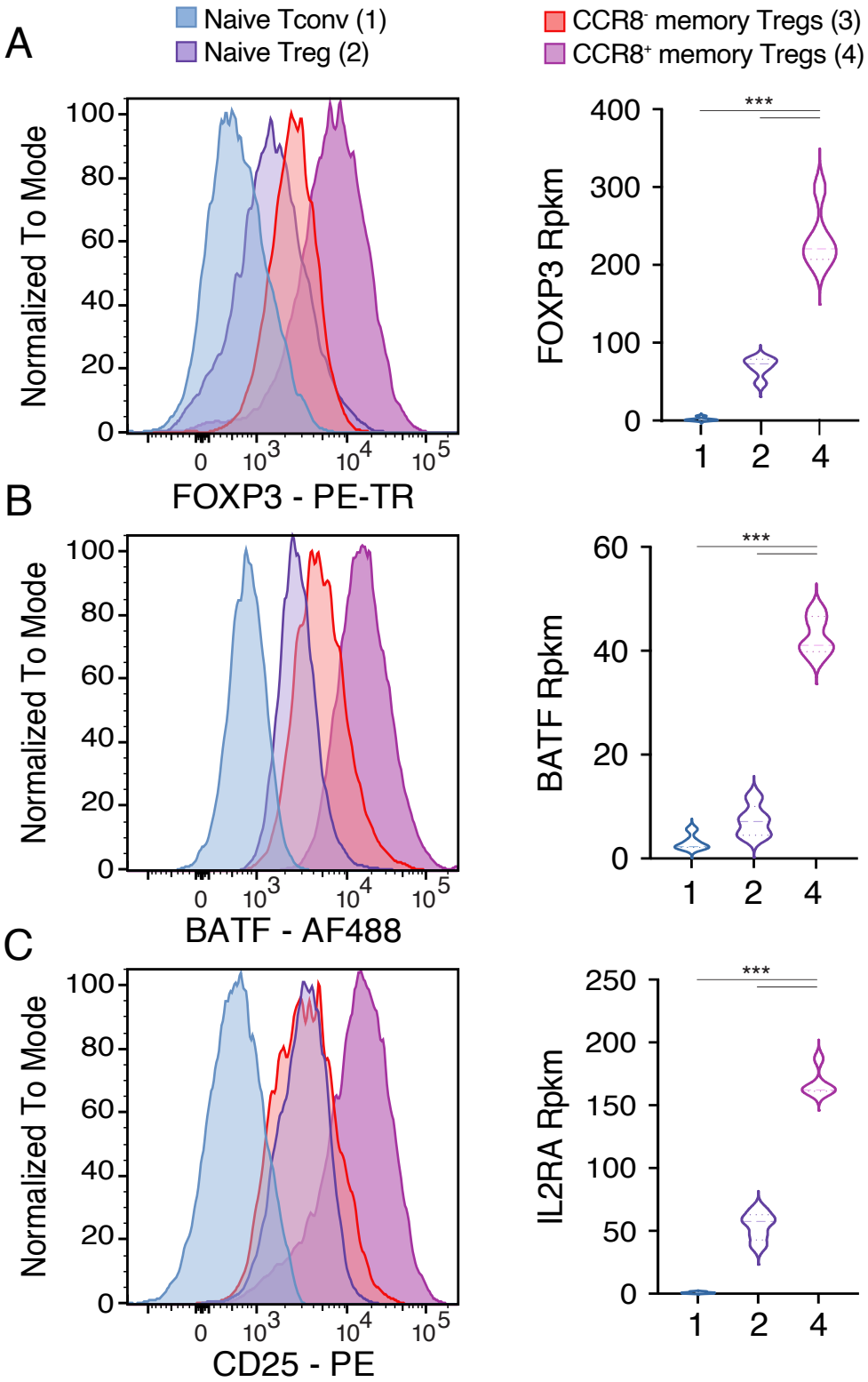

Figure 17. ***Blood derived CCR8+ Tregs have increased BATF, FOXP3 and CD25 levels.*** *Right: Flow cytometry plots of FOXP3 (A) , BATF (B) and CD25 (C)in various blood derived CD4+ T-cell populations. Left: RPKM graphs showing RNA expression level of genes corresponding to flow cytometry plots on the right (N=5, Deseq2). RPKM tables and Deseq2 analysis was performed by Agnes Hotz-Wagenblatt (DKFZ)*

Combined these data show that CCR8 can reliably be used as a way to identify a specific subset of memory human Treg cells. They also show an increased expression of BATF in CCR8$^+$ Tregs present in the blood, pointing to a potential relation between blood derived CCR8$^+$ Tregs and Tissue Tregs.

4.5. LEGENDScreen™ identifies further surface markers for potential tissue Treg progenitor population in CCR8$^+$ treg subpopulation in peripheral blood

After identifying CCR8 as a reliable surface marker for human tissue resident Tregs, the next question was whether other surface markers could be identified, that are co-expressed on CCR8$^+$ Tregs. To examine this, PMBCs were isolated out of peripheral blood, enriched for CD25, and subjected to a LEGENDScreen™. 381 surface markers were assessed for protein expression through flow cytometry, by measuring the level of PE expression compared to isotype controls (Figure 18). 5 groups were compared, namely; CD45RO$^-$ Tconv, CD45RO$^-$ Treg, CD45RO$^+$ Tconv, CD45RO$^+$ CCR8$^-$ CD45RO$^+$ Tregs and CCR8$^+$ CD45RO$^+$ Tregs. 287 of these markers (group 9) were not expressed at all. This group contained primarily markers that are not expressed on T-cells, as well as isotype controls. 47 markers were markers ubiquitously expressed (group 8). 7 markers were present on all cells but naïve Tregs (Group 7). 2 markers were downregulated all CD45RO$^+$ Tregs (Group 6). 3 markers were downregulated on all CD45RO$^+$ cells (Group 5). 13 markers were only upregulated on CD45RO$^+$ Tconv (Group 4). 6 markers were upregulated on all CD45RO$^+$ T-cells (Group 3).

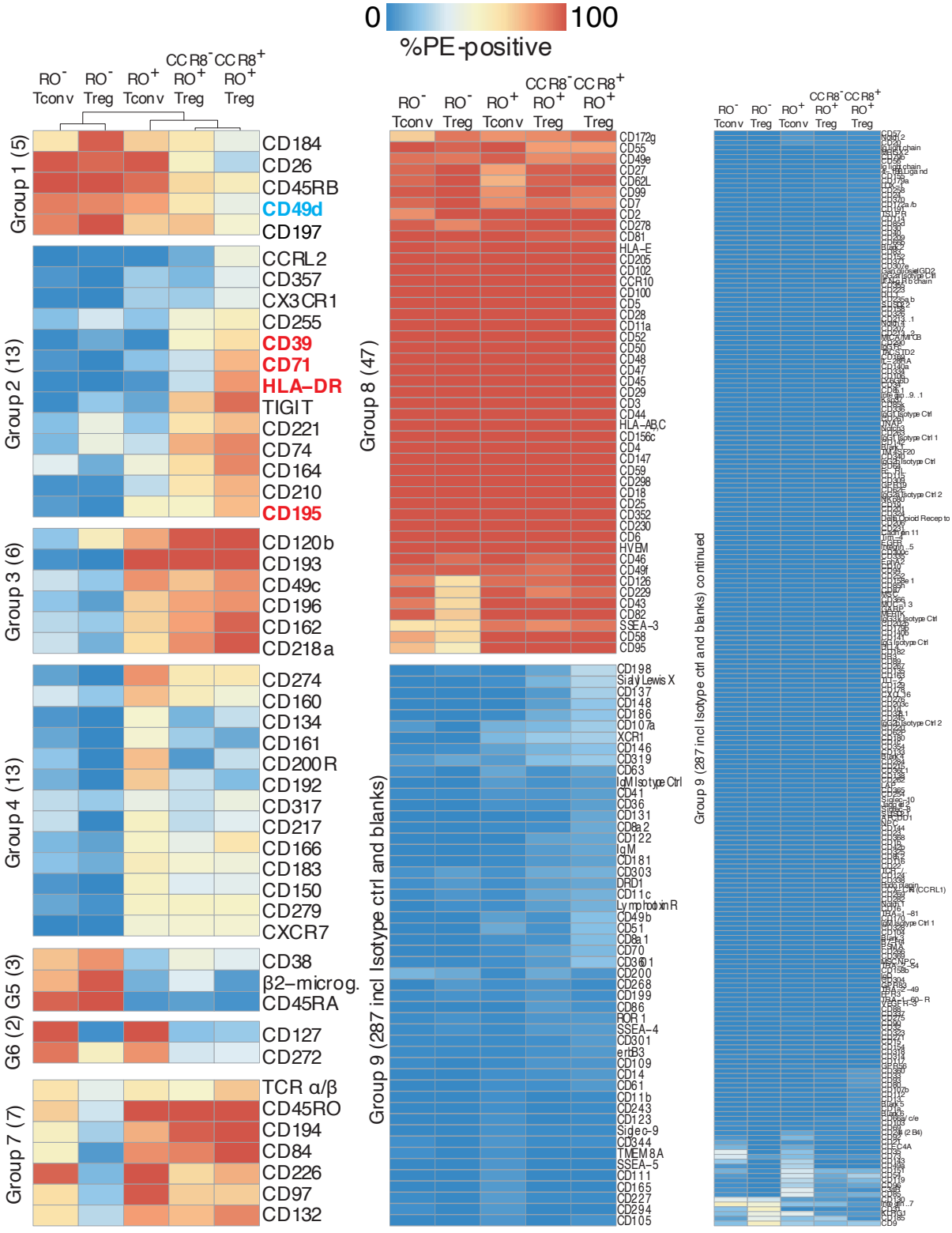

Figure 18. ***LEGENDScreen™ identifies surface markers that are co-expressed on CCR8⁺ Tregs.*** *Heatmap of PE expression in different subsets of human CD4⁺ cells. PBMCs were isolated and enriched for CD25. Enriched cells were stained for CD3, CD4, CD25, CD127, CD45RO and CCR8. After collective staining, cells were submitted to LEGENDScreen™ in which they were stained for 361 individual surface markers. Expression of those individual markers is shown as PE expression ranging from low to high, with low=blue and high=red.*

13 Markers were upregulated on CCR8$^+$ Tregs (Group 2) and 6 Markers were downregulated on CCR8$^+$ Tregs (Group 1) compared to the other groups.

5 proteins from group 1 and 2 were chosen for more careful examination on CD45RO$^+$ Tregs. HLA-DR, CD39, CD71, CCR5 (CD195) and CD49d were plotted against CCR8 (Figure 19). An isotype control from group 9 was picked as a negative control for protein expression (Figure 19A). HLA-DR was shown to have an increased expression as CCR8$^+$ expression increased as well (Figure 19B). CD39 expression was expressed on a subpopulation of CD45RO$^+$ Tregs independent from CCR8 expression, but on the subpopulation of Tregs expression both CD39 and CCR8, CD39 increased with CCR8 expression (Figure 19C). CD71 followed the same dynamic as HLA-DR, in which CD71 expression went up with CCR8 expression on all CD45RO$^+$ Tregs (Figure 19D). CCR5 was not present on Tregs not expressing CCR8, but evenly expressed on mid to high CCR8 expressing Tregs (Figure 19E). CCR5 expression, however, did not increase with CCR8 expression. CD49d expression was present on CCR8$^-$ Tregs (Figure 19F). Expression of CD49d decreased as CCR8 expression increased.

With these markers, 4 more positive selection markers were identified for CCR8$^+$ Tregs in blood, as well as one negative selection marker.

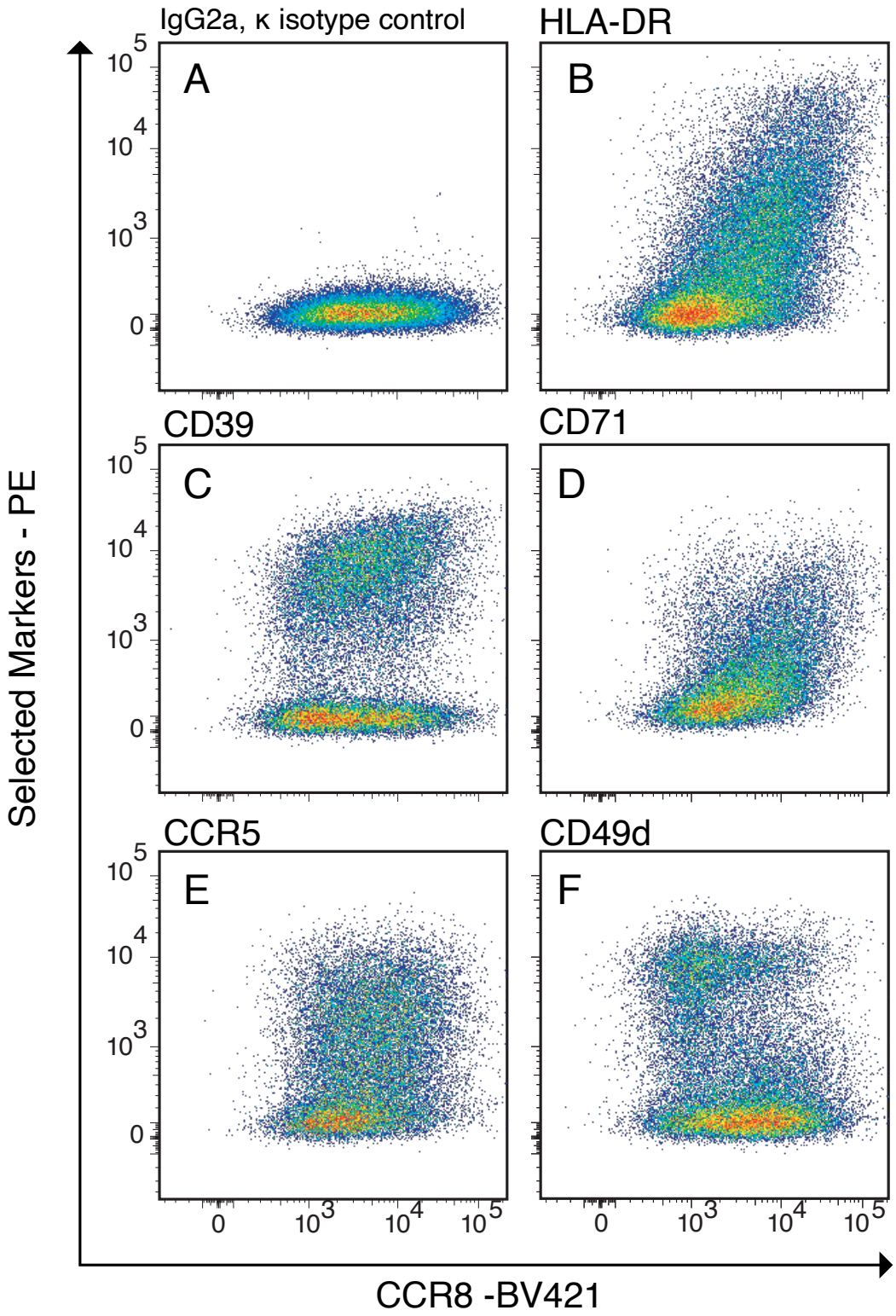

Figure 19. ***Several surface markers correlate with CCR8 expression in memory Tregs.*** *Individual flow cytometry plots of CCR8 and selected surface markers in memory Tregs. Markers are listed above the plots. IgG2a, κ was used an isotype control. Data derived from one independent experiment with 3 combined donors.*

After these 5 markers had been identified, the next question was whether they would also be expressed in a similar fashion in tissues Treg cells, if at all.

To investigate this, human skin and fat tissues were digested as stated above and PMBCs were isolated out of blood. Naïve blood derived Tregs and memory blood derived Tregs were compared to Tregs isolated from skin and fat (Figure 20).

Once again, HLA-DR was not present on Naïve Tregs. On Memory blood derived Tregs a small HLA-DR$^+$ subpopulation could be seen. In both skin and fat, HLA-DR was shown to be expressed on the majority of Tregs, mirroring the expression of CCR8 on tissue derived Tregs (Figure 20A).

Like in the LEGENDScreen™, CD39 was not present on naïve Tregs, but a CD39$^+$ subpopulations could be seen in memory Tregs. However, CD39 was not ubiquitously expressed in tissue Tregs. Only a subpopulation on Tregs in both fat and skin showed CD39 expression (Figure 20B).

CD71 expression in memory Tregs compared to naïve Tregs was distinguished even cleared in this plot, with naïve Tregs having no CD71 expression, but memory Tregs showing a majority CD71$^+$ population (Figure 20C). In skin, a majority of Tregs had CD71 expression. In the fat, this was not the case, where a CD71$^-$ population could be seen, and overall expression of CD71 was lower compared to both fat and memory Tregs.

CCR5 expression in blood contradicted the LEGENDScreen™, because a CCR5$^+$ subpopulation could be seen in naïve Tregs (Figure 20D). This CCR5$^+$ subpopulation was still present in memory Tregs; however, it was shown to be much smaller than in naïve Tregs. In tissues, CCR5 expression could only be seen in a small subpopulation in the fat. In the skin, no CCR5 expression could be seen.

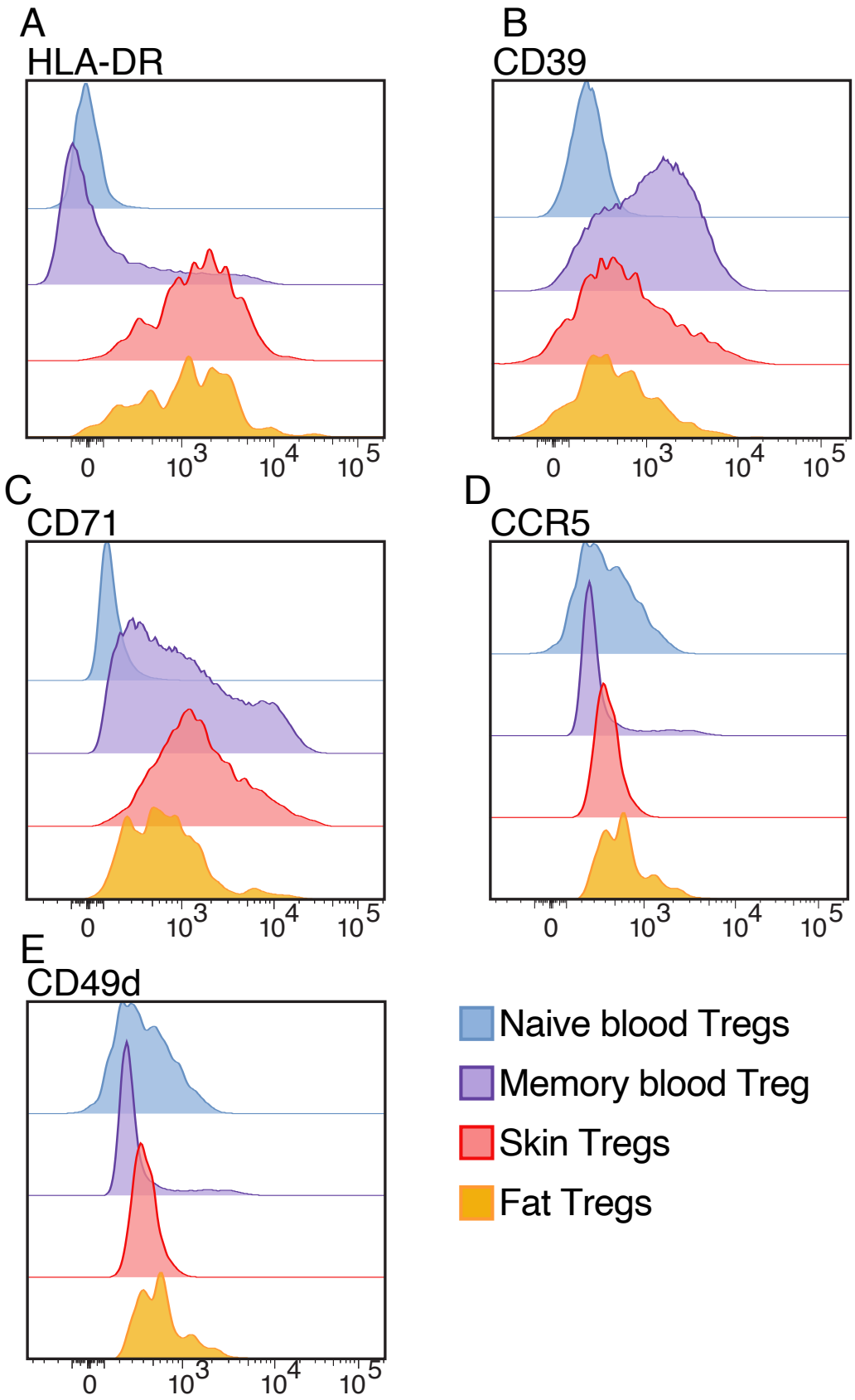

Figure 20. ***Surface markers expressed on CCR8+ Tregs in LEGENDScreen™ are also expressed on tissue Tregs.*** *Flow cytometry plots of Tregs from several tissues. Markers derived from LEGENDScreen™ were stained individually in tissues. Markers are listed above the plots. N=3 donors. Representative plots were chosen for all proteins.*

CD49d expression, however, did behave as it did in the LEGENDScreen™ (Figure 20E). Naïve Tregs had a larger subpopulation of CD49d$^+$ Tregs, whereas this population was much smaller in memory Tregs. In the skin, CD49d was completely absent in the skin, but not in the fat. In the fat, a small CD49d positive population could be seen.

Together, these data show that besides CCR8, HLA-DR and to an extent, CD71, could also reliably be used to identify tissue resident Tregs. The fact that these factors are both expressed on CCR8$^+$ Tregs in the blood as well as in tissues, increases the likeliness of a relation between CCR8$^+$ Tregs in the blood with tissue derived Tregs.

4.6. Single Cell TCR and RNA sequencing reveals clonality between CCR8$^+$ Tregs from peripheral blood and fat and skin derived Tregs

With the identification of multiple markers that are present on both CCR8$^+$ Tregs from the blood as well as tissue Tregs, came the question what the relationship between these populations entailed. To research this, the clonal relationship of the populations was examined. This is possible with T-cells due to their built-in barcoding feature, the TCR-sequence. To this end, different populations from the blood were sorted, namely: total CD4$^+$ cells (all CD4 T cells), CD4$^+$CD25$^+$CD127$^-$ cells (all Treg cells), CD4$^+$CD25$^+$CD127$^-$CD45RO$^+$ (all memory Treg cells) cells and CD4$^+$CD25$^+$CD127$^-$CD45RO$^+$CCR8$^+$ cells (CCR8$^+$ memory Treg cells). From skin and fat, CD4$^+$CD25$^+$CD127$^-$ were sorted as well. All these groups were subjected to single cell RNA sequencing (scRNA-seq) and single cell TCR sequencing (scTCR-seq). for 2 donors, all info from the same donor were combined, and UMAPs were generated for

each donor (Figure 21). Every group that was sorted was assigned its own colour (Figure 21A). For both donors, the blood populations grouped together, and the tissue populations grouped together. *FOXP3* was used to identify the Tregs in each of the plots (Figure 21B). *CCR8* expressing cells were found to colocalize was with *FOXP3* expressing cells in both donors (Figure 21B). The same was true for *HLADRB1* expressing cells, which colocalized with both *CCR8* expressing cells as well as *FOXP3* expressing cells (Figure 21C). Next, all TCR sequences derived from Tregs from fat and skin tissue were identified, and all corresponding cells with the same TCR sequences in blood were highlighted on a UMAP plot (Figure 21D). This UMAP shows that blood derived Tregs with a tissue Treg TCR are in the same place in the plot as Tregs expressing *CCR8* and *HLADRB1*, indicating a relation between these populations.

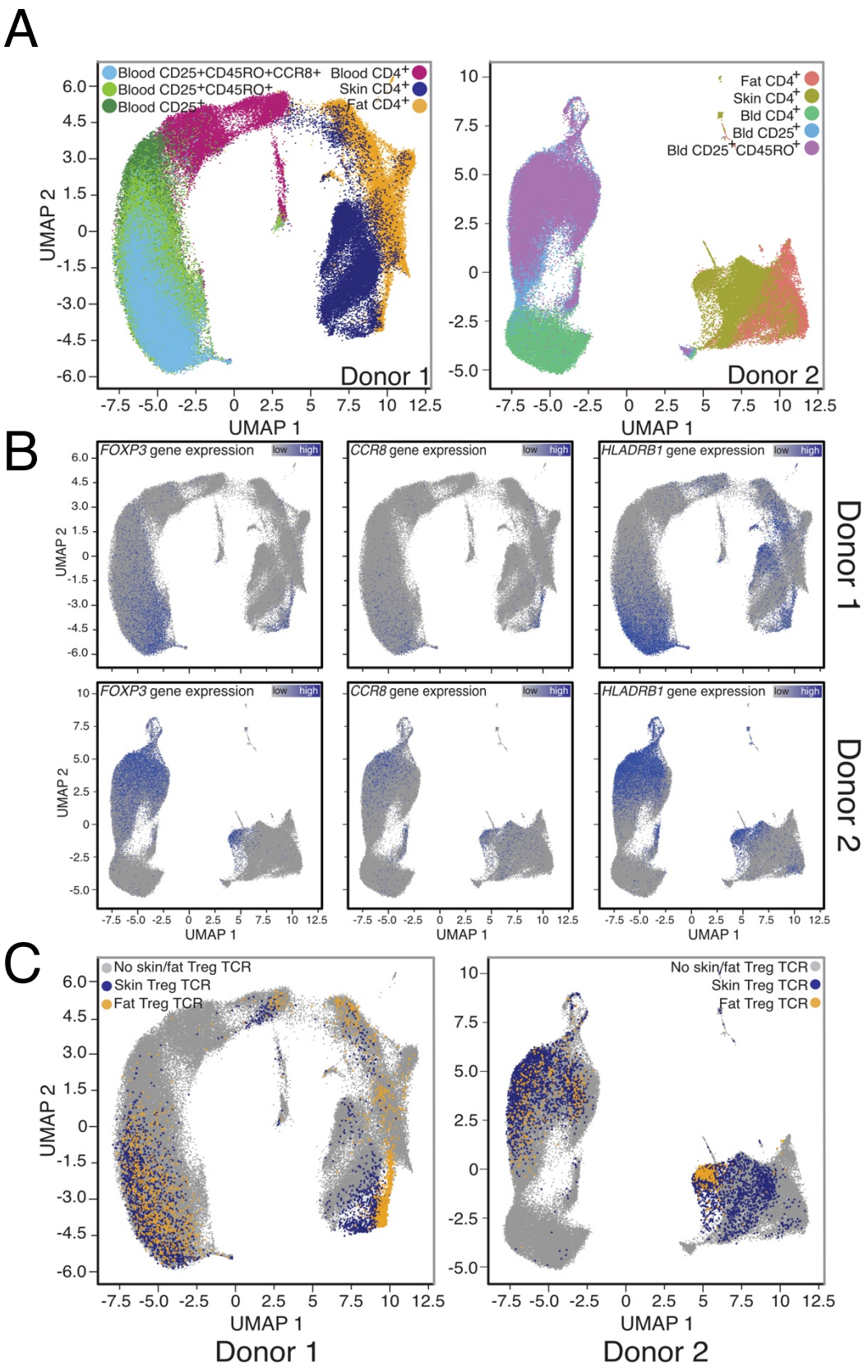

Figure 21. ***TCR-sequences from tissue Tregs can be found in CCR8⁺ Tregs in the blood.*** *A: UMAPs of scRNA-seq data from several CD4⁺ cell subpopulations. Each sorted populations was assigned its own colour. B: gene expression of FOXP3, CCR8, and HLADRB1. Genes listed inside of plots. Gene expression shown as colours, with blue = high and grey = low. C: TCR sequences from skin (blue) and fat (yellow) are highlighted. Bioinformatic analysis and UMAP generation was done by Malte Simon and Charles Imbusch (DKFZ).*

To be able to confirm this relationship, the amount of tissue TCR sequence clones present in the different blood derived populations was examined (Figure 22). For this experiment, one of the donors was selected.

Fat Treg derived TCR sequences accounted for 0,52% of all blood $CD4^+$ cells; 1,14% of blood Tregs; 1,62% of blood memory Tregs, and 4,42% of blood $CCR8^+$ Tregs (Figure 22A).

Skin TCR sequences accounted for 1,21% of all blood $CD4^+$ cells; 2,67% of blood Tregs; 3,61% of blood memory Tregs, and 7,18% of blood $CCR8^+$ Tregs (Figure 22B).

These data, from both donors, show a confirmation that there is a relation between $CCR8^+$ Tregs and tissue derived Tregs from both fat and skin.

A

B

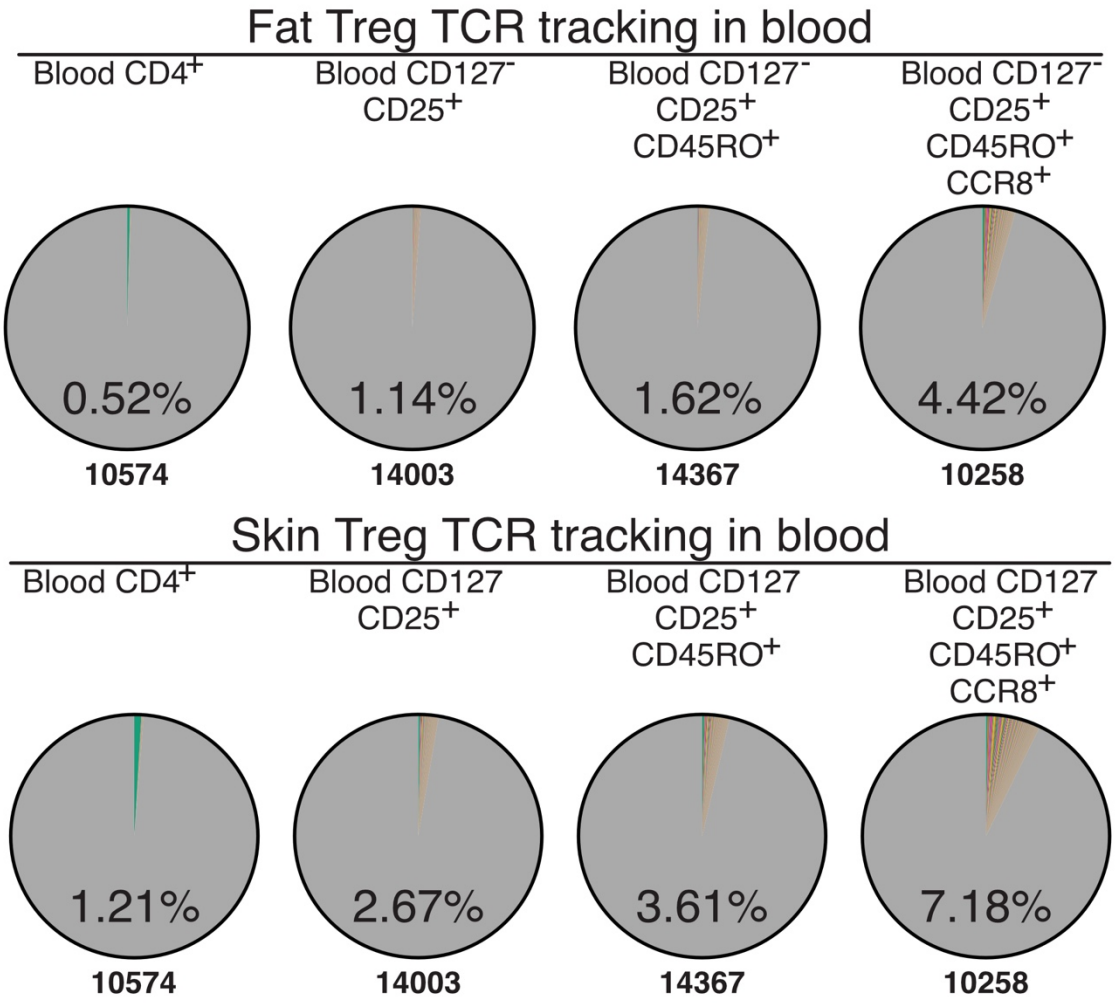

Figure 22. ***TCRs derived from fat and skin tissue Tregs are enriched in blood CCR8+ Tregs.*** *TCR sequencing from fat (up) and skin (down) were extracted and compared against blood CD4+ TCR sequences. Overlapping sequences were given a colour in the pie charts. Percentage indicates the share of overlapping sequences out of total. Total amount of TCR sequences shown below pie chart. Bioinformatic analysis and pie chart generation was done by Malte Simon and Charles Imbusch (DKFZ).*

4.7. A tissue-like phenotype can be induced in naïve human Tregs from peripheral blood using Tfh polarizing cytokines

4.7.1. A Tfh-like signature can be found in human tissue resident Tregs

Having identified human tissue resident Tregs on a single cell chromatin accessibility level, surface markers for their identification in tissue and a clonally related population in blood that share the same surface markers, the next question was whether a tissue-like profile could be induced, like in the mouse system. This had to be approached from a different angle, because where murine tissue Tregs had shown an obvious Th2 bias, this was not the case in the human system. What could be seen however, is that BATF played an important role in both, as indicated by the large amount of binding BATF binding sites on the shared peakset (Figure 10). Since BATF is also an important factor in T follicular Helper (Tfh) cell differentiation, this was an interesting profile to examine for tissue-like induction in naïve Tregs. In order to confirm this idea, a scATAC-seq dataset from a tumour identifying profiles of tumour T-cells was extracted (Satpathy *et al.*, 2019). This team found that this tumour harboured Tfh-like $CD4^+$ cells. The Tfh-signature of these cells was projected upon the scATAC UMAP showing healthy fat skin and blood CD4s (Figure 23A). This signature shows a clear increase in fat and skin tissue resident Tregs, supporting the idea that human tissue Tregs are Tfh-biased. This could also be confirmed on RNA level, by examining important transcription factors involved in Tfh differentiation (Figure 23B). *MAF* expression went up significantly in $CCR8^+$ Tregs compared to naïve Tregs. This level of *MAF* expression was equally high in both fat and skin Tregs. *BCL6*, the master transcription factor for Tfh differentiation, was upregulated in fat and skin Tregs, but not in $CCR8^+$ Tregs in the blood.

Typical surface markers for Tfh cells were also examined. *CXCR5*, the most common marker for Tfh cells, was found to be significantly downregulated on CCR8^{+} Tregs

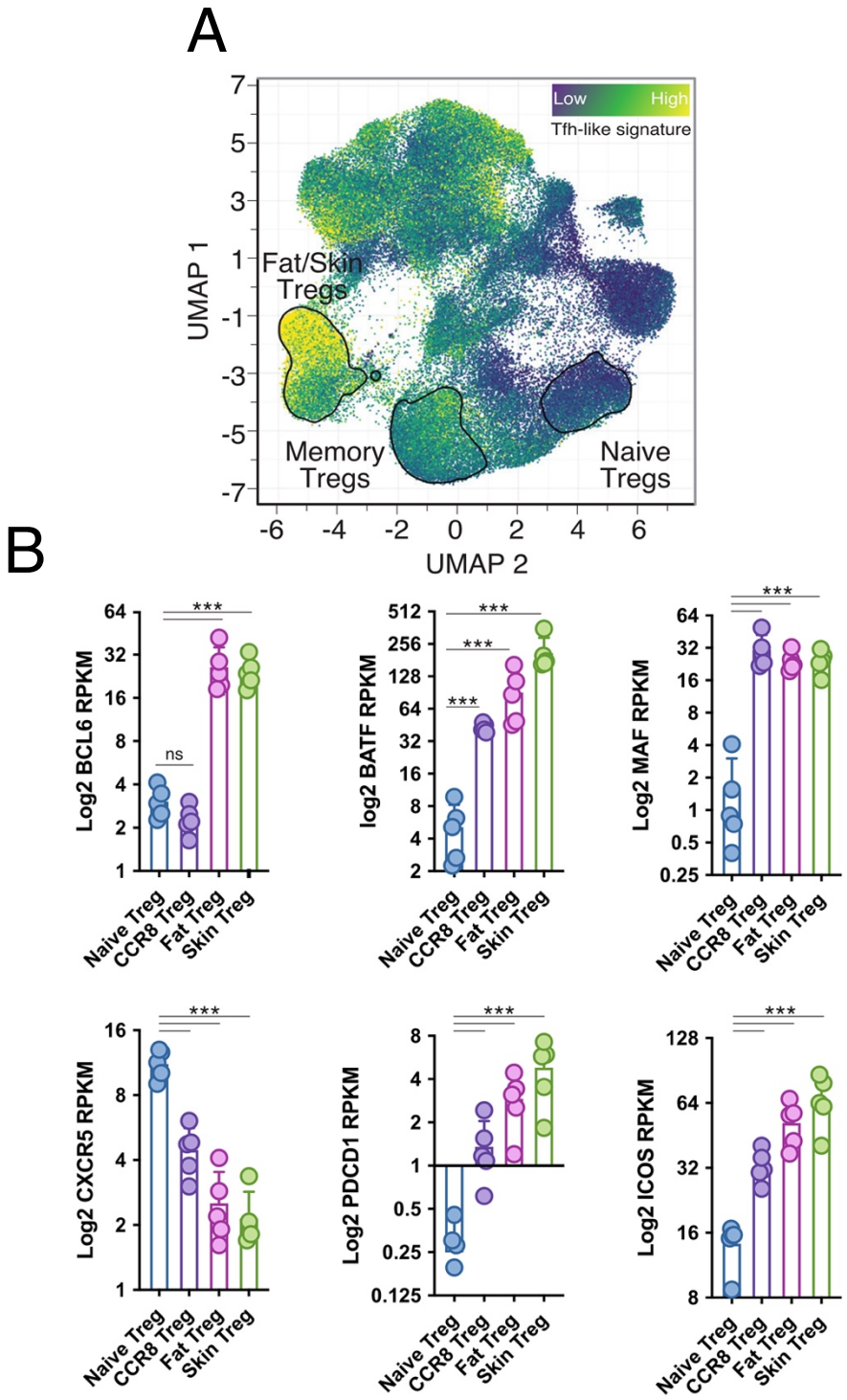

Figure 23. ***A Tfh-like signature can be seen in tissue Tregs.*** *A: UMAP of Tfh signature, counting 3,099 peaks. Tfh signature derived from literature (Satpathy et al., 2019). Populations of interest are circled. B: RNA-seq data of BCL6, BATF, MAF, CXCR5, PDCD1 and ICOS from several different tissues (N=5, Deseq2). UMAP was generated by Malte Simon (DKFZ). RPKM tables and Deseq2 table were generated by Agnes Hotz-Wagenblatt (DKFZ).*

compared to Naïve Tregs. The same was found to be true for fat and skin Tregs, indicating that tissue Treg cells are not identical to germinal canter Tfh cells.

PDCD1 (encoding for PD1), another Tfh expressed gene, and a marker for murine tissue Tregs and T-cell exhaustion in humans, was found to be significantly upregulated in CCR8^{+} Tregs compared to naïve Tregs. This expression level was increased in both skin and fat derived Tregs.

ICOS, another important surface marker for Tfh Cells, was, like *PDCD1*, upregulated in CCR8^{+} Tregs compared to naïve Tregs. this expression was also increased in fat and skin Tregs.

This data shows that human tissue Tregs have a Tfh-biased profile, which can be seen on both chromatin accessibility level as well as RNA level.

4.7.2. A Tfh-like signature can be induced form peripheral blood derived naïve Tregs

With the knowledge that human Tregs had a Tfh-biased expression profile, came the question if a Tfh-profile could be induced *in-vitro*. To investigate this, naïve blood derived Tregs were cultured with cytokines described to induce a Tfh-like phenotype (Qin et al., 2018). These cytokines were IL-2, TGFβ, IL-12, IL-21 and IL-23. Within this cocktail, TGFβ and IL-12 served to induce a Tfh phenotype, and IL-21 and IL-23 served to stabIL-ize this phenotype. Naïve Tregs were cultured for 5 days with this cocktail, or only with Th2 as a control. After 5 days, RNA expression of key Tfh Transcription factors *BATF*, *MAF* and *BCL6* was examined (Figure 24). In Tfh-like cultured cells, *BATF*, *BCL6* and *MAF* were all significantly upregulated, compared to the IL-2 only control. This shows that a Tfh-like program can be induced in naïve Tregs *in-vitro*.

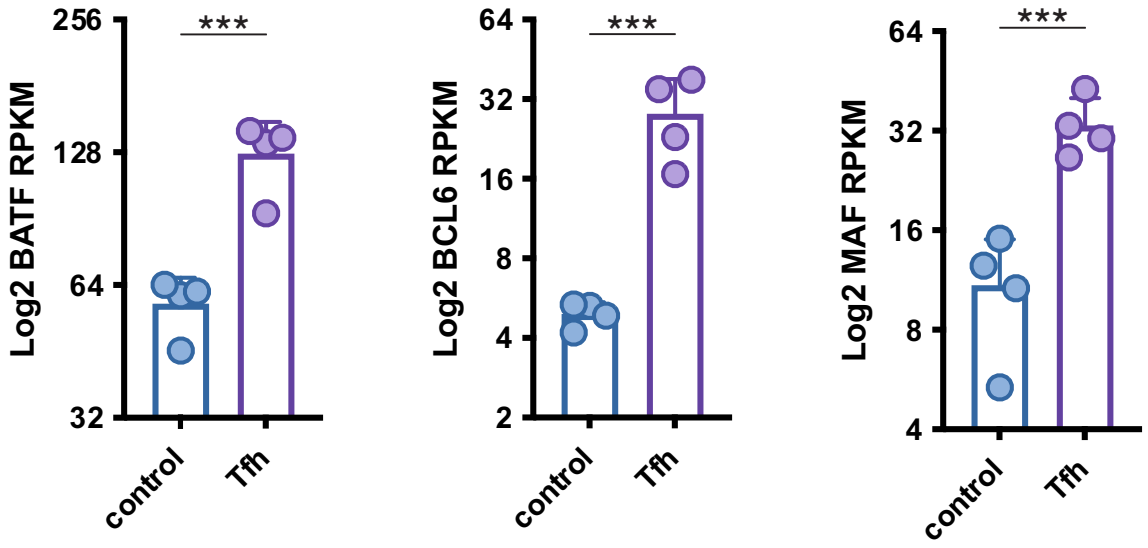

Figure 24. ***A Tfh phenotype can be iduced in-vitro.*** *Naïve Tregs were cultured with IL-2 or with IL-2, TGFb, IL-12, IL-21 and IL-23 for 6 days, and subsequently subjected to RNA-seq. RKPM values for BATF, BCL6, and MAF (N=4, Deseq2). RPKM tables and Deseq2 table were generated by Agnes Hotz-Wagenblatt (DKFZ).*

4.7.3. bulk ATAC sequencing shows that Tfh culture induces many of the same factors that are present in tissue resident Tregs

With a Tfh-like induction protocol established, the next step was to research how alike tissue derived Tregs and *in-vitro* generated Tfh-like were exactly. To research this, bulk ATAC-seq and bulk RNA-seq ofh Tfh-like Tregs and IL-2 only Tregs was carried out. Naïve Tregs were cultured for 6 days with either the Tfh inducing cocktail or IL-2 only as a control. Before the cultured Tregs were subjected to sequencing, a quality was carried out to insure Tfh induction (Figure 25). A portion of the cells was fixed and stained intracellularly for BATF, BCL6 and FOXP3, before and after culture. Both BATF and BCL6 expression was significantly upregulated in Tfh-like cells compared to IL-2 only cells (Figure 25A). FOXP3 expression was stable, with around 90% $FOXP3^{+}$ cells after culture in Tfh-like cells, and 95% in IL-2 only Tregs (Figure 25B).

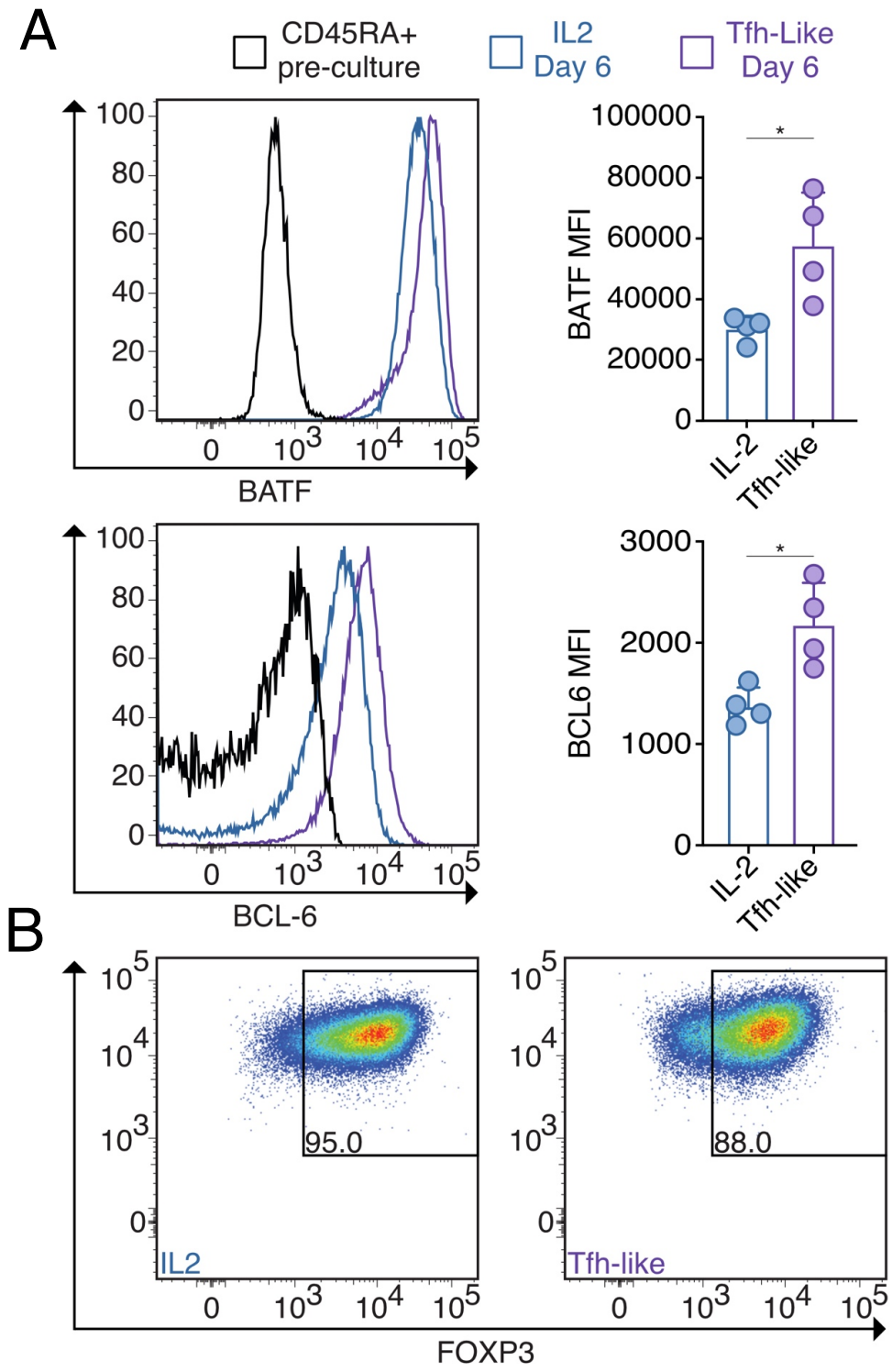

Figure 25. ***BCL6 and BATF are significantly higher in Tfh-like Tregs, while FOXP3 stays stable.*** *Naïve Tregs were cultured with IL-2 or with IL-2, TGFβ, IL-12, IL-21 and IL-23 for 6 days. A: left; flow cytometry plots for BATF and BCL6 for different conditions, listed above. Right; MFI for BATF and BCL6 (N=4, unpaired T-test). B: FOXP3 expression after 6 days of culture with cocktails named in the plots. Representative dot plots have been chosen.*

Once the cells passed the QC of BATF induction, BCL6 induction and FOXP3 stability, they were subjected to either ATAC or RNA sequencing (Figure 26). For both groups, gene expression profiles as well as chromatin accessibility profiles were established. About 4500 differentially expressed genes were identified between IL-2 and Tfh-like Tregs on an RNA level (Figure 26A). 2719 genes were upregulated in Tfh-like cells compared to IL-2 only cells. 1800 genes were downregulated in Tfh-like cells compared to IL-2 cells. *BCL6*, *BATF* and *MAF* were, as expected, all in the group of genes that was upregulated.

On a chromatin accessibility level, more than 17.500 differentially accessible peaks could be identified between Tfh-like and IL-2 Tregs (Figure 26B). 12623 peaks were present in Tfh-like Tregs that were not present in IL-2 Tregs. Multiple peaks each could be identified for *BCL6*, *BATF* and *MAF* within this group.

These results show that different gene expression profiles exist between these 2 groups, and that *BATF*, *BCL6* and *MAF* are part of the differentially expressed genes in Tfh-like cells, mirroring the tissue-derived Treg vs Naïve Treg data.

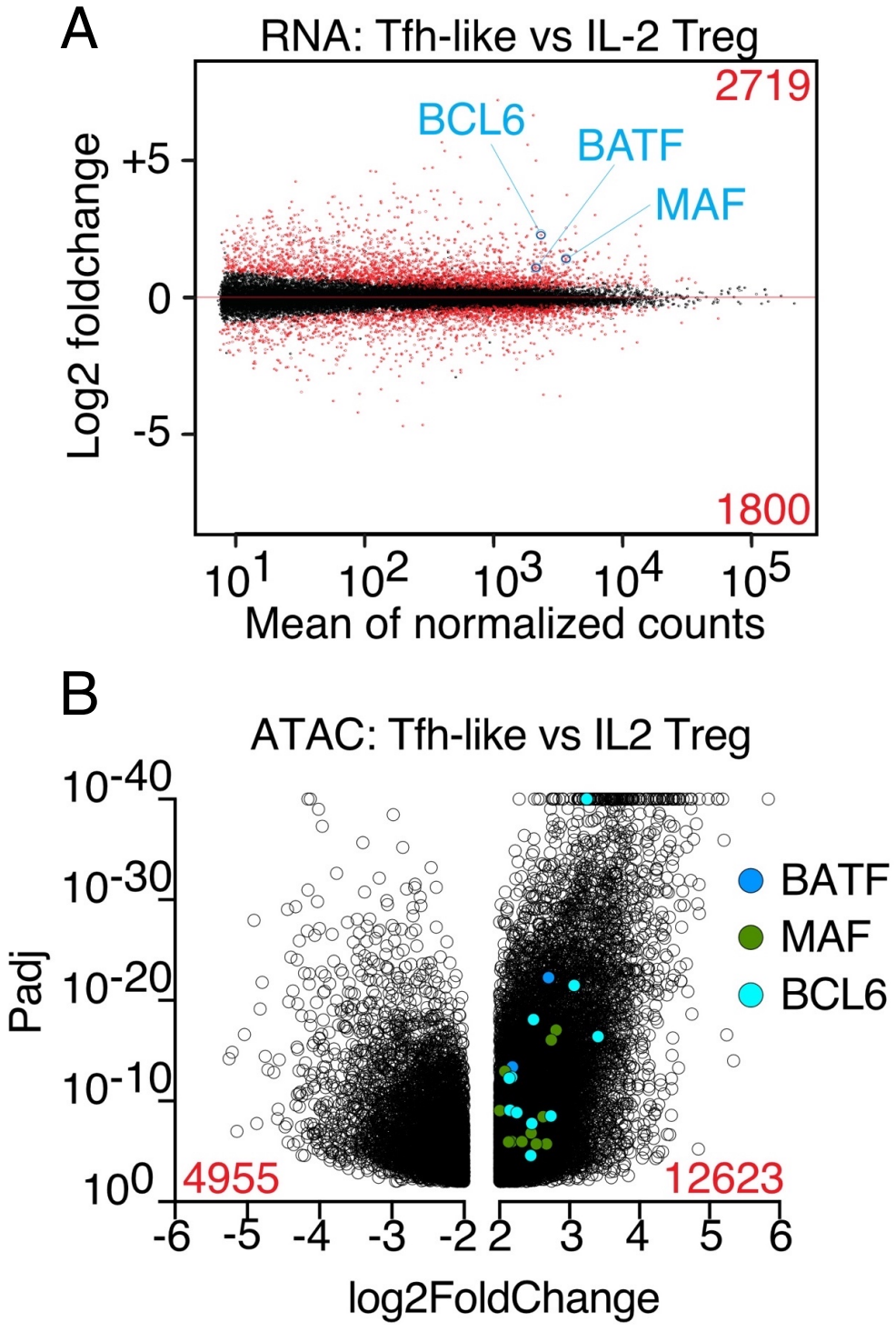

Figure 26. ***ATAC-seq an RNA-seq identify different factors induced in Tfh-like Tregs.*** *Naïve Tregs were cultured with IL-2 or with IL-2, TGFβ, IL-12, IL-21 and IL-23 for 6 days (N=4, Deseq2). Loci for BATF, BCL6, BATF highlighted. Bioinformatic analysis and plot generation was perfomed by Malte Simon (DKFZ) Agnes Hotz-Wagenblatt (DKFZ) and Michael Delacher (RCI/JGU).*

To investigate how many factors were shared between *in-vitro* induced Tfh-like Tregs and tissue derived Tregs from fat and skin, differentially expressed genes from RNA-seq from fat or skin vs naïve blood derived Tregs were plotted against differentially expressed genes from RNA-seq from Tfh-like vs IL-2 Tregs (Figure 27).

In total, 228 genes were upregulated in both Tfh-like Tregs as well as skin derived Tregs (Figure 27A). among these were *BCL6*, *BATF* and *MAF*. Other factors included *PDGFA* (platelet-derived growth factor alpha), which is a factor that induces proliferation in fibroblasts, and *GRN*, which encodes for progranulin, a granulin precursor. Granulin has been implicated in cell proliferation, wound healing and tumorigenesis (Bateman et al., 2018). Two interesting families of genes that have been upregulated are the MMPs (matrix metalloproteinases) and the ADAMs (disintegrin and metalloproteinases). Proteins encoded by these 2 families of genes are involved in extracellular matrix reorganisation.

The same comparison was made for fat derived tissue Tregs vs Naïve Tregs and Tfh-like Tregs vs IL-2 Tregs (Figure 27B). In total, 219 genes were upregulated in fat derived tissue Tregs and Tfh-like Tregs. Once again, *BATF*, *BCL6* and *MAF* were part of this group of genes. Other genes that were upregulated in the skin were present like *PDGFA* and *GRN*. MMPs and ADAMs were also represented within these 219 genes.

These data show that *in-vitro* induced Tfh-like Tregs share similarities with tissue resident Tregs from both fat and skin. Upregulated genes in all 3 groups have been shown to be involved in development, as well as tissue remodelling and repair.

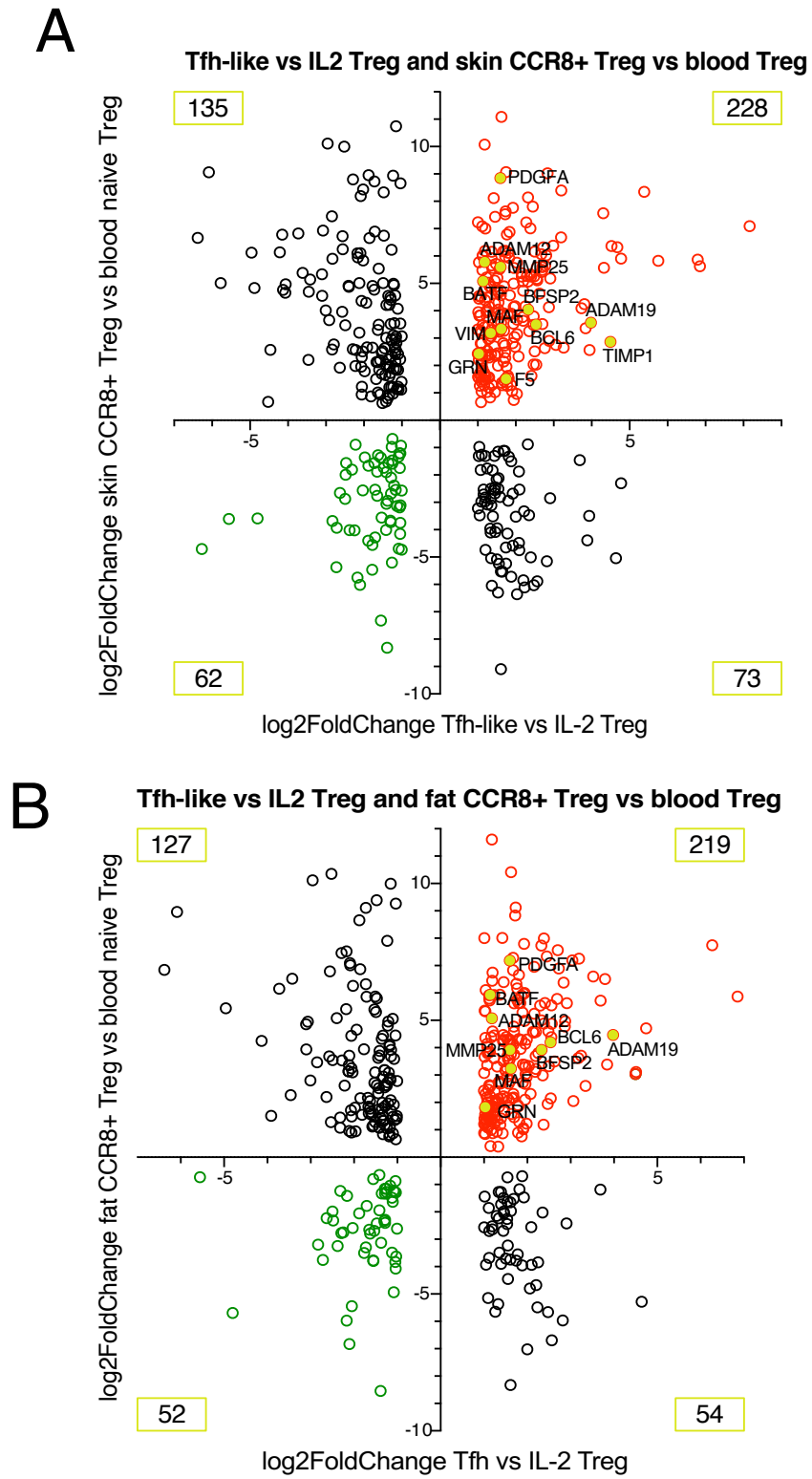

Figure 27. ***ATAC-seq identifies shared factors between tissue derived Tregs and Tfh-like Tregs.*** *RNA-seq data of skin Tregs (A) or fat Tregs (B) vs naïve blood Tregs compared to IL-2 vs Tfh-like. Number of loci that gain accessibility in boxes within each quadrant. Bioinformatic analysis performed by Malte Simon (DKFZ) and Michael Delacher (RCI/JGU).*

4.8. Tregs cultured with Tfh polarizing cytokines produce supernatant that is superior at wound healing

Having identified a Tfh induction protocol that induces factors in naïve Tregs that can also be found *in-situ* in tissue derived Tregs, the question was to investigate whether these Tfh-like Tregs had wound healing capacities. This was especially interesting, since many of the factors that were shared between tissue Tregs and Tfh-like Tregs were related to wound healing and proliferation (Figure 28). To examine this, a scratch wound healing assay was performed. Naïve Tregs were cultured for 6 days, with either Tfh inducing cytokines or IL-2 only. This was followed by washing steps to get rid of any traces of added cytokines. Cells were provided with TCR stimulation overnight, in order to produce factors to secrete into the environment. The supernatant of this overnight culture was collected and added to HaCaT cells. These HaCaT cells had been seeded in 96 wells plate, at 10.000/well and were allowed to grow overnight. Shortly before supernatant addition, HaCaT cells were wounded with a woundmaker™ (Essen Bioscience). HaCaT cells were observed for 72 hours in an IncuCyte™ (Essen Bioscience), which was programmed to take a picture of each well every hour. As a control, TexMACS© medium (Miltenyi), which the Tregs had been cultured in, was added to HaCaT cells as a separate condition. In the first 24 hours, no significant difference between the groups could be observed. After 24 hours however, supernatant from Tregs with a Tfh-like profile was significantly superior at mediating wound healing compared both supernatant from IL-2 only Tregs as well as the TexMACS© only control (Figure 28A). After 36 hours, the wound had already closed in Tfh-like wells, whereas wound healing was still in progress in the IL-2 wells (Figure

28B). No significant difference between IL-2-only Treg supernatant and the TexMACS© only control could be observed.

These data show that Tfh-like Tregs produce factors that mediate wound healing and are superior at wound healing compared to IL-2 only Tregs.

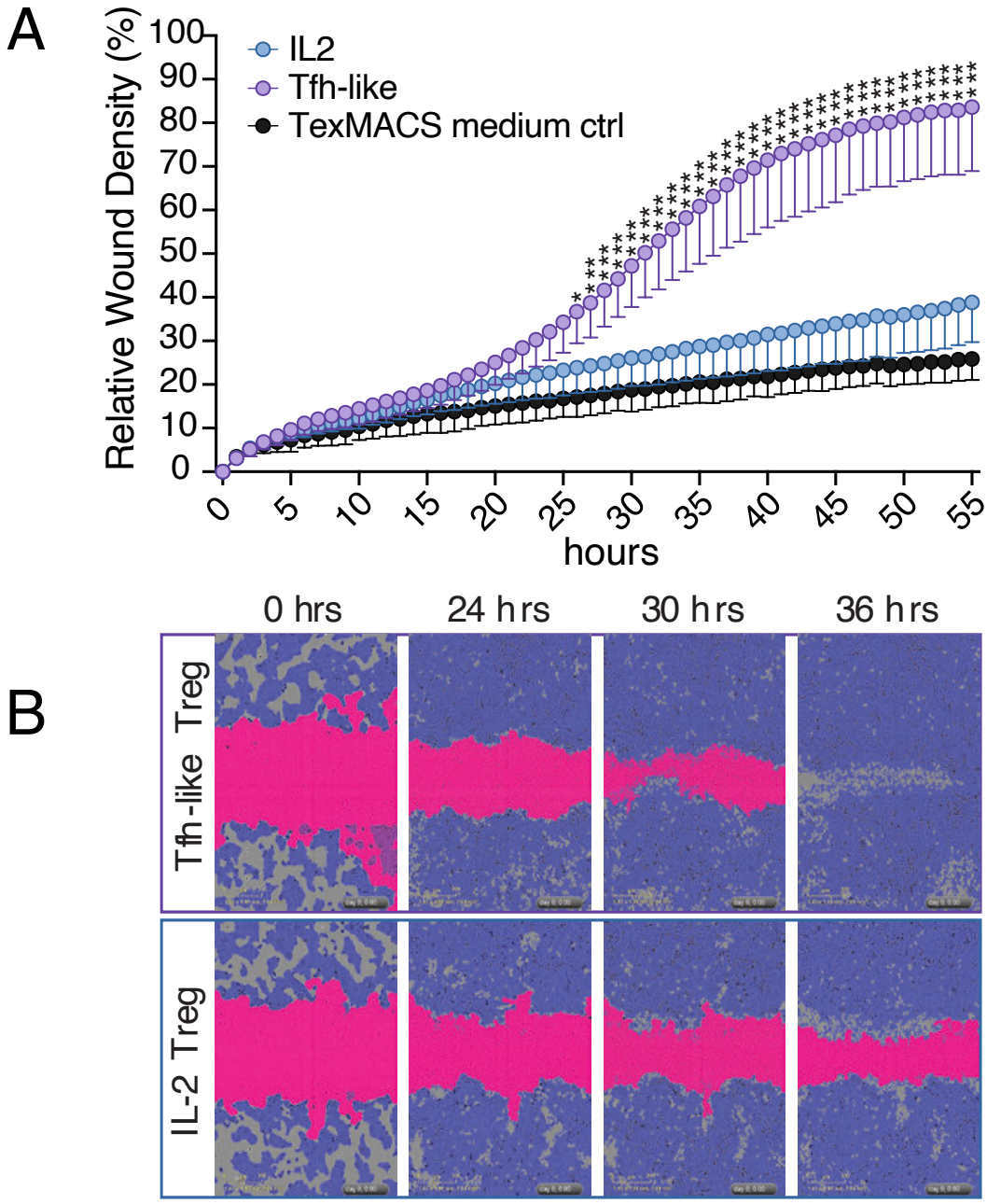

Figure 28. ***Tfh-like Tregs are superior at woundhealing compared to IL-2 Tregs in scratch wound assay.*** *Naïve Tregs were cultured with IL-2 or with IL-2, TGFb, IL-12, IL-21 and IL-23 for 6 days, washed, and given TCR stimulation overnight. Treg culture supernatant was diluted 1:8 and given to wounded HaCaT cells. Cells were monitored for 55 hours (N=5 donors, unpaired T-test).*

To strengthen these claims, and to study the effect of this Tfh-like Tregs supernatant on human skin repair, an open-sourced reconstructed epidermis (OSREp) model was used (Figure 29). Experiments with these models were performed by Florian Groeber-Becker and Verena Scheider (Frauenhofer ISC), as follows; human keratinocytes were cultured on a polycarbonate membrane and formed models of a physiological human epidermis containing all layers found in an adult human epidermis (Groeber et al., 2015). After these models had formed, they were punched, resulting in a hole that was 2mm in diameter. Trans-epithelial electrical resistance (TEER) was used to keep track of wound healing, and a baseline measurement was performed after the initial punch. All following TEER measurements were normalized to this baseline. 3 models were used per condition; No supernatant, IL-2 Treg Supernatant, or Tfh-like supernatant, and combined supernatant of 4 donors was applied to each model. Two days after wounding, no difference between the condition in TEER measurements could be seen yet (Figure 29A). However, 4 days after wounding, models which had received Tfh-like supernatant showed significantly increased TEER100hz values compared to both control conditions. This increase in wound healing compared to both control conditions stayed significant until the end of the assay, at 7 days after wounding.

After 7 days, histological analysis of the stratum corneum was performed (Figure 29B-C). for quantitative analysis, the surface area (μm^2) of the stratum corneum was normalized to the 2mm punch. After 7 days, the surface area of models that received Tfh-like supernatant was significantly larger compared to both control groups.

These data show that Tfh-like supernatant is superior in mediating wound-healing both in cell lines, as well as human epidermis skin models.

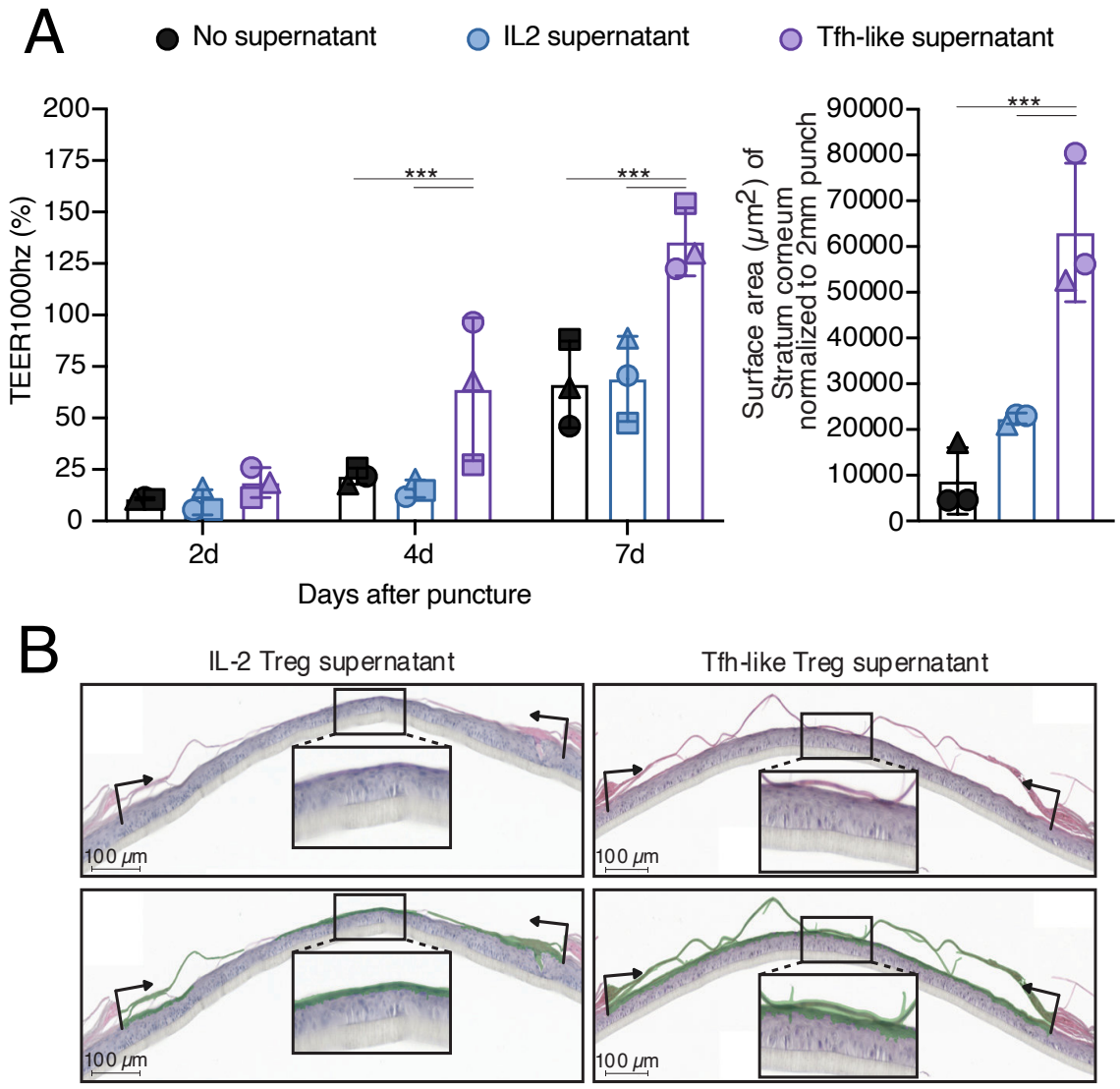

Figure 29. ***Tfh-like Tregs are superior at woundhealing compared to IL-2 Tregs in primary human keratinocytes.*** *Naïve Tregs were cultured with IL-2 or with IL-2, TGFβ, IL-12, IL-21 and IL-23 for 6 days, washed, and given TCR stimulation overnight. Treg culture supernatant was diluted 1:8 and applied to reconstructed human epidermis models, which had been punched shortly before. A: left; electrical impedance, right; stratum corneum surface area (N=3 models composed of 4 donors each, ANOVA). B: histology of epidermis after assay. Green identifies regrown epidermis after punch. Experiments, analysis and Histology performed by Florian Groeber-Becker, Verena Scheider (Frauenhofer ISC) and Uwe Ritter (RCI).*

4.9. Tumour resident Tregs share commonalities with healthy tissue resident Tregs.

Having identified factors that contribute to a wound healing phenotype in tissue resident Tregs, as well as surface factors to identify these cells, it became increasingly clear that many of these factors had previously been identified as being exclusive to tumour Tregs. CCR8 had already been identified as a marker for Tregs in multiple different human tumours (Alvisi et al., 2020; De Simone et al., 2016; Plitas *et al.*, 2016). Indeed, many of the factors shared by Tfh-like Tregs and tissue Tregs are also involved in tumourigenesis. This led to the question, how alike tumour Tregs and healthy tissue resident Tregs were exactly. To address this question, Tregs from healthy skin and fat, as well as matching blood, were compared to Tregs from Hepatocellular Carcinomas (HCCs), normal tumour adjacent liver tissue (NAT), and matching blood. First, comparisons were made through flow cytometry, and compared populations were sorted and subjected to RNA sequencing.

In blood from healthy donors as well as tissue donors, a $CCR8^+$ population in the blood could be seen, that was present in $CD45RA^-$ Tregs (Figure 30). Shifting the focus to skin and fat, the data showing that a majority of tissue Tregs express CCR8, could once again be repeated. In NAT this number was slightly less, with 47,8% $CCR8^+$ Tregs. in HCC however, the same could be seen as in healthy fat and skin, with a majority of Tregs being $CCR8^+$.

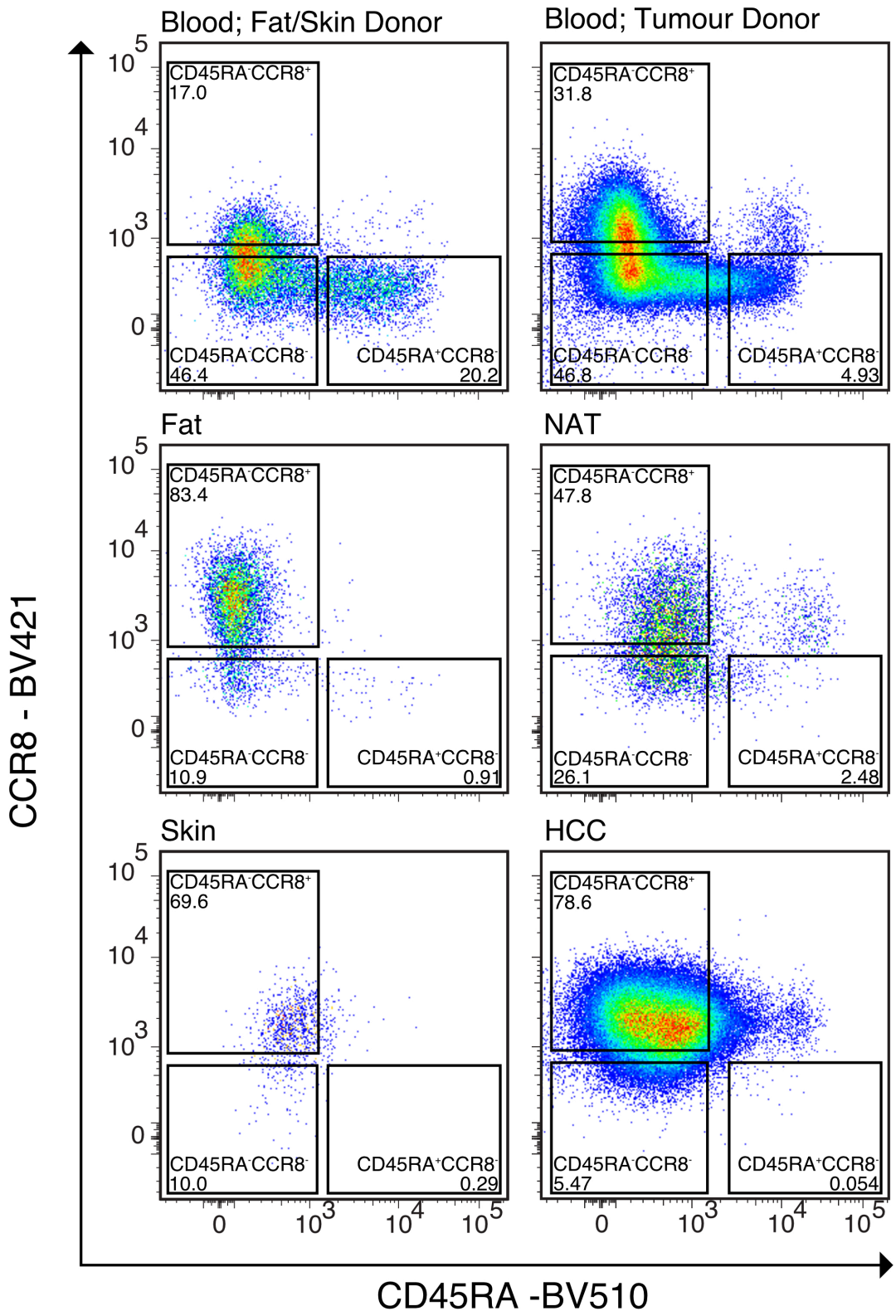

Figure 30. ***CCR8 expression in Tumour tissue looks comparable to healthy tissue.*** *Flow cytometry plots of CCR8 vs CD45RA expression in Tregs from several tissues. Tissues are listed above the plots. NAT = Normal tumour Adjacent Tissue. HCC = Hepatocellular carcinoma.*

These results could be repeated in multiple donors. HCC, skin and fat all had a significantly higher percentage of CCR8^{+} cells compared to blood. however, no significance could be found among the tissue and tumour groups (figure 31).

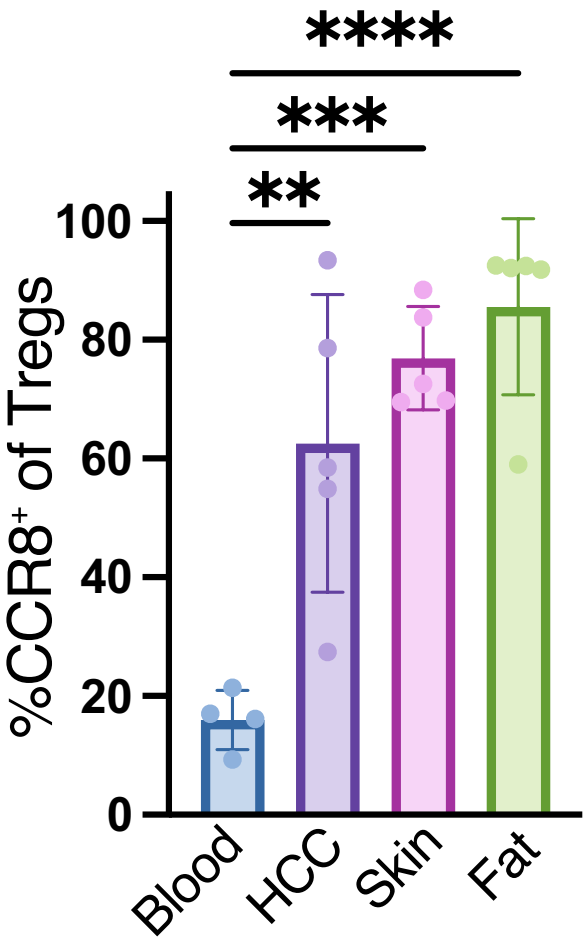

Figure 31. ***CCR8 expression is similar in HCC and tissues.*** *Quantification of percentage of CCR8 expressing cells found in blood, HCC, skin and fat. N=4 donors for blood, N=5 donors for HCC, skin and fat. One-way ANOVA.*

The populations shown in figure 30 were sorted and subjected to RNA sequencing, to allow for deeper, more thorough comparison (Figure 32).

First, blood CD45RA$^-$ Tregs and NAT CCR8$^+$ Tregs from the same donor were separately compared to tumour CCR8$^+$ Tregs (Figure 32A). In total, more than 1900 Differentially expressed genes could be identified between CD45RA$^-$ blood derived Tregs and CCR8$^+$ tumour Tregs. 1307 genes were upregulated in tumour Tregs vs blood CD45RA$^-$ Tregs. Among these upregulated genes were genes that were also identified in tissue Tregs; *PDCD1*, *HLADRA*, *BATF*, *BCL6* and *CCR8*.

Next, NAT CCR8$^+$ Tregs were compared to Tumour CCR8$^+$ Tregs (Figure 32A). These 2 populations were almost identical, with 17 identifiable differentially expressed genes between the 2 populations. None of those 17 genes were the ones previously mentioned, that were upregulated in tumour CCR8$^+$ vs blood CD45RA$^-$ Tregs.

To further examine the overlap between tumour Tregs and healthy tissue Tregs, a healthy tissue Treg signature was calculated from RNA-seq data from skin and fat Tregs (Figure 32B). This signature was plotted for all sorted population and plotted out in a heatmap. While a sizeable overlap in gene expression could be seen between fat, skin, NAT and HCC, the same could not be observed for CD45RA$^-$ or CD45RA$^+$ populations from the blood. To confirm this, a tumour signature was established in the same way, from CCR8$^+$ Tregs derived from the tumour. This signature showed similar findings.

These data show that healthy tumour resident Tregs are indeed very similar to Tumour Tregs, on a surface marker level, as well as on gene expression profile level.

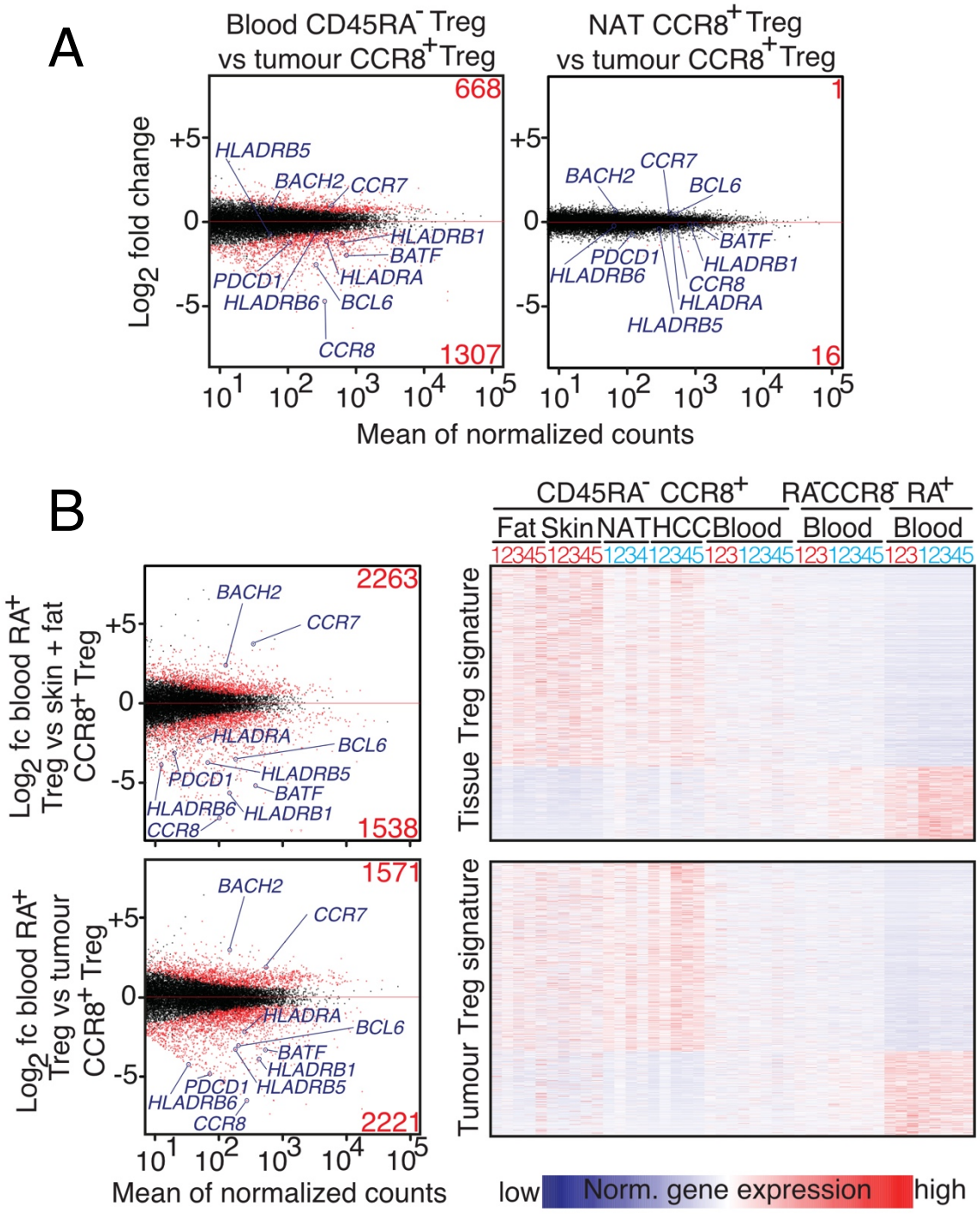

Figure 32. ***RNA-seq identifies virtual indistinguishabIL-ity between normal liver and tumour Tregs.*** *A: left; differentially expressed genes between blood CD45RA- Tregs and tumour Tregs. right; differentially expressed genes between normal tumour adjacent liver Tregs and tumour Tregs. B: top; differentially expressed genes between naïve Tregs and tissue Tregs, with heatmap of healthy tissue signature. Bottom; differentially expressed genes between naïve Tregs and Tumour Tregs, with heatmap of tumour signature. N=10 donors. Bioinformatic analysis and figure generation was performed by Malte Simon and Agnes Hotz-Wagenblatt (DKFZ).*

5. Discussion

Tregs are an integral part of the immune system, in that they modulate the immune response to avoid autoimmunity. Tregs are the main agents in controlling immune responses in peripheral immunity and can migrate to tissues to become tissue resident Tregs. Tregs that have migrated to the tissue gain different functionalities compared to their lymphoid tissue counterparts, on top of the classical Tregs functions. Murine Tissue resident Tregs have been studied and have been shown to aid in healing after infection (Arpaia *et al.*, 2015) and tissue injury (Burzyn *et al.*, 2013). Batf has been shown to be the main transcription factor for tissue phenotype differentiation in mice (Delacher *et al.*, 2020). Murine Tregs have, all in all, been well studied in the murine system (Delacher *et al.*, 2017; Delacher *et al.*, 2019; Schmidl *et al.*, 2018). The human counterpart of this population, however, remained poorly understood. A few studies have addressed Tregs in tumours (Azizi *et al.*, 2018; Plitas *et al.*, 2016; Sakaguchi *et al.*, 2020; Szabo *et al.*, 2019), and in healthy tissue (James et al., 2020; Miragaia et al., 2019; Wu et al., 2019) but the repair capacity of human tissue Tregs has not yet been studied. In this study, we performed single cell studies to characterise human tissue Tregs. We looked at chromatin accessibility of Tregs derived from skin, fat, colon lungs and spleen from mice, and Tregs derived from skin, fat and blood from humans and established a tissue signature for both. This allowed us to compare these signatures and identify shared factors.

With this knowledge, we set about trying to track potential progenitor Tregs in the blood and found a clonal relationship between CCR8^{+} Tregs in blood and tissues.

In other experiments using this newly acquired dataset, we found that human tissue Tregs upregulated many classical Tfh factors. This led us to induce a Tfh phenotype

in naïve blood derived Tregs and examine their wound healing capacity. We found that Tfh-like Tregs are superior at mediating tissue regeneration compared to IL-2 only Tregs.

Lastly, we compared tissue Tregs from healthy tissues to tumour derived Tregs and found many shared factors between the two groups.

5.1. Tissue repair program cannot be initiated *in-vitro* in BATF$^{-/-}$ mice

Previously, Batf had been identified as one of the major factors involved murine tissue Treg development (Delacher *et al.*, 2017). In BATF$^{-/-}$ mice, a los of tissue resident Tregs has been described by our lab and by others (Hayatsu et al., 2017). In tissue Treg progenitor cells, a large subset of genes that gains accessibility in tissue Tregs are direct targets of Batf, including *Il1rl1* (ST2), *IL10*, and *Pparg* (Delacher *et al.*, 2020). It has also been shown that Batf modulates the Th2 locus control region (Li and Rudensky, 2016), with this this knowledge, we wondered if BATF was necessary for tissue phenotype inducting *in-vitro*. We found that a cytokine mix of IL-4 and IL-33 successfully induced a tissue-like phenotype, where many of the same factors were induced as can be found in tissue derived Tregs. this aligns with the knowledge that murine tissue Tregs are Th2 biased, since IL-4 is responsible for inducing a Th2 profile In CD4 tissues (Gadani et al., 2012). IL-33 is the ligand for ST2, thereby explaining the induction of ST2, as the ST2/IL-33 axis has been shown to be a positive feedback loop (Griesenauer and Paczesny, 2017). However, we found that a combination of IL-4 and IL-33 led to a stronger induction of ST2, suggesting that IL-4 may increase the effect of IL-33 on ST2 expression. It has also been shown that IL-33 is essential for

development and maintenance of murine VAT Tregs, which validated our results (Vasanthakumar *et al.*, 2015).

When this protocol was applied to both BATF$^{-/-}$ and WT Tregs, ATAC sequencing revealed that many of the loci that gain accessibility in WT Tregs treated with IL-4^{+}IL-33, did not gain accessibility in BATF$^{-/-}$ Tregs treated with the same cocktail. Indeed, BATF$^{-/-}$ Tregs treated with this cocktail bore more similarities to WT Tregs treated with IL-2, than with WT Tregs treated with IL-4/IL-33, based on chromatin accessibility data. Looking at specific gene loci, the same could be shown. This could be explained by the fact that these loci all had BATF binding sites. Indeed, WT Tregs treated with IL-4^{+}IL-33 had similar looking peaks to VAT derived Tregs. From this, we can conclude that BATF is essential in the induction of a tissue program both *in-vivo* and in vitro.

5.2. Human tissue Tregs can be recognized by surface molecules classically associated with tumour infiltrating Tregs.

In recent years, a handful of studies Tregs in tissue context have been performed (James *et al.*, 2020; Miragaia *et al.*, 2019; Wu *et al.*, 2019). However, most of them have been focused on Tregs in the context of the tumour microenvironment (Azizi *et al.*, 2018; Plitas *et al.*, 2016; Sakaguchi *et al.*, 2020; Szabo *et al.*, 2019), and so, most of the factors that have been identified on tumour derived Tregs have been described as tumour specific Treg markers. Here, we show a healthy human Treg signature containing many of the factors. Many of these studies postulate that Tregs infiltrate the tumour and then gain these factors due to their interaction with the tumour environment (Cinier et al., 2021). Some of these factors are exhaustion markers, like PD-1 (Ishida *et al.*, 1992), that are claimed to be induced because of the high state of

activation induced in the tumour microenvironment. However, we suggest that these markers might be upregulated not due to exhaustion, but to induce senescence in order to induce tolerance in tissue Tregs, and possibly other tissue resident T-cells, and redirect them towards other functions that expand upon the functions already present, like wound healing. We have found that multiple surface receptors that have been described as tumour specific, like CCR8, TIGIT, ICOS and CD39 to also already be present on Tregs derived from healthy human tissue. Our findings suggest that this makes these Tregs not Tumour specific, but tumour specific.

A high number of Tregs present in the tumour is often associated with a poor prognosis (Ménétrier-Caux *et al.*, 2012; Tanaka and Sakaguchi, 2017) except for in a few cases. It has been shown that T-cells with high FOXP3 expression correlate to a poor prognosis, and T-cells with a low FOXP3 expression are associated with a good prognosis (Saito *et al.*, 2016). It has been suggested that this is because $FOXP3^{lo}$ T-cells are activated T-cells and as opposed to Tregs, which might very well be true. However, there might be more to the story. Our data show that human tissue Tregs have a higher FOXP3 expression compared to their lymphoid counterparts. Tissue Tregs also secrete many factors that contribute to tissue remodelling. This could also contribute to the poor prognosis associated with $FOXP3^{hi}$ Tregs in tumours, since they would both suppress the immune response and help the tissue grow. The fact that this is especially the case in Colorectal cancer is telling, since it has been described that iTregs play a large role in immune modulation in the colon (Murphy *et al.*, 2017). Our data suggests that tissue Tregs with tissue remodelling capabilities are thymus derived, and thus not induced in the periphery. iTregs could potentially have a lower level of FOXP3 expression, and no tissue remodelling capabilities. This might be

another explanation for the different prognoses depending on which tissue the tumour resides in, and the level of Tregs in these tissues and tumours. However, this is just speculation, and would need to be further researched.

CCR8$^+$ Tregs have been described as drivers of immune suppression in experimental autoimmune encephalitis (EAE), an experimental model of Multiple Sclerosis. They do this by acting through the CCL1-CCR8 axis, which increases production of IL-10, CD39, and granzyme B (Barsheshet et al., 2017). The authors claim these cells ameliorate EAE solely through immunosuppression. However, since our data suggest that tissue Tregs secrete many factors that are associated with tissue remodelling, this axis may exact a similar function to the IL-33-ST2 axis in murine Tregs, which leads to the production of wound healing factors, like amphiregulin (Arpaia *et al.*, 2015). This could suggest that immunosuppression is not the only process leading to the amelioration of EAE. This question, however, would require further study.

Blood derived CCR8$^+$ Tregs have also been described as tumour progenitors (Wang et al., 2019). However, after performing TCR tracking of CCR8$^+$ cells from skin and fat in the blood, we have found a connection between those populations, suggesting that CCR8$^+$ Tregs in the blood may either be progenitors that are poised to travel to the tissue, or recirculating tissue Tregs. Either way, they are also present in healthy tissue, and our data suggest they are more likely to be tissue specific than tumour specific.

One population of human Tregs that has been described are the so-called ‘fraction II’ or 'effector’ Tregs (Sakaguchi *et al.*, 2020). This population was described to have a heightened expression of both CD25 and FOXP3, as well as an increased

suppressive capacity. From our data, we see that CCR8^{+} Tregs in blood also have an increased expression of CD25 and FOXP3 compared to other blood derived Tregs. This suggests that CCR8 Tregs may also be part of this population, especially since Barsheshet et al. also described this population as having increased suppressive capacity.

From these data, we can conclude that human tissue Tregs, derived from healthy tissue Tregs share many features with Tregs found in the tumour microenvironment. This raises the question, is the phenotype we see in tumour derived Tregs truly due to exhaustion from being in the tumour microenvironment, or is it always induced when Tregs migrate to the tissue? Our data suggest the latter, but more research needs to be done to validate this.

5.3. The human tissue Treg signature is Tfh biased and *in-vitro* induced Tregs are superior at wound healing.

Recently, a study has been published that assigned signatures of different known subsets of T-cells to skin tumour derived T-cells (Satpathy *et al.*, 2019). The tumour resident Tregs in this study were found to have a Tfh-like signature. From what we have learned from our data, there was a possibility this is not just tumour specific, but tissue specific. Indeed, our data show that tissue Tregs in healthy skin and fat also have a Tfh-like signature. Multiple factors that have been classically associated with Tfh cells, like BCL6, BATF, MAF, IOCS, and PD-1, are upregulated in tissue Tregs compared to blood Tregs (Qin *et al.*, 2018). CCR8^{+} Tregs also show an upregulated Tfh-like profile, further strengthening the theory that these two populations of cells are related.

A population of Tregs, called T follicular regulatory cells (Tfr cells), has recently been described (Wollenberg et al., 2011). This population of cells is responsible for regulating germinal center (GC) responses, by repressing proliferation of both Tfh cells and B cells. Like Tfh cells, Tfr cells express high levels of CXCR5, as well as PD-1 and ICOS. They can also express BCL-6, the master TF for Tfh induction. These cells are derived mostly from tTregs, with only a small amount induced in the periphery. These cells seem to have a lot in common with our tissue Tregs. however, our data show that human tissue Tregs, even though they have a Tfh-like signature, do not express CXCR5, a key marker for both Tfh cells and Tfr cells (Xie and Dent, 2018). This suggests that these 2 populations are not the same population, but rather similar, but different, populations of Tregs specialised to their own tissue environment.

We could also show a successful induction of a Tfh-like phenotype in vitro. A combination of IL-2, TGFβ, and IL-12 has been described to induce a Tfh progam in $CD4^+$ cells, and IL-21 and IL-23 have been described as Tfh stabilising cytokines, through their upregulation of BCL6. Our data confirmed this on both chromatin accessibility level as well as RNA level. A large of shared factors could be identified between tissue Tregs and *in-vitro* induced Tfh-like Tregs. Many of these shared factors belonged to a group of proteins involved in wound healing and tissue remodelling (Bateman *et al.*, 2018; Verma and Hansch, 2007; Wolfsberg et al., 1995), suggesting that these *in-vitro* generated cells may also have a wound healing capability. We could confirm in 2 separate models, that this is in fact the case. *In-vitro* induced Tfh-like Tregs secrete factors into the supernatant that increases wound healing capacities of both a human skin keratinocyte cell line as well as a primary human epidermis.

5.4. The future of tissue Tregs in clinical applications

Allogeneic bone marrow transplant has been a treatment option for multiple haematologic diseases for multiple decades (Majhail et al., 2015). Donor, or graft, derived T cells can mediate the graft-versus-Leukemia effect (GvL) and enable stem cell engraftment (Horowitz et al., 1990). Allogeneic BMT however, has not been without complications, as graft T-cells can see the healthy tissue as the recipient as foreign, and move to attack this healthy tissue. This complication of allogeneic BMT is called Graft versus Host Disease (GvHD) (Ferrara et al., 2009).

The natural suppressive capacity of Tregs was seen as a possibility to rein in GvHD. Studies were conducted that researched the effect of adoptive Treg transfer on GvHD and the GvL effect (Hoffmann et al., 2002; Nguyen et al., 2007; Riegel et al., 2020). These studies found that co-transfer of donor Tregs along with BMT can retain GvL effect but protect against acute GvHD. Tregs that are used for co-transfer are first expanded in culture, before they are transferred. In our study, we established a protocol for the induction of a wound healing phenotype from blood derived Tregs. this knowledge could potentially be combined, and a protocol for the expansion of Tregs that not only combats GvHD but also heals wounded tissue, could potentially be established. This, however, requires more research.

Since Tregs have been shown to be bad prognostic marker in Tregs (Shang et al., 2015), efforts have been made to try and remove them from the tumour microenvironment (Galdino et al., 2018; Ohue and Nishikawa, 2019). Modulation and depletion strategies have been applied, but not without adverse effects. Due to lack of specify for tumour Tregs, healthy Tregs can also be targeted by these therapies. One

study tried to improve upon this by only targeting CCR8$^+$ Tregs, since CCR8 has been described to be present on tumour Tregs, as opposed to circulating Tregs, however, our data shows that CCR8 is also present on healthy tissue Tregs, as well as a subpopulation of circulating Tregs, so this strategy might not be as successful as originally thought. Our data could serve as reference base for what factors healthy Tregs express, so they can be excluded. This might work to increase specificity in these types of therapies.

5.5. Limitations of the study

In this study, we did not research the wound healing capabilities of human tissue Tregs or CCR8$^+$ blood derived Tregs *in-vivo*. Wound healing capabilities of human tissue Tregs were also not tested *in-vitro*, since the number of cells needed for these assays was higher than what could be retrieved from the tissues. We did not perform wound healing studies with CCR8$^+$ blood derived Tregs either, because we found no successful way to expand them *in-vitro*. We did not research if CCR8$^+$ Tregs promote tumour growth. This question would require further research. We identified a clonal relationship between blood derived CCR8$^+$ Tregs and tissue Tregs, but the exact nature of this relationship has yet to be determined. We did not research how human Tregs develop. More research remains to be done on this. We were successful in inducing a tissue phenotype in naïve blood derived Tregs. This protocol, however, needs optimisation, especially for potential clinical applications in the future.

5.6. Conclusion

In this study, we successfully described human tissue Tregs on a single cell chromatin accessibility level, as well as a population of circulating CCR8^{+} Tregs that are clonally related to tissue Tregs. We also identified a method for induction of a tissue-like program from naïve blood derived Tregs. We discovered that, as in mouse, BATF plays a pivotal role in this population, and that they can be recognised by CCR8 expression, a factor that was previously believed to be tumour Treg exclusive.

We are just at the surface of what can be done with these Tregs, and this dataset could serve as a basis for many other studies researching Tregs in both healthy and diseased settings.

Part of the here presented data were published in the journal *Immunity* in 2021, and in 2020, both as open access papers.

1) Single-cell chromatin accessibility landscape identifies tissue repair program in human regulatory T cells.

Delacher M*, Simon M*, **Sanderink L***, Hotz-Wagenblatt A, Wuttke M, Schambeck K, Schmidleithner L, Bittner S, Pant A, Ritter U, Hehlgans T, Riegel D, Schneider V, Groeber-Becker FK, Eigenberger A, Gebhard C, Strieder N, Fischer A, Rehli M, Hoffmann P, Edinger M, Strowig T, Huehn J, Schmidl C, Werner JM, Prantl L, Brors B, Imbusch CD, Feuerer M. Immunity. 2021 Apr 13;54(4):702-720.e17.

***Equally contributing first author**

2) Precursors for Nonlymphoid-Tissue Treg Cells Reside in Secondary Lymphoid Organs and Are Programmed by the Transcription Factor BATF.

Delacher M, Imbusch CD, Hotz-Wagenblatt A, Mallm JP, Bauer K, Simon M, Riegel D, Rendeiro AF, Bittner S, **Sanderink L**, Pant A, Schmidleithner L, Braband KL, Echtenachter B, Fischer A, Giunchiglia V, Hoffmann P, Edinger M, Bock C, Rehli M, Brors B, Schmidl C, Feuerer M. Immunity. 2020 Feb 18;52(2):295-312.e11.

6. References

Alvisi, G., Brummelman, J., Puccio, S., Mazza, E.M., Tomada, E.P., Losurdo, A., Zanon, V., Peano, C., Colombo, F.S., Scarpa, A., et al. (2020). IRF4 instructs effector Treg differentiation and immune suppression in human cancer. J Clin Invest *130*, 3137-3150. 10.1172/JCI130426.

Arpaia, N., Green, J.A., Moltedo, B., Arvey, A., Hemmers, S., Yuan, S., Treuting, P.M., and Rudensky, A.Y. (2015). A Distinct Function of Regulatory T Cells in Tissue Protection. Cell *162*, 1078-1089. 10.1016/j.cell.2015.08.021.

Au - He, X., Au - de Oliveira, V.L., Au - Keijsers, R., Au - Joosten, I., and Au - Koenen, H.J.P.N. (2016). Lymphocyte Isolation from Human Skin for Phenotypic Analysis and Ex Vivo Cell Culture. JoVE, e52564. doi:10.3791/52564.

Azizi, E., Carr, A.J., Plitas, G., Cornish, A.E., Konopacki, C., Prabhakaran, S., Nainys, J., Wu, K., Kiseliovas, V., Setty, M., et al. (2018). Single-Cell Map of Diverse Immune Phenotypes in the Breast Tumor Microenvironment. Cell *174*, 1293-1308.e1236. 10.1016/j.cell.2018.05.060.

Barsheshet, Y., Wildbaum, G., Levy, E., Vitenshtein, A., Akinseye, C., Griggs, J., Lira, S.A., and Karin, N. (2017). CCR8(+)FOXp3(+) T(reg) cells as master drivers of immune regulation. Proceedings of the National Academy of Sciences of the United States of America *114*, 6086-6091. 10.1073/pnas.1621280114.

Bateman, A., Cheung, S.T., and Bennett, H.P.J. (2018). A Brief Overview of Progranulin in Health and Disease. Methods Mol Biol *1806*, 3-15. 10.1007/978-1-4939-8559-3_1.

Bonilla, F.A., and Oettgen, H.C. (2010). Adaptive immunity. Journal of Allergy and Clinical Immunology *125*, S33-S40. https://doi.org/10.1016/j.jaci.2009.09.017.

Brunkow, M.E., Jeffery, E.W., Hjerrild, K.A., Paeper, B., Clark, L.B., Yasayko, S.A., Wilkinson, J.E., Galas, D., Ziegler, S.F., and Ramsdell, F. (2001). Disruption of a new forkhead/winged-helix protein, scurfin, results in the fatal lymphoproliferative disorder of the scurfy mouse. Nat Genet *27*, 68-73. 10.1038/83784.

Buenrostro, J.D., Giresi, P.G., Zaba, L.C., Chang, H.Y., and Greenleaf, W.J. (2013). Transposition of native chromatin for fast and sensitive epigenomic profiling of open chromatin, DNA-binding proteins and nucleosome position. Nat Methods *10*, 1213-1218. 10.1038/nmeth.2688.

Burzyn, D., Kuswanto, W., Kolodin, D., Shadrach, J.L., Cerletti, M., Jang, Y., Sefik, E., Tan, T.G., Wagers, A.J., Benoist, C., and Mathis, D. (2013). A special population of regulatory T cells potentiates muscle repair. Cell *155*, 1282-1295. 10.1016/j.cell.2013.10.054.

Butler, A., Hoffman, P., Smibert, P., Papalexi, E., and Satija, R. (2018). Integrating single-cell transcriptomic data across different conditions, technologies, and species. Nat Biotechnol *36*, 411-420. 10.1038/nbt.4096.

Chen, J., Guan, L., Tang, L., Liu, S., Zhou, Y., Chen, C., He, Z., and Xu, L. (2019). T Helper 9 Cells: A New Player in Immune-Related Diseases. DNA Cell Biol *38*, 1040-1047. 10.1089/dna.2019.4729.

Chu, Y., and Corey, D.R. (2012). RNA sequencing: platform selection, experimental design, and data interpretation. Nucleic Acid Ther *22*, 271-274. 10.1089/nat.2012.0367.
Cinier, J., Hubert, M., Besson, L., Di Roio, A., Rodriguez, C., Lombardi, V., Caux, C., and Ménétrier-Caux, C. (2021). Recruitment and Expansion of Tregs Cells in the Tumor Environment-How to Target Them? cancers (Basel) *13*. 10.3390/cancers13081850.
Cipolletta, D., Feuerer, M., Li, A., Kamei, N., Lee, J., Shoelson, S.E., Benoist, C., and Mathis, D. (2012). PPAR-gamma is a major driver of the accumulation and phenotype of adipose tissue Treg cells. Nature *486*, 549-553. 10.1038/nature11132.
Copeland, N.G., Jenkins, N.A., and Court, D.L. (2001). Recombineering: a powerful new tool for mouse functional genomics. Nat Rev Genet *2*, 769-779. 10.1038/35093556.
Corces, M.R., Trevino, A.E., Hamilton, E.G., Greenside, P.G., Sinnott-Armstrong, N.A., Vesuna, S., Satpathy, A.T., Rubin, A.J., Montine, K.S., Wu, B., et al. (2017). An improved ATAC-seq protocol reduces background and enables interrogation of frozen tissues. Nat Methods *14*, 959-962. 10.1038/nmeth.4396.
Cossarizza, A., Chang, H.D., Radbruch, A., Acs, A., Adam, D., Adam-Klages, S., Agace, W.W., Aghaeepour, N., Akdis, M., Allez, M., et al. (2019). Guidelines for the use of flow cytometry and cell sorting in immunological studies (second edition). Eur J Immunol *49*, 1457-1973. 10.1002/eji.201970107.
Curotto de Lafaille, M.A., and Lafaille, J.J. (2009). Natural and Adaptive Foxp3⁺ Regulatory T Cells: More of the Same or a Division of Labor? Immunity *30*, 626-635. 10.1016/j.immuni.2009.05.002.
De Simone, M., Arrigoni, A., Rossetti, G., Gruarin, P., Ranzani, V., Politano, C., Bonnal, R.J.P., Provasi, E., Sarnicola, M.L., Panzeri, I., et al. (2016). Transcriptional Landscape of Human Tissue Lymphocytes Unveils Uniqueness of Tumor-Infiltrating T Regulatory Cells. Immunity *45*, 1135-1147. 10.1016/j.immuni.2016.10.021.
De Simone, M., Rossetti, G., and Pagani, M. (2018). Single Cell T Cell Receptor Sequencing: Techniques and Future Challenges. Frontiers in Immunology *9*. 10.3389/fimmu.2018.01638.
Delacher, M., Imbusch, C.D., Hotz-Wagenblatt, A., Mallm, J.P., Bauer, K., Simon, M., Riegel, D., Rendeiro, A.F., Bittner, S., Sanderink, L., et al. (2020). Precursors for Nonlymphoid-Tissue Treg Cells Reside in Secondary Lymphoid Organs and Are Programmed by the Transcription Factor BATF. Immunity *52*, 295-312 e211. 10.1016/j.immuni.2019.12.002.
Delacher, M., Imbusch, C.D., Weichenhan, D., Breiling, A., Hotz-Wagenblatt, A., Trager, U., Hofer, A.C., Kagebein, D., Wang, Q., Frauhammer, F., et al. (2017). Genome-wide DNA-methylation landscape defines specialization of regulatory T cells in tissues. Nat Immunol *18*, 1160-1172. 10.1038/ni.3799.
Delacher, M., Schmidl, C., Herzig, Y., Breloer, M., Hartmann, W., Brunk, F., Kagebein, D., Trager, U., Hofer, A.C., Bittner, S., et al. (2019). Rbpj expression in regulatory T cells is critical for restraining TH2 responses. Nat Commun *10*, 1621. 10.1038/s41467-019-09276-w.
Dobin, A., Davis, C.A., Schlesinger, F., Drenkow, J., Zaleski, C., Jha, S., Batut, P., Chaisson, M., and Gingeras, T.R. (2013). STAR: ultrafast universal RNA-seq aligner. Bioinformatics *29*, 15-21. 10.1093/bioinformatics/bts635.

Dombrowski, Y., O'Hagan, T., Dittmer, M., Penalva, R., Mayoral, S.R., Bankhead, P., Fleville, S., Eleftheriadis, G., Zhao, C., Naughton, M., et al. (2017). Regulatory T cells promote myelin regeneration in the central nervous system. Nat Neurosci *20*, 674-680. 10.1038/nn.4528.
Durinck, S., Spellman, P.T., Birney, E., and Huber, W. (2009). Mapping identifiers for the integration of genomic datasets with the R/Bioconductor package biomaRt. Nat Protoc *4*, 1184-1191. 10.1038/nprot.2009.97.
Easton, D.F., Pooley, K.A., Dunning, A.M., Pharoah, P.D.P., Thompson, D., Ballinger, D.G., Struewing, J.P., Morrison, J., Field, H., Luben, R., et al. (2007). Genome-wide association study identifies novel breast cancer susceptibility loci. Nature *447*, 1087-1093. 10.1038/nature05887.
Ferrara, J.L., Levine, J.E., Reddy, P., and Holler, E. (2009). Graft-versus-host disease. Lancet *373*, 1550-1561. 10.1016/s0140-6736(09)60237-3.
Feuerer, M., Herrero, L., Cipolletta, D., Naaz, A., Wong, J., Nayer, A., Lee, J., Goldfine, A.B., Benoist, C., Shoelson, S., and Mathis, D. (2009). Lean, but not obese, fat is enriched for a unique population of regulatory T cells that affect metabolic parameters. Nat Med *15*, 930-939. 10.1038/nm.2002.
Fuller, C.W., Middendorf, L.R., Benner, S.A., Church, G.M., Harris, T., Huang, X., Jovanovich, S.B., Nelson, J.R., Schloss, J.A., Schwartz, D.C., and Vezenov, D.V. (2009). The challenges of sequencing by synthesis. Nature Biotechnology *27*, 1013-1023. 10.1038/nbt.1585.
Gadani, S.P., Cronk, J.C., Norris, G.T., and Kipnis, J. (2012). IL-4 in the brain: a cytokine to remember. J Immunol *189*, 4213-4219. 10.4049/jimmunol.1202246.
Galdino, N.A.L., Loures, F.V., de Araújo, E.F., da Costa, T.A., Preite, N.W., and Calich, V.L.G. (2018). Depletion of regulatory T cells in ongoing paracoccidioidomycosis rescues protective Th1/Th17 immunity and prevents fatal disease outcome. Scientific Reports *8*, 16544. 10.1038/s41598-018-35037-8.
Goswami, R., and Awasthi, A. (2020). Editorial: T Cell Differentiation and Function in Tissue Inflammation. Frontiers in Immunology *11*. 10.3389/fimmu.2020.00289.
Griesenauer, B., and Paczesny, S. (2017). The ST2/IL-33 Axis in Immune Cells during Inflammatory Diseases. Frontiers in Immunology *8*. 10.3389/fimmu.2017.00475.
Groeber, F., Engelhardt, L., Egger, S., Werthmann, H., Monaghan, M., Walles, H., and Hansmann, J. (2015). Impedance spectroscopy for the non-destructive evaluation of in vitro epidermal models. Pharm Res *32*, 1845-1854. 10.1007/s11095-014-1580-3.
Groeber, F., Schober, L., Schmid, F.F., Traube, A., Kolbus-Hernandez, S., Daton, K., Hoffmann, S., Petersohn, D., Schafer-Korting, M., Walles, H., and Mewes, K.R. (2016). Catch-up validation study of an in vitro skin irritation test method based on an open source reconstructed epidermis (phase II). Toxicol In Vitro *36*, 254-261. 10.1016/j.tiv.2016.07.008.
Guler, R., Roy, S., Suzuki, H., and Brombacher, F. (2015). Targeting Batf2 for infectious diseases and cancer. Oncotarget *6*.
Hayatsu, N., Miyao, T., Tachibana, M., Murakami, R., Kimura, A., Kato, T., Kawakami, E., Endo, T.A., Setoguchi, R., Watarai, H., et al. (2017). Analyses of a Mutant Foxp3 Allele Reveal BATF as a Critical Transcription Factor in the Differentiation and Accumulation of Tissue Regulatory T Cells. Immunity *47*, 268-283.e269. 10.1016/j.immuni.2017.07.008.

Heinz, S., Benner, C., Spann, N., Bertolino, E., Lin, Y.C., Laslo, P., Cheng, J.X., Murre, C., Singh, H., and Glass, C.K. (2010). Simple combinations of lineage-determining transcription factors prime cis-regulatory elements required for macrophage and B cell identities. Mol Cell *38*, 576-589. 10.1016/j.molcel.2010.05.004.
Henriksson, J., Chen, X., Gomes, T., Ullah, U., Meyer, K.B., Miragaia, R., Duddy, G., Pramanik, J., Yusa, K., Lahesmaa, R., and Teichmann, S.A. (2019). Genome-wide CRISPR Screens in T Helper Cells Reveal Pervasive Crosstalk between Activation and Differentiation. Cell *176*, 882-896 e818. 10.1016/j.cell.2018.11.044.
Hoffman, W., Lakkis, F.G., and Chalasani, G. (2016). B Cells, Antibodies, and More. Clin J Am Soc Nephrol *11*, 137-154. 10.2215/CJN.09430915.
Hoffmann, P., Ermann, J., Edinger, M., Fathman, C.G., and Strober, S. (2002). Donor-type CD4(+)CD25(+) regulatory T cells suppress lethal acute graft-versus-host disease after allogeneic bone marrow transplantation. J Exp Med *196*, 389-399. 10.1084/jem.20020399.
Horowitz, M.M., Gale, R.P., Sondel, P.M., Goldman, J.M., Kersey, J., Kolb, H.J., Rimm, A.A., Ringdén, O., Rozman, C., Speck, B., and et al. (1990). Graft-versus-leukemia reactions after bone marrow transplantation. Blood *75*, 555-562.
Hosseini, H., Obradovic, M.M.S., Hoffmann, M., Harper, K.L., Sosa, M.S., Werner-Klein, M., Nanduri, L.K., Werno, C., Ehrl, C., Maneck, M., et al. (2016). Early dissemination seeds metastasis in breast cancer. Nature *540*, 552-558. 10.1038/nature20785.
Hünefeld, C., Mezger, M., Röcken, M., and Röcken, M. (2012). The Three Dimensions of Functional T-Cell Tolerance: From Research to Practice. Journal of Investigative Dermatology *132*, 508-511. https://doi.org/10.1038/jid.2011.465.
Ishida, Y., Agata, Y., Shibahara, K., and Honjo, T. (1992). Induced expression of PD-1, a novel member of the immunoglobulin gene superfamily, upon programmed cell death. Embo j *11*, 3887-3895.
Islam, S., Zeisel, A., Joost, S., La Manno, G., Zajac, P., Kasper, M., Lönnerberg, P., and Linnarsson, S. (2014). Quantitative single-cell RNA-seq with unique molecular identifiers. Nat Methods *11*, 163-166. 10.1038/nmeth.2772.
Ito, M., Komai, K., Mise-Omata, S., Iizuka-Koga, M., Noguchi, Y., Kondo, T., Sakai, R., Matsuo, K., Nakayama, T., Yoshie, O., et al. (2019). Brain regulatory T cells suppress astrogliosis and potentiate neurological recovery. Nature *565*, 246-250. 10.1038/s41586-018-0824-5.
James, K.R., Gomes, T., Elmentaite, R., Kumar, N., Gulliver, E.L., King, H.W., Stares, M.D., Bareham, B.R., Ferdinand, J.R., Petrova, V.N., et al. (2020). Distinct microbial and immune niches of the human colon. Nat Immunol *21*, 343-353. 10.1038/s41590-020-0602-z.
Jiang, H., Lei, R., Ding, S.W., and Zhu, S. (2014). Skewer: a fast and accurate adapter trimmer for next-generation sequencing paired-end reads. BMC Bioinformatics *15*, 182. 10.1186/1471-2105-15-182.
Kiesewetter, L., Littau, L., Walles, H., Boccaccini, A.R., and Groeber-Becker, F. (2019). Reepithelialization in focus: Non-invasive monitoring of epidermal wound healing in vitro. Biosens Bioelectron *142*, 111555. 10.1016/j.bios.2019.111555.
Komatsu, N., Mariotti-Ferrandiz, M.E., Wang, Y., Malissen, B., Waldmann, H., and Hori, S. (2009). Heterogeneity of natural Foxp3+ T cells: a committed regulatory T-

cell lineage and an uncommitted minor population retaining plasticity. Proc Natl Acad Sci U S A *106*, 1903-1908. 10.1073/pnas.0811556106.
König, R., Huang, L.Y., and Germain, R.N. (1992). MHC class II interaction with CD4 mediated by a region analogous to the MHC class I binding site for CD8. Nature *356*, 796-798. 10.1038/356796a0.
Korsunsky, I., Millard, N., Fan, J., Slowikowski, K., Zhang, F., Wei, K., Baglaenko, Y., Brenner, M., Loh, P.R., and Raychaudhuri, S. (2019). Fast, sensitive and accurate integration of single-cell data with Harmony. Nat Methods *16*, 1289-1296. 10.1038/s41592-019-0619-0.
Kuhn, R.M., Haussler, D., and Kent, W.J. (2013). The UCSC genome browser and associated tools. Brief Bioinform *14*, 144-161. 10.1093/bib/bbs038.
Kurachi, M., Barnitz, R.A., Yosef, N., Odorizzi, P.M., DiIorio, M.A., Lemieux, M.E., Yates, K., Godec, J., Klatt, M.G., Regev, A., et al. (2014). The transcription factor BATF operates as an essential differentiation checkpoint in early effector CD8+ T cells. Nature Immunology *15*, 373-383. 10.1038/ni.2834.
Langmead, B., and Salzberg, S.L. (2012). Fast gapped-read alignment with Bowtie 2. Nat Methods *9*, 357-359. 10.1038/nmeth.1923.
Li, M.O., and Rudensky, A.Y. (2016). T cell receptor signalling in the control of regulatory T cell differentiation and function. Nature reviews. Immunology *16*, 220-233. 10.1038/nri.2016.26.
Liesz, A., Suri-Payer, E., Veltkamp, C., Doerr, H., Sommer, C., Rivest, S., Giese, T., and Veltkamp, R. (2009). Regulatory T cells are key cerebroprotective immunomodulators in acute experimental stroke. Nat Med *15*, 192-199. 10.1038/nm.1927.
Liu, X., Nurieva, R.I., and Dong, C. (2013). Transcriptional regulation of follicular T-helper (Tfh) cells. Immunological reviews *252*, 139-145. 10.1111/imr.12040.
Love, M.I., Huber, W., and Anders, S. (2014). Moderated estimation of fold change and dispersion for RNA-seq data with DESeq2. Genome Biol *15*, 550. 10.1186/s13059-014-0550-8.
Macián, F., García-Cózar, F., Im, S.H., Horton, H.F., Byrne, M.C., and Rao, A. (2002). Transcriptional mechanisms underlying lymphocyte tolerance. Cell *109*, 719-731. 10.1016/s0092-8674(02)00767-5.
Majhail, N.S., Farnia, S.H., Carpenter, P.A., Champlin, R.E., Crawford, S., Marks, D.I., Omel, J.L., Orchard, P.J., Palmer, J., Saber, W., et al. (2015). Indications for Autologous and Allogeneic Hematopoietic Cell Transplantation: Guidelines from the American Society for Blood and Marrow Transplantation. Biol Blood Marrow Transplant *21*, 1863-1869. 10.1016/j.bbmt.2015.07.032.
Ménétrier-Caux, C., Curiel, T., Faget, J., Manuel, M., Caux, C., and Zou, W. (2012). Targeting regulatory T cells. Target Oncol *7*, 15-28. 10.1007/s11523-012-0208-y.
Meyer, M., and Kircher, M. (2010). Illumina sequencing library preparation for highly multiplexed target capture and sequencing. Cold Spring Harb Protoc *2010*, pdb.prot5448. 10.1101/pdb.prot5448.
Miragaia, R.J., Gomes, T., Chomka, A., Jardine, L., Riedel, A., Hegazy, A.N., Whibley, N., Tucci, A., Chen, X., Lindeman, I., et al. (2019). Single-Cell Transcriptomics of Regulatory T Cells Reveals Trajectories of Tissue Adaptation. Immunity *50*, 493-504 e497. 10.1016/j.immuni.2019.01.001.

Morman, R.E., Poston, S., and Taparowsky, E.J. (2016). Identification of BATF target genes critical to its function in immune responses. The Journal of Immunology *196*, 58.14-58.14.
Mortazavi, A., Williams, B.A., McCue, K., Schaeffer, L., and Wold, B. (2008). Mapping and quantifying mammalian transcriptomes by RNA-Seq. Nat Methods *5*, 621-628. 10.1038/nmeth.1226.
Murphy, K., Weaver, C., and Janeway, C. (2017). Janeway's immunobiology.
Nguyen, V.H., Zeiser, R., Dasilva, D.L., Chang, D.S., Beilhack, A., Contag, C.H., and Negrin, R.S. (2007). In vivo dynamics of regulatory T-cell trafficking and survival predict effective strategies to control graft-versus-host disease following allogeneic transplantation. Blood *109*, 2649-2656. 10.1182/blood-2006-08-044529.
Ohue, Y., and Nishikawa, H. (2019). Regulatory T (Treg) cells in cancer: Can Treg cells be a new therapeutic target? cancer Sci *110*, 2080-2089. 10.1111/cas.14069.
Pham, D., Silberger, D.J., Hatton, R.D., and Weaver, C.T. (2019). Batf promotes and stabilizes Th17 cell development by antagonizing the actions of STAT5. The Journal of Immunology *202*, 124.110-124.110.
Pliner, H.A., Packer, J.S., McFaline-Figueroa, J.L., Cusanovich, D.A., Daza, R.M., Aghamirzaie, D., Srivatsan, S., Qiu, X., Jackson, D., Minkina, A., et al. (2018). Cicero Predicts cis-Regulatory DNA Interactions from Single-Cell Chromatin accessibility Data. Mol Cell *71*, 858-871 e858. 10.1016/j.molcel.2018.06.044.
Plitas, G., Konopacki, C., Wu, K., Bos, P.D., Morrow, M., Putintseva, E.V., Chudakov, D.M., and Rudensky, A.Y. (2016). Regulatory T Cells Exhibit Distinct Features in Human Breast cancer. Immunity *45*, 1122-1134. 10.1016/j.immuni.2016.10.032.
Pope, B.D., Ryba, T., Dileep, V., Yue, F., Wu, W., Denas, O., Vera, D.L., Wang, Y., Hansen, R.S., Canfield, T.K., et al. (2014). Topologically associating domains are stable units of replication-timing regulation. Nature *515*, 402-405. 10.1038/nature13986.
Qin, L., Waseem, T.C., Sahoo, A., Bieerkehazhi, S., Zhou, H., Galkina, E.V., and Nurieva, R. (2018). Insights Into the Molecular Mechanisms of T Follicular Helper-Mediated Immunity and Pathology. Front Immunol *9*, 1884. 10.3389/fimmu.2018.01884.
Quinlan, A.R., and Hall, I.M. (2010). BEDTools: a flexible suite of utilities for comparing genomic features. Bioinformatics *26*, 841-842. 10.1093/bioinformatics/btq033.
Riegel, C., Boeld, T.J., Doser, K., Huber, E., Hoffmann, P., and Edinger, M. (2020). Efficient treatment of murine acute GvHD by in vitro expanded donor regulatory T cells. Leukemia *34*, 895-908. 10.1038/s41375-019-0625-3.
Round, J.L., O'Connell, R.M., and Mazmanian, S.K. (2010). Coordination of tolerogenic immune responses by the commensal microbiota. J Autoimmun *34*, J220-J225. 10.1016/j.jaut.2009.11.007.
Saito, T., Nishikawa, H., Wada, H., Nagano, Y., Sugiyama, D., Atarashi, K., Maeda, Y., Hamaguchi, M., Ohkura, N., Sato, E., et al. (2016). Two FOXP3(+)CD4(+) T cell subpopulations distinctly control the prognosis of colorectal cancers. Nat Med *22*, 679-684. 10.1038/nm.4086.
Sakaguchi, S., Mikami, N., Wing, J.B., Tanaka, A., Ichiyama, K., and Ohkura, N. (2020). Regulatory T Cells and Human Disease. Annu Rev Immunol *38*, 541-566. 10.1146/annurev-immunol-042718-041717.

Sakaguchi, S., Wing, K., Onishi, Y., Prieto-Martin, P., and Yamaguchi, T. (2009). Regulatory T cells: how do they suppress immune responses? International Immunology *21*, 1105-1111. 10.1093/intimm/dxp095.
Sanger, F., Nicklen, S., and Coulson, A.R. (1977). DNA sequencing with chain-terminating inhibitors. Proc Natl Acad Sci U S A *74*, 5463-5467. 10.1073/pnas.74.12.5463.
Satpathy, A.T., Granja, J.M., Yost, K.E., Qi, Y., Meschi, F., McDermott, G.P., Olsen, B.N., Mumbach, M.R., Pierce, S.E., Corces, M.R., et al. (2019). Massively parallel single-cell chromatin landscapes of human immune cell development and intratumoral T cell exhaustion. Nat Biotechnol *37*, 925-936. 10.1038/s41587-019-0206-z.
Schmid, M., Dufner, B., Durk, J., Bedal, K., Stricker, K., Prokoph, L.A., Koch, C., Wege, A.K., Zirpel, H., van Zandbergen, G., et al. (2015). An Emerging Approach for Parallel Quantification of Intracellular Protozoan Parasites and Host Cell Characterization Using TissueFAXS Cytometry. PLoS One *10*, e0139866. 10.1371/journal.pone.0139866.
Schmidl, C., Delacher, M., Huehn, J., and Feuerer, M. (2018). Epigenetic mechanisms regulating T-cell responses. J Allergy Clin Immunol *142*, 728-743. 10.1016/j.jaci.2018.07.014.
Shang, B., Liu, Y., Jiang, S.-j., and Liu, Y. (2015). Prognostic value of tumor-infiltrating FoxP3+ regulatory T cells in cancers: a systematic review and meta-analysis. Scientific reports *5*, 15179-15179. 10.1038/srep15179.
Sprent, J., and Kishimoto, H. (2001). The thymus and central tolerance. Philos Trans R Soc Lond B Biol Sci *356*, 609-616. 10.1098/rstb.2001.0846.
Stuart, T., Butler, A., Hoffman, P., Hafemeister, C., Papalexi, E., Mauck, W.M., 3rd, Hao, Y., Stoeckius, M., Smibert, P., and Satija, R. (2019). Comprehensive Integration of Single-Cell Data. Cell *177*, 1888-1902 e1821. 10.1016/j.cell.2019.05.031.
Szabo, P.A., Levitin, H.M., Miron, M., Snyder, M.E., Senda, T., Yuan, J., Cheng, Y.L., Bush, E.C., Dogra, P., Thapa, P., et al. (2019). Single-cell transcriptomics of human T cells reveals tissue and activation signatures in health and disease. Nat Commun *10*, 4706. 10.1038/s41467-019-12464-3.
Tanaka, A., and Sakaguchi, S. (2017). Regulatory T cells in cancer immunotherapy. Cell Res *27*, 109-118. 10.1038/cr.2016.151.
Tarasov, A., Vilella, A.J., Cuppen, E., Nijman, I.J., and Prins, P. (2015). Sambamba: fast processing of NGS alignment formats. Bioinformatics *31*, 2032-2034. 10.1093/bioinformatics/btv098.
Tay, R.E., Richardson, E.K., and Toh, H.C. (2021). Revisiting the role of CD4+ T cells in cancer immunotherapy—new insights into old paradigms. cancer Gene Therapy *28*, 5-17. 10.1038/s41417-020-0183-x.
Vasanthakumar, A., Moro, K., Xin, A., Liao, Y., Gloury, R., Kawamoto, S., Fagarasan, S., Mielke, L.A., Afshar-Sterle, S., Masters, S.L., et al. (2015). The transcriptional regulators IRF4, BATF and IL-33 orchestrate development and maintenance of adipose tissue-resident regulatory T cells. Nat Immunol *16*, 276-285. 10.1038/ni.3085.
Verma, R.P., and Hansch, C. (2007). Matrix metalloproteinases (MMPs): chemical-biological functions and (Q)SARs. Bioorg Med Chem *15*, 2223-2268. 10.1016/j.bmc.2007.01.011.

Vignali, D.A., Collison, L.W., and Workman, C.J. (2008). How regulatory T cells work. Nat Rev Immunol *8*, 523-532. 10.1038/nri2343.
Wang, L., Simons, D.L., Lu, X., Tu, T.Y., Solomon, S., Wang, R., Rosario, A., Avalos, C., Schmolze, D., Yim, J., et al. (2019). Connecting blood and intratumoral T(reg) cell activity in predicting future relapse in breast cancer. Nat Immunol *20*, 1220-1230. 10.1038/s41590-019-0429-7.
Wildin, R.S., Ramsdell, F., Peake, J., Faravelli, F., Casanova, J.L., Buist, N., Levy-Lahad, E., Mazzella, M., Goulet, O., Perroni, L., et al. (2001). X-linked neonatal diabetes mellitus, enteropathy and endocrinopathy syndrome is the human equivalent of mouse scurfy. Nat Genet *27*, 18-20. 10.1038/83707.
Wolfsberg, T.G., Straight, P.D., Gerena, R.L., Huovila, A.P., Primakoff, P., Myles, D.G., and White, J.M. (1995). ADAM, a widely distributed and developmentally regulated gene family encoding membrane proteins with a disintegrin and metalloprotease domain. Dev Biol *169*, 378-383. 10.1006/dbio.1995.1152.
Wollenberg, I., Agua-Doce, A., Hernández, A., Almeida, C., Oliveira, V.G., Faro, J., and Graca, L. (2011). Regulation of the germinal center reaction by Foxp3+ follicular regulatory T cells. J Immunol *187*, 4553-4560. 10.4049/jimmunol.1101328.
Wu, D., Han, J.M., Yu, X., Lam, A.J., Hoeppli, R.E., Pesenacker, A.M., Huang, Q., Chen, V., Speake, C., Yorke, E., et al. (2019). Characterization of regulatory T cells in obese omental adipose tissue in humans. Eur J Immunol *49*, 336-347. 10.1002/eji.201847570.
Xie, M.M., and Dent, A.L. (2018). Unexpected Help: Follicular Regulatory T Cells in the Germinal Center. Frontiers in Immunology *9*. 10.3389/fimmu.2018.01536.
Yano, H., Andrews, L.P., Workman, C.J., and Vignali, D.A.A. (2019). Intratumoral regulatory T cells: markers, subsets and their impact on anti-tumor immunity. Immunology *157*, 232-247. 10.1111/imm.13067.
Zhang, J., Xu, X., and Liu, Y. (2004). Activation-induced cell death in T cells and autoimmunity. Cell Mol Immunol *1*, 186-192.
Zhang, N., and Bevan, M.J. (2011). CD8(+) T cells: foot soldiers of the immune system. Immunity *35*, 161-168. 10.1016/j.immuni.2011.07.010.